arXiv:quant-ph/0211035v1 7 Nov 2002

CHAOS AND QUANTUM-CLASSICAL CORRESPONDENCE FOR TWO COUPLED SPINS

by

Joseph V. Emerson

M.Sc., Simon Fraser University, 1995

B.Sc., McGill University, 1993

A THESIS SUBMITTED IN PARTIAL FULFILLMENT
OF THE REQUIREMENTS FOR THE DEGREE OF
DOCTOR OF PHILOSOPHY
in the Department
of
Physics

© Joseph V. Emerson 2001

SIMON FRASER UNIVERSITY

May 2001

All rights reserved. This work may not be
reproduced in whole or in part, by photocopy
or other means, without the permission of the author.

APPROVAL

Name: Joseph V. Emerson

Degree: Doctor of Philosophy

Title of thesis: Chaos and Quantum-Classical Correspondence for Two Coupled Spins

Examining Committee: Dr. Mike Hayden
Chair

Dr. Leslie E. Ballentine, Senior Supervisor

Dr. Howard Trottier, Supervisor

Dr. Michael Wortis, Supervisor

Dr. Igor Herbut, Internal Examiner

Dr. Jorge V. Jose, External Examiner
Department of Physics, Northeastern University

Date Approved: _____

Abstract

Two approaches to quantum-classical correspondence are distinguished according to the classical dynamical theory with which quantum theory is compared. The first of these, Ehrenfest correspondence, defines a dynamical regime in which the quantum expectation values follow approximately a classical trajectory. The second of these, Liouville correspondence, applies when the quantum probability distributions remain well approximated by a density in the classical phase space. The former applies only for narrow states, whereas the latter may remain valid even for quantum states that have spread to the system size.

A spin model is adopted for this correspondence study because the quantum state is discrete and finite-dimensional, and thus no articifical truncation of the Hilbert space is required. The quantum time-evolution is given by a discrete unitary mapping. The corresponding classical model is volume-preserving (non-dissipative) and the time-evolution is given by a symplectic map.

In classically chaotic regimes, the widths of initially narrow quantum states grow, on average, exponentially with time, until saturation at the system size. This initial spreading rate is well approximated by the classical Lyapunov exponent when the accessible classical phase space is predominantly chaotic. Because of the exponential growth rate of the quantum variance, the Ehrenfest regime is delimited by a break-time that grows logarithmically with increasing quantum numbers.

The small differences between quantum expectation values and corresponding Liouville averages of dynamical variables also grow exponentially, initially, if the classical behaviour is chaotic. This exponential rate is independent of $\hbar$ and consistently larger than the classical Lyapunov exponent by at least a factor of two. Interestingly, this exponential growth rate does not continue until these differences approach magnitudes of order the system size, but crosses over to power-law growth (or simply saturates), when the differences have

reached magnitudes no larger than order $\hbar$. Because of the exponential growth of these quantum-classical differences, the Liouville regime is also delimited by a break-time that grows logarithmicly with increasing quantum numbers. However, due to the early saturation of the exponential growth of the differences, the Liouville log break-time applies only in a restricted domain.

After spreading to the system size, the quantum states relax to an approximately time-independent state. This is characterised by equilibrium distributions that are subject to rapidly oscillating fluctuations about the coarse-grained classical steady-state. If the accessible classical phase space is predominantly chaotic, then the equilibrium quantum probability distributions are nearly microcanonical. Otherwise the steady-state quantum probability distributions accurately reflect the details of the KAM surfaces in the classical phase space. The equilibrium regime quantum fluctuations, which are quantum-classical differences, are shown to approach zero as a negative power of the quantum numbers.

Since the differences between quantum expectation values and *individual* classical trajectories grow exponentially in time to a magnitude that scales with the system size, the Ehrenfest regime is delimited by an *unrestricted* log break-time. The log break-time may be short compared to experimental time-scales for some chaotic macroscopic bodies, and, as a result, an observable *breakdown* of Ehrenfest correspondence may arise for some macroscopic systems. Although the Liouville regime is also delimited by a log break-time, an observable *breakdown* of correspondence between quantum mechanics and Liouville mechanics for macroscopic bodies is not likely since their differences, expressed relative to the dimensions of the observable, approach zero in the limit of large quantum numbers.

For Coyote

Acknowledgments

I would like to thank my thesis advisor, Dr. Leslie Ballentine, and the Faculty of Science for financial support provided throughout my doctoral studies. I would also like to thank the Centre for Experimental and Constructive Mathematics for access to their computational resources.

I am indebted to several individuals for their intellectual support: Dr. Leslie Ballentine, for his critical insights and numerous clarifications, and several careful readings of the manuscript; Karn Kallio, my office mate and friend, for sharing his vast knowledge of mathematics and, more importantly, his infectious enthusiasm for learning the art of physics; and my old friend Rob Spekkens, for the many thought-provoking discussions that stimulated my interest in the physics and philosophy of quantum mechanics.

Finally, I wish to thank my family and friends for their encouragement, the Bookman for his advice, and, especially, Julia Lianne Bevin Shugarman - for seeing me through.

Contents

Approval **ii**

Abstract **iii**

Dedication **v**

Acknowledgments **vi**

List of Figures **x**

1 Introduction **1**

1.1 Classical Trajectories and Quantum Expectation Values 3

1.2 Classical Chaos and Quantum Chaos 7

1.3 Chaos and Ehrenfest Correspondence 9

1.4 Quantum Correspondence with Liouville Mechanics 12

2 Description of the Model **20**

2.1 The Model 20

2.1.1 The Quantum Dynamics 20

2.1.2 Classical Map 22

2.1.3 The Liouville Dynamics 27

2.1.4 Correspondence Between Quantum and Classical Models 28

2.2 Initial States 29

2.2.1 Initial Quantum State 29

2.2.2 Initial Classical State and Correspondence in the Macroscopic Limit . 30

2.3 Numerical Methods 33

3 Correspondence for Low Order Moments **35**
3.1 Introduction . . . 35
3.2 Characteristics of the Quantum and Liouville Dynamics . . . 37
3.2.1 Mixed Phase Space . . . 37
3.2.2 Regime of Global Chaos . . . 40
3.3 Time-Domain Characteristics of Quantum-Classical Differences . . . 45
3.4 Correspondence Scaling in the Macroscopic Limit . . . 49
3.5 Discussion . . . 54

4 Correspondence for the Probability Distributions **57**
4.1 Introduction . . . 57
4.2 Dynamical Behaviour of Probability Distributions . . . 59
4.2.1 Mixed Regime Chaos . . . 62
4.2.2 Regime of Global Chaos . . . 64
4.3 Rates of Relaxation to Equilibrium . . . 67
4.4 Time-dependence of Quantum-Classical Differences . . . 71
4.5 Correspondence in the Classical Limit . . . 75
4.6 Discussion . . . 79

5 Breakdown of Ehrenfest Correspondence **81**
5.1 Introduction . . . 81
5.2 Ehrenfest Correspondence Conditions . . . 84
5.3 The Ehrenfest Break-Time . . . 85
5.4 The Breakdown of Ehrenfest Correspondence . . . 87
5.5 Macroscopic Deviations and Kinematic Constraints . . . 88
5.6 Case Study: Coupled Spins . . . 89
5.7 Discussion . . . 95
5.7.1 Liouville Correspondence Does Not Breakdown . . . 95
5.7.2 Can Decoherence Restore Ehrenfest Correspondence? . . . 96
5.7.3 Consequences for Interpretation of the Quantum State . . . 96
5.8 Is Quantum Mechanics Complete? . . . 97

A Nonclassical Moments for SU(2) Coherent States **99**

B Wigner-Weyl Representation of Quantum Mechanics **102**

Bibliography **104**

List of Figures

2.1 Behaviour of the classical mapping for different values of $r = |\mathbf{L}|/|\mathbf{S}|$ and $\gamma = c|\mathbf{S}|$ with $a = 5$. Circles correspond to parameter values for which at least 99% of the surface area $\mathcal{P}$ produces regular dynamics and crosses correspond to parameter values for which the dynamics are at least 99% chaotic. Superpositions of circles and crosses correspond to parameter values which produce a mixed phase space. We investigate quantum-classical correspondence for the parameter values $\gamma = 1.215$ (mixed regime) and $\gamma = 2.835$ (global chaos), with $r = 1.1$, which are indicated by filled circles. 24

2.2 Stroboscopic trajectories on the unit sphere launched from a regular zone of the mixed regime with $\gamma = 1.215$, $r = 1.1$, $a = 5$ and $\vec{\theta}(0) = (5^o, 5^o, 5^o, 5^o)$. . 26

2.3 Same parameters as Fig. 2.2 but the trajectory is launched from a chaotic zone of the mixed regime with initial condition $\vec{\theta}(0) = (20^o, 40^o, 160^o, 130^o)$. . 27

2.4 A chaotic trajectory for mixed regime parameters $\gamma = 0.06$, $r = 100$, and $a = 5$ with $\vec{\theta}(0) = (27^o, 27^o, 27^o, 27^o)$. The motion of the larger spin appears to remain confined to a narrow band on the surface of the sphere. 28

3.1 Growth of normalized quantum and classical variances in a chaotic zone (a) and a regular zone (b) of the mixed phase space regime $\gamma = 1.215$ and $r \simeq 1.1$ with $l = 154$. Quantum and classical results are nearly indistinguishable on this scale. In the chaotic case, the approximately exponential growth of both variances is governed by a much larger rate, $\lambda_w = 0.13$ (solid line), than that predicted from the largest Lyapunov exponent, $\lambda_L = 0.04$ (dotted line). . . . 38

3.2 Comparison of quantum expectation value and corresponding classical average $\langle L_z \rangle_c$ in the regime of global chaos $\gamma = 2.835$ and $r \simeq 1.1$ with $l = 154$ and initial condition $\vec{\theta}_o = (45^o, 70^o, 135^o, 70^o)$. The points of the stroboscopic map are connected with lines to guide the eye. The quantum expectation value and the Liouville average exhibit esentially the same rate of relaxation to microcanonical equilibrium, a behaviour which is qualitatively distinct from that of the single trajectory. 41

3.3 Growth of normalized quantum and classical variances in the regime of global chaos, $\gamma = 2.835$ and $r \simeq 1.1$ with l=154, for the two initial conditions cited in the text. Quantum-classical differences are nearly imperceptible on this scale. In this regime the largest Lyapunov exponent $\lambda_L = 0.45$ provides a much better estimate of the initial variance growth rate. 42

3.4 Initial probability distributions for L_z for $\vec{\theta}(0) = (45^o, 70^o, 135^o, 70^o)$ with $l = 154$. The quantum and classical distributions are indistinguishable on the scale of the figure. 43

3.5 Same as Fig. 3.4 but the states have evolved to $n = 6$ in the regime of global chaos $\gamma = 2.835$ and $r \simeq 1.1$. Both the quantum and classical distribution have spread to system dimension and exhibit their largest differences on this saturation time-scale. 44

3.6 Same as Fig. 3.5, but for $n = 15$. Both quantum and classical distributions have relaxed close to the microcanonical equilibrium. 45

3.7 Time-dependence of quantum-classical differences in a regular zone (open circles) and a chaotic zone (filled circles) of mixed regime ($\gamma = 1.215$ and $r \simeq 1.1$) with $l = 154$. For the chaotic state, $\delta L_z = |\langle L_z \rangle - \langle L_z \rangle_c|$ is contrasted with the Ehrenfest difference $|\langle L_z \rangle - L_z|$ between the quantum expectation value and a single trajectory (plus signs), which grows until saturation at system dimension. The solid line corresponds to (3.5) using $\lambda_{qc} = 0.43$. The horizontal lines indicate two different values of the difference tolerance p which may be used to determine the break-time; for $p = 0.1$ (dotted line) t_b occurs on a logarithmic time-scale, but for $p = 15.4$ (sparse dotted line) t_b is not defined over numerically accessible time-scales. 46

3.8 Growth of the quantum-classical difference δL_z in the chaotic zone of a mixed regime, $\gamma = 1.215$ and $r \simeq 1.1$, with $l = 22$ (filled circles) and $l = 220$ (open circles). For $l = 220$ the exponential growth rate (3.5) is plotted using the classical Lyapunov exponent, $\lambda_L = 0.04$ (sparse dotted line), and for both l values (3.5) is plotted using the exponent $\lambda_{qc} = 0.43$ (solid line for $l = 22$, dotted line for $l = 220$), which is obtained from a fit of (3.6) to the corresponding break-time data in Fig. 3.10. 47

3.9 Growth of quantum-classical differences in the regime of global chaos, $\gamma = 2.835$ and $r \simeq 1.1$, with $l = 154$, for the two initial conditions cited in text. The exponential growth rate (3.5) is plotted using the classical Lyapunov exponent, $\lambda_L = 0.45$ (dotted line), and the exponent $\lambda_{qc} = 1.1$ (solid line), which is obtained from a fit of (3.6) to the corresponding break-time data in Fig. 3.10. 48

3.10 Scaling of the break-time using tolerance $p = 0.1$ as a function of increasing quantum number for the mixed regime parameters $\gamma = 1.215$ and $r \simeq 1.1$ with $\vec{\theta}(0) = (20^o, 40^o, 160^o, 130^o)$ (filled circles) and for the global chaos parameters $\gamma = 2.835$ and $r \simeq 1.1$ with $\vec{\theta}(0) = (45^o, 70^o, 135^o, 70^o)$ (open circles). We also plot the results of fits to the log rule (3.6), which produced exponents $\lambda_{qc} = 0.43$ for $\gamma = 1.215$ and $\lambda_{qc} = 1.1$ for $\gamma = 2.835$. 51

3.11 Maximum quantum-classical difference occuring over the first 200 kicks in the regime of global chaos ($\gamma = 2.835$, $r \simeq 1.1$) plotted against increasing quantum number. These maximum values provide an upper bound on $\delta L_z(t^*)$ for each l. The data corresponding to the initial condition $\vec{\theta}(0) = (20^o, 40^o, 160^o, 130^o)$ (filled circles) represent a typical case in which the maximum quantum-classical differences do not vary significantly with l. The large deviations observed for the initial condition $\vec{\theta}(0) = (45^o, 70^o, 135^o, 70^o)$ (open circles) are an exceptional case, with maximum differences growing rapidly for small quantum numbers but tending asymptotically toward independence of l. These curves provide an upper bound on the tolerance values p for which the break-time measure scales logarithmically with l. 53

4.1 Quantum and classical probability distributions for L_z with $l = 154$ in chaotic zone of mixed regime ($\gamma = 1.215, r = 1.1, a = 5$). The dots are visible because they are shifted to the right by half of their width. The figure on the left is the initial state ($n = 0$) and that on the right is at time-step $n = 6$. 62
4.2 Same as Fig. 4.1 but for time-steps $n = 99$ on the left and $n = 100$ on the right. Both quantum and classical distributions have reached the system dimension and are relaxing towards equilibrium. 63
4.3 Same as Fig. 4.1 but for $n = 199$ on the left and $n = 200$ on the right. The quantum distribution is fluctuating about a classical steady-state. 64
4.4 Same as in the previous figure, but for $P_{L_x}(m_l)$ on the left and $P_{J_z}(m_j)$ on the right, at time-step $n = 200$. Both $P_{J_z}(m_j)$ and $P^c_{J_z}(m_j)$ are localised relative to the projected microcanonical distribution $P^{mc}_{J_z}(m_j)$. 65
4.5 The equilibrium shapes of $P_{L_z}(m_l)$ and $P_{J_z}(m_j)$ at time-step $n = 50$ with $l = 154$ for a state launched in the global chaos regime ($\gamma = 2.835, r = 1.1, a = 5$). The quantum distributions exhibit small rapidly oscillating fluctuations about the projected microcanonical distributions. The classical distributions are not visible since the points lie within the fluctuating quantum data. . . . 66
4.6 Comparison of the quantum and classical entropies for $s = 140$ and $l = 154$ in (a) regime of global chaos ($\gamma = 2.835$); (b) chaotic zone of the mixed regime ($\gamma = 1.215$); (c) regular zone of the mixed regime ($\gamma = 1.215$). 68
4.7 Comparison of the quantum and classical subsystem entropies for increasing system sizes in the global chaos regime of Fig. 4.6. 69
4.8 Time dependence of the standard deviation $\sigma[L_z]$ of quantum-classical differences (4.13) for states launched from a regular zone (dotted line) of the mixed regime ($\gamma = 1.215$), from a chaotic zone of the same mixed regime (middle solid line), and from the regime of global chaos (lower solid line,$\gamma = 2.835$). The initial discrepancy is relatively large, but quickly decreases, and then increases until reaching an asymptotic equilibrium value. This occurs more slowly for the mixed regime case, for which the asymptotic value is also larger. In all cases $s = 140$ and $l = 154$. 72
4.9 Same as Fig. 4.8 but for the standard deviation of quantum-classical differences of the total angular momentum, $\sigma[J_z]$, given by (4.14). 73

4.10 Scaling of relative quantum-classical differences (4.15 in the equilibrum time-domain versus increasing system size. Scatter of crosses corresponds to time-steps $191 \leq n \leq 200$, for a state launched in the chaotic zone of the mixed regime ($\gamma = 1.215$). Scatter of plus signs corresponds to time-steps $41 \leq n \leq 50$, for a state launched in the global chaos regime. Data sets in both of these regimes are consistent with the scaling law $R \simeq {N_l}^{-1/2}$, where $N_l = 2l + 1$. . 76

4.11 Same as Fig. 4.10 but using $R[J_z]$, as given by (4.16). Data sets in both types of chaotic regime are consistent with the scaling law $R \simeq {N_j}^{-1/2}$, where $N_j = 2(l + s) + 1$. 77

5.1 The time-development of the Ehrefest differences for L_z for classical parameters $\gamma = 2.835$, $r = 1.1$ and $a = 5$ for which the phase space is predominantly chaotic. Open circles correspond to quantum numbers $(s, l) = (20, 22)$ and filled circle correspond to $(s, l) = (200, 220)$. In both cases the approximately exponential growth of the Ehrenfest differences persists until saturation at the system size $|\mathbf{L}|$, indicated by horizontal lines. 91

5.2 The time-development of the differences between the classical constant of the motion $\mathbf{L}^2 = l^2$ and the quantum prediction for $\langle L \rangle^2$ for the same classical parameters as in Fig. 5.1. The data are compared to an exponential growth rate given by twice the classical Lyapunov exponent, $\lambda_L = 0.45$. Open circles correspond to quantum numbers $(s, l) = (20, 22)$ and filled circle correspond to $(s, l) = (200, 220)$. In both cases the exponential growth of the Ehrenfest differences persists until saturation at the maximum possible value $\mathbf{L}^2$, indicated by horizontal lines. 92

5.3 The break time obtained by the condition (5.32), using a threshold $f\mathbf{L}^2 = 0.25\mathbf{L}^2$, plotted against quantum number l ranging from 11 to 220. The data are obtained using the same classical parameters as in Fig. 5.2 and initial condition $\vec{\theta} = 20^o, 40^o, 160^o, 130^o)$. The solid line corresponds to Eq. 5.33 with exponent $\lambda = 0.51$ obtained by a least-squares fit. The dotted line corresponds to Eq. 5.33 using the largest Lyapunov exponent $\lambda_L = 0.45$. . . 94

Chapter 1

Introduction

Though it is widely accepted that classical mechanics should emerge from quantum theory in an appropriate limit, this "correspondence principle" meets with severe difficulties when the classical dynamics exhibit chaos. Research into the physical conditions required for the emergence of classical chaos from the underlying quantum description has become a topic of active investigation, and has led to a number of differing perspectives.

Ford and coworkers [42, 43, 44] have considered the criterion of *algorithmic complexity*, which has led them to the conclusion that classical chaos can not emerge from quantum theory in the macroscopic limit, and, therefore, that quantum-classical correspondence must break down for chaotic motion. While Zurek and Paz [96, 97] and others [62, 56, 99] agree that a breakdown of correspondence does arise, they have argued that the required correspondence is restored when the effect of a weak-coupling to an environment, a process sometimes called *decoherence* [61, 50], is taken into account. Alternatively, Ballentine [8], Takahashi [91], and Casati and Chirikov [23] have emphasized that correspondence should emerge in the macroscopic limit given an appropriate degree of coarse-graining which may be considered to represent the finite resolution of macroscopic measurements. The variety of perspectives on this issue is due in part to differing views on which observable properties must be taken into consideration in order to demonstrate a formal correspondence in the macroscopic limit [7, 8, 11, 56].

The details of the quantum-classical transition and the quantum manifestations of classical chaos are of considerable interest also for the accurate and practical description of mesoscopic systems. The onset of widespread chaos in the *classical* Hamiltonian model

of the highly excited states of hydrogen has been shown to accurately predict the unexpected onset of ionization observed in these states under increasing microwave fields [14, 64]. In the classical model, the microwave field itself provides the non-integrable perturbation to the otherwise integrable classical dynamics. Under strong magnetic fields, the energy level statistics of these Rydberg atoms exhibit the characterisitic distribution of spacings predicted from random matrix theory precisely when the classical model exhibits chaotic behaviour [60].

A better understanding of the quantum-classical transition is required also for practical computation in the mesoscopic regime. On the one hand, the *exact* theoretical description of even simple microscopic and mesoscopic systems in quantum theory demands computational resources (specifically, *classical* computational resources!) that increase as a power of the quantum numbers and exponentially with the number of interacting subsystems. On the other hand, the semiclassical techniques developed by Gutzwiller [53] and others become computationally impractical due to the proliferation of (unstable) periodic orbits in the case of chaotic motion. Moreover, the accuracy of the semiclassical approximation is not well understood in either the time-domain [92] or the energy domain [21], and remains a topic of active investigation. The results in this thesis suggest that purely classical techniques may be applied to accurately describe the time-domain behaviour of chaotic systems even in the case of surprisingly small quantum numbers.

The theoretical identification of the characteristic properties of quantum systems with chaotic classical counterparts has been an interesting and illuminating topic of research in its own right. This nascent area of research, sometimes called "quantum chaos," is not a unified field but encompasses a wide variety of approaches. In analogy with the manner in which classical chaos came to be understood, much of the theoretical progress in quantum chaos has proceeded through the study of idealized model systems, usually taking the form of stroboscopic mappings. Some of this research will be reviewed further below. I should also mention here that, whereas a fairly complete understanding of the microscopic underpinnings of irreversible thermodynamics has recently emerged from the perspective of classical dynamical systems theory [49, 30], very little is known about how these characteristic properties emerge from the more fundamental quantum mechanical treatment of these models. The results presented in this thesis will clarify how these statistical properties emerge from the underlying quantum dynamics specifically when the classical model exhibits chaotic behaviour.

Certainly the most intellectually intriguing aspect of this research pertains to the possibility of demonstrating that *experimentally distinct* predictions result from two very different interpretations of the quantum state. This pedagogical issue is tied to the following practical question about quantum-classical correspondence: which classical theory of mechanics actually emerges from the quantum description of macroscopic systems? One alternative is Hamilton's equations of motion (Newton's laws); another is the classical Liouville equation that describes the dynamics of probability densities with non-vanishing support. The former describes the exact, deterministic evolution of single macroscopic systems, whereas the latter provides only probabilistic predictions for ensembles of similarly prepared systems.

The central focus of the work in this thesis is to demonstrate that, for the chaotic motion of some macroscopic systems, standard quantum mechanics may be unable to reproduce Newton's laws of motion over experimentally relevant time-scales. Moreover, contrary to the conclusion of a recent argument by Zurek [99], I will provide evidence that this specific *breakdown* of quantum-classical correspondence is not circumvented by taking into account the decoherence effects of a stochastic environment. This striking conclusion does not imply a failure of the correspondence principle, however, since the statistical predictions of Liouville mechanics are shown to be compatible with the predictions of quantum theory for such systems. The decisive implications of this scenario for the interpretation of the correspondence principle, as well as the interpretation of quantum theory itself, will be drawn out and related to some of the historical debate on this topic.

In the remainder of this Introduction I will review the relevant literature on quantum chaos and quantum-classical correspondence, before undertaking, in the body of this thesis, a detailed comparison of the quantum and classical dynamics of a non-integrable model system comprised of two coupled spins. The perspective developed from the results of this analysis will generalize and extend much of the earlier work on the dynamical properties of quantum chaos and quantum-classical correspondence that has been developed through the study of different model systems.

1.1 Classical Trajectories and Quantum Expectation Values

A convenient starting point for this subject follows from considering an old theorem due to Ehrenfest [33] and the oft-repeated correspondence argument that derives from it [65, 88, 67, 68]. For a simple Hamiltonian system of the form $H = p^2/2m + V(q)$, the time-dependence

of the expectation values $\langle q(t)\rangle = \langle\psi(t)|q|\psi(t)\rangle$ and $\langle p(t)\rangle = \langle\psi(t)|p|\psi(t)\rangle$, in an arbitrary quantum state $\psi(t)$, is prescribed by the differential equations,

$$\begin{aligned} \frac{d\langle q(t)\rangle}{dt} &= \frac{\langle p(t)\rangle}{m} \\ \frac{d\langle p(t)\rangle}{dt} &= \langle F(q)\rangle. \end{aligned} \tag{1.1}$$

These equations do not form a closed set since the time-dependence of the force function,

$$\langle F(q)\rangle = \langle\psi(t)|F(q)|\psi(t)\rangle \neq F(\langle q\rangle) \tag{1.2}$$

has not been specified. However, if the operator $F(q) = dV/dq$ can be expanded in a Taylor series about the position centroid of the quantum state, $\langle q(t)\rangle$, then,

$$\langle F(q)\rangle = F(\langle q\rangle) + \frac{(\Delta q)^2}{2}\left.\frac{d^2F}{dq^2}\right|_{q=\langle q\rangle} + \ldots \tag{1.3}$$

where $(\Delta q)^2 = \langle q^2\rangle - \langle q\rangle^2$ is the state variance. When the quadratic and higher-order terms of this expansion are negligible, the system of differential equations (1.1) becomes closed and the expectation values of the dynamical variables reduce to Hamilton's canonical equations of motion,

$$\begin{aligned} \frac{dq_c(t)}{dt} &= \frac{p_c(t)}{m} \\ \frac{dp_c(t)}{dt} &= \{H, p_c\} = F(q_c), \end{aligned} \tag{1.4}$$

In the above, $\{\cdot,\cdot\}$ is a Poisson bracket and $q_c(t)$ and $p_c(t)$ are classical dynamical variables.

At this point it is natural to ask: under what conditions may we expect this approximation to apply? Clearly, if the potential $V(q)$ is either linear or quadratic in q, as for a harmonic oscillator, then the quantum equations are identical to the classical ones. More generally, this correspondence follows provided the state variance is narrow compared to significant non-linear variation in the prescribed force,

$$(\Delta q)^2 \ll L^2 \sim \frac{F(\langle q\rangle)}{\left.\frac{d^2F}{dq^2}\right|_{q=\langle q\rangle}}, \tag{1.5}$$

and higher-order contributions to the expansion (1.3) are also negligible. The dynamical regime in which (1.5) holds is sometimes called the *Ehrenfest* regime [7, 11, 35].

A common textbook argument [65, 67, 68] maintains that the approximation (1.5) should be valid, quite generally, for *macroscopic* systems. This arguments holds that, for a macroscopic body, the width of a well-localised state may be extremely narrow compared to characteristic variation in the macroscopic potential (or some other relevant system dimension). Consequently, the approximation,

$$\langle F(q)\rangle = F(\langle q\rangle), \tag{1.6}$$

should hold for a generic macroscopic system described by such a localised state. The important conclusion is that the differential equations governing the time-evolution of the expectation values (1.1) then accurately approximate Hamilton's equations of motion (1.4). Provided it is possible to match the classical initial conditions, quantum theory can then describe the *deterministic* motion of a single macroscopic body by *associating* expectation values with the classical dynamical variables. The requirement on the initial conditions is simply that the quantum centroids must be set equal to the initial phase space coordinates of the classical trajectory; that is, $\langle q(0)\rangle = q_c(0)$ and $\langle p(0)\rangle = p_c(0)$.

These observations may be taken as means of justifying the "correspondence principle", that is, the view that the predictions of quantum mechanics must coincide with those of classical mechanics in cases where the latter is known to be valid [68, 67]. In the present context, "classical mechanics" is taken to refer specifically to Hamilton's equations of motion. I will call this interpretation of the correspondence principle the *Ehrenfest* correspondence principle. This conjecture may be stated heuristically as,

$$\left.\begin{array}{l} |\langle q\rangle - q_c| \to 0, \\ |\langle p\rangle - p_c| \to 0, \end{array}\right\} \quad \text{for} \quad \frac{\mathcal{J}}{\hbar} \to \infty, \tag{1.7}$$

where $\mathcal{J}$ is a characteristic action and $\hbar$ is Planck's constant. I will provide a more useful statement of this conjecture in Chapter 5.

Of course, the ratio $\mathcal{J}/\hbar$ is actually finite for real physical systems. Moreover, initially localised quantum states will generally diffuse with time, and the accuracy of the approximation (1.6) eventually breaks down. Therefore, to confirm the validity of the conjecture (1.7) as a principle of correspondence, it is important to determine the time-scale on which significant deviations between the quantum and classical predictions arise. Let $\mathbf{x}_c$ denote the generalised classical coordinates, *e.g.* $\mathbf{x}_c = (q_c, p_c)$, and $\langle \mathbf{x}\rangle$ denote the corresponding quantum expectation values. Then, the magnitude of their difference

$$\epsilon(t) = |\langle \mathbf{x}\rangle - \mathbf{x}_c| \tag{1.8}$$

is a time-dependent measure of the degree of correspondence. Given some criterion defining *adequate* correspondence, *i.e.*, a threshold χ, one may define [25, 57] a time-scale t_{Ehr} over which Ehrenfest correspondence holds from the condition,

$$\epsilon(t) \leq \chi \quad \text{for} \quad t < t_{Ehr}. \tag{1.9}$$

This threshold-dependent condition delineates the Ehrenfest regime more precisely than the approximation (1.5). This condition differs slightly from the "narrow state" condition (1.5), though both definitions will coincide, approximately, as a result of Eqs. (1.3) and (1.1), if the tolerance threshold χ for the position is set at the characteristic system size, L, given by the RHS of (1.5) and the explicit degree of correspondence for the momentum is ignored.

The time-scale of Ehrenfest correspondence will generally depend on the details of the potential and other system parameters, but it is worthwhile to get some sense of the duration of this regime by considering the simplest case of a free-particle. For a particle of mass m, starting from a Gaussian state with initial standard deviation $\Delta q(0) = a_o$ and momentum $\hbar k_o$, the time-dependent probability distribution is given by,

$$P(q,t) = |\psi(q,t)|^2 = \frac{1}{a\sqrt{2\pi}(1+t^2/\tau^2)^{1/2}} \exp\left[-\frac{(q-(\hbar k_o t/m)^2}{2a_o^2(1+t^2/\tau^2)}\right]. \tag{1.10}$$

The width Δq of this Gaussian doubles on the time-scale $\tau = 2ma_o^2/\hbar$. The time it takes this width to grow to a size $\Delta q >> a_o$ is given by

$$t \sim \frac{\Delta q \; a_o \; m}{\hbar}. \tag{1.11}$$

Therefore, in the case of a quantum state describing a macroscopic object, such as a baseball, initially localised to within 1 Angstrom, the time it takes this state to diffuse to a width of 1 cm is of order 10^{14} years [33, 65]. This is much longer than the estimated lifetime of the universe!

Thus it appears plausible to conclude that quantum expectation values can adequately describe the deterministic motion of individual macroscopic objects over time-scales much longer than the duration of any conceivable experiment. In the following section I will explain how the presence of chaos in the classical dynamics challenges this simple picture, as well as the adequacy of the conjecture (1.7) as a principle of quantum-classical correspondence.

1.2 Classical Chaos and Quantum Chaos

The task of identifying criteria for chaos in quantum mechanics in a manner that extends or generalizes the criteria for chaos in classical mechanics meets with several immediate difficulties. Classical chaos is characterized by "extreme sensitivity to initial conditions." This property is normally identified with an exponential divergence, on average, in the separation between initially nearby classical trajectories. The rate of this divergence is characterized by a set of exponents, called Lyapunov exponents. In the simplest case of a mapping, $\mathbf{x}(n+1) = \mathbf{F}(\mathbf{x}(n))$, the largest such exponent, λ_L, may be defined in the following way. Let $\mathbf{d}(n) = \mathbf{x}_a(n) - \mathbf{x}_b(n)$ designate the difference between the phase space coordinates, $\mathbf{x}_a$ and $\mathbf{x}_b$, of two nearby classical trajectories. For small enough $|\mathbf{d}|$, the growth of this difference vector is governed by the tangent matrix,

$$M_{ij}(x) = \left.\frac{\partial F_i(\mathbf{x})}{\partial x_j}\right|_{x(n)}. \tag{1.12}$$

The eigenvalues of this matrix characterize the local stability of the mapping about the trajectory $\mathbf{x}(n)$ [66, 2]. (If the mapping describes a Hamiltonian system, then these eigenvalues must sum to zero.) In particular, the Lyapunov exponents are obtained from the geometric mean of these matrices evaluated along some reference trajectory. The largest of these exponents may be defined from the double limit [90],

$$\lambda_L = \lim_{n\to\infty} \lim_{|\mathbf{d}(0)|\to 0} \frac{1}{n} \ln \frac{|\mathbf{d}(n)|}{|\mathbf{d}(0)|}. \tag{1.13}$$

A more general definition (one that may be applied for practical computation) is provided in Chapter 2.

However, there is no definite concept of "trajectory" in quantum theory. Each quantum state, if pure, is specified by a vector in Hilbert space, and not a point in phase space. Moreover, the time-dependent Schrodinger equation is linear (more generally, the quantum time-development is given by a unitary transformation), whereas classical chaos requires a nonlinear tranformation of the coordinates. For bounded systems, the eigenvalue spectrum is discrete, and the quantum dynamics are at most quasi-periodic.

The significance of these differences may be illustrated by considering some measure of proximity that applies to quantum states, and then determining how this measure evolves in time. One definition of proximity that may be constructed in Hilbert space is the degree of overlap between two quantum states, $|\langle\psi|\phi\rangle|$. Nearby states are then those that the

satisfy, $|\langle\psi|\phi\rangle| = 1 - \delta$ with $\delta \ll 1$. However, this scalar quantity is invariant under unitary time-evolution,

$$|\langle\psi(t)|\phi(t)\rangle| = |\langle\psi(0)|\, U^{-1}(t)\, U(t)\, |\phi(0)\rangle| = |\langle\psi(0)|\phi(0)\rangle|. \tag{1.14}$$

Therefore, *any* two quantum states do not separate at all with time, for any system!

This attempt at characterizing chaos in quantum mechanics, though unsuccessful, draws attention to two of the central questions that have motivated research in the field of "quantum chaos." The first of these pertains to identifying signatures of chaos that arise in quantum mechanics: which criteria, if any, distinguish chaotic systems from regular ones in quantum theory? The second pertains to quantum-classical correspondence: how does classical chaos emerge from the underlying quantum description in the macroscopic limit? In particular, how can quantum theory reproduce the exponential divergence exhibited by the classical *trajectories*?

Much of the work that attempts to identify manifestations of chaos in quantum theory has been obtained from numerical computation of the properties of specific Hamiltonian models. These results have suggested a few, possibly universal, signatures of chaos in quantum systems. Before proceeding to introduce some of these approaches, it is important to clarify that there is currently no *definitive* criterion for chaos in quantum theory. Consequently, in this thesis, when the term "chaotic" is invoked to describe a quantum system, this should be understood as a shorthand expression denoting that the classical counterpart to the quantum system exhibits chaotic behaviour.

Perhaps the most well-known signature of "quantum chaos" arises in the distribution of spacings between consecutive energy eigenvalues. Quantum systems with chaotic classical counterparts exhibit the same characteristic distributions for these spacings as those of a random matrix with the same symmetry properties as the Hamiltonian. These distributions exhibit *level repulsion* relative to their integrable counterparts: small spacings are suppressed (leading to "avoided crossings") and most spacings are clustered about an average value [55]. This signature exhibited in the eigenvalue spectrum has no obvious classical analogue.

Although there is no sensitivity to changes in the initial conditions in quantum mechanics (given the same unitary evolution for both initial conditions), the presence of classical chaos is evident in the quantum state's sensitivity to small perturbations in the Hamiltonian. This distinctive feature of the chaotic quantum dynamics has been demonstrated in several model systems, although the perturbations have been applied using very different techniques

[74, 75, 83, 84, 85, 10]. The basic idea is to evolve a given initial state, $|\psi(0)\rangle$, according to a unitary transformation, $|\psi(t)\rangle = U|\psi(0)\rangle$, where $U = \exp(-iHt/\hbar)$ for some Hamiltonian H, and then examine the overlap, $|\langle\psi'(t)|\psi(t)\rangle|$, defined between this final state with another *perturbed* final state, $|\psi'(t)\rangle = U'|\psi(0)\rangle$. Here U' may differ from U according to some small perturbation in the Hamiltonian, or by some small coordinate transformation applied at the end of the unpertubed evolution [10]. If the classical Hamiltonian is chaotic, then the overlap decreases much more rapidly, and to a lower mean asymptotic value, than if the classical Hamiltonian is regular [75]. As noted by several authors [82, 10], this sensitivity criterion arises also in the case of a classical density that is evolved according to the Liouville equation. As will be demonstrated further below, much can be learned about quantum mechanics, and quantum chaos, from the connection between quantum mechanics and the classical Liouville equation.

1.3 Chaos and Ehrenfest Correspondence

Several authors have addressed the question of quantum-classical correspondence for chaotic systems by comparing the dynamical behaviour of the quantum expectation values with that of the classical dynamical variables satisfying Hamilton's equations of motion [15, 48, 54]. This approach is clearly motivated by the Ehrenfest correspondence conjecture explained in the previous section (1.7). On this view, the quantum dynamics may be identified as chaotic provided the quantum expectation values approximately follow a chaotic classical trajectory. If nearby classical trajectories are diverging, on average, exponentially, then the quantum expectation values will exhibit a similar exponential divergence, at least while the quantum state remains well-localised, that is, in the initial Ehrenfest regime, $t < t_{Ehr}$.

Accordingly, one of the main interests has been to determine how the correspondence time, t_{Ehr}, increases with increasing system size. In the literature this limit is often denoted using the short-hand expression "$\hbar \to 0$", where in this context $\hbar$ always denotes the dimensionless ratio $(\hbar/\mathcal{J})$, and the magnitude of $\mathcal{J}$ is given by the quantum numbers or some combination of the system parameters. It is also useful to note that $(\hbar/\mathcal{J})$ does not actually denote a mathematical limit in quantum theory, but refers to a sequence of quantum models with increasing values of the ratio $(\mathcal{J}/\hbar)$, but with other parameters adjusted so that each quantum model is associated with the same classical model.

Haake *et al.* have stuided this time-scale in the special case of a simple non-autonomous

spin model which they call the kicked top [54]. The length of the spin is conserved, so the quantum number j is a measure of the system dimension $j\hbar \sim \mathcal{J}$. For initial SU(2) coherent states, they obtain an approximate mapping relation for the *expectation values* of the angular momentum components, $\langle J_k \rangle$, that consists of the corresponding classical mapping modifed by correction terms in powers of $(1/j)$. They are able to relate the growth of the first-order corrections to the tangent matrix of the classical mapping. The eigenvalues of this matrix govern the local stability of the classical motion. For mappings, the definition of the Lyapunov exponent is obtained from the geometric mean of these matrices evaluated along the classical trajectory (see Chapter 2). If the classical motion is regular, then the perturbation should grow, at most, as some power of the time. Consequently, for large j, significant deviations from the classical map occur on a very late time-scale,

$$t \sim (\frac{\mathcal{J}}{\hbar})^{1/\alpha}, \tag{1.15}$$

where $\alpha \simeq 1$. This scaling is consistent with the example of the baseball considered above. On the other hand, if the classical mapping is chaotic, then the first-order quantum corrections terms should grow, on average, exponentially with time. For chaotic dynamics, the quantum mapping therefore deviates from the classical one on the time-scale,

$$t \sim \lambda_L^{-1} \ln(\mathcal{J}/\hbar). \tag{1.16}$$

The above correspondence scaling results for regular (1.15) and chaotic (1.16) motion are consistent with estimates derived by other authors in several different model systems [15, 16, 95, 24, 48], though under a variety of different approximation techniques. In Chapter 5, I will provide a simpler and much more general argument than the one outlined above, which demonstrates that Eqs. (1.15) and (1.16) should hold (for regular and chaotic systems respectively) in the general case of a system of particles interacting only through position dependent potentials.

There are a few features of the above break-time rules that are worth stressing immediately. First, Eqs. (1.15) and (1.16) apply specifically in the case of initial minimum uncertainty states, and in this sense they *maximize* the time-scale of correspondence. Second, these scaling results are guaranteed to apply only when considering the onset of very small differences, since the exponential growth of the differences is derived on the basis of the local stability of the classical flow. The scaling for large differences, that is, differences given by a significant fraction of the system dimension, is left undetermined. Finally, under

the restrictive conditions noted just above, these expressions may be taken as an estimate of how the Ehrenfest break-time, defined by (1.9), scales with increasing system size for chaotic systems. This follows from the fact that the coordinate centroids of the quantum states are associated with the phase space coordinates of a classical trajectory. Consequently, although the time-scale (1.16) is usually called simply the "break-time" of quantum-classical correspondence for a chaotic system, in this thesis I will refer to this result more specifically as the *Ehrenfest* break-time, for reasons that will become clear shortly. As a result of the time-scale (1.16), several authors have argued that deterministic chaos can exist only as a transient phenomena in quantum mechanics [22, 25].

Another distinct feature of quantum chaos was first identified by Fox and coworkers in numerical studies of the kicked top and the kicked rotor (which they call the kicked pendululm) [47, 46]. These authors showed that, when the classical dynamics are chaotic, the widths of initially localised quantum states grow exponentially with time, until saturation at the system size. Specifically, their numerical studies showed that,

$$\Delta q(t) \simeq \Delta q(0) \exp \lambda_w t, \tag{1.17}$$

where $\Delta q^2 = \langle q^2 \rangle - \langle q \rangle^2$ is the variance of the quantum state and λ_w is a characteristic exponent of order the largest Lyapunov exponent.

A separate, though equally important, contribution of their work was to recognize that the exponential spreading of the quantum state mimicks that of a classical distribution of trajectories concentrated around the initial quantum centroids. More precisely, they constructed initial classical densities which matched the moments of the Husimi phase space functions for the initial coherent states [46]. This close correspondence in the growth rates of quantum states and classical densities has been characterized more carefully in recent work by Ballentine and McRae [11, 12], who have studied this problem in the Henon-Heiles model. The exponential growth of quantum and classical variances is demonstrated also for the chaotic states of the coupled spin model examined in this thesis (see Chapter 3).

This exponential spreading of quantum states is closely related to the earlier estimate (1.16) that Ehrenfest correspondence is governed by a $\log(\mathcal{J}/\hbar)$ break-time. As noted above, the width of the quantum state gives rise to the first correction term in the expansion (1.3), and the precision of the correspondence between the quantum expectation values and the classical trajectory is limited by the magnitude of this correction term. In particular, for an initial minimum-uncertainty state, $\Delta q(0) \simeq \hbar/\Delta p(0)$, the time at which the width in

position space has grown sufficiently large that (1.5) no longer holds is obtained by setting the RHS of (1.17) equal to the RHS of (1.5) and solving for the Ehrenfest break-time. This gives,

$$t \sim \lambda_w^{-1} \ln(\frac{L\Delta p(0)}{\hbar}), \tag{1.18}$$

where L is a characteristic length defined *relative* to the system size. The magnitude L may be interpreted as a threshold indicating a "break" between the quantum and classical predictions. It is important to stress that the validity of (1.18) is based on a numerical result (1.17), rather than derived, but is more general than the earlier estimate of the break-time scaling (1.16), since the derivation of Eq. (1.16) applied strictly in the limit of vanishingly small differences. As noted earlier, the results of Fox *et al.* indicate that this exponential growth persists until the state width reaches the system size; therefore the scaling rule (1.18) remains valid even for estimating the onset of very large quantum-classical differences.

Clearly, for a macroscopic system, the ratio $\mathcal{J}/\hbar$ is astronomically large. The incredibly large magnitude of this ratio is a crucial ingredient in Ehrenfest's approach to extracting Newton's Laws from quantum mechanics [33]. However, Zurek and Paz [97] have observed that a $\log(\mathcal{J}/\hbar)$ time-scale may be short even for systems of macroscopic dimension, *i.e.*, systems with $\mathcal{J}/\hbar >> 1$. Specifically, they have estimated that the time-scale $t \simeq \lambda_L^{-1} \ln(\mathcal{J}/\hbar)$ is comparable to experimentally relevant time-scales in the case of Hyperion, one of the moons of Saturn, which is known to exhibit a chaotic tumble [94, 20]. Therefore the Ehrenfest correspondence principle is at risk of *breaking down* in the case of chaotic motion. I will examine this possibility in detail in Chapter 5, and conclude that such a breakdown actually may be subject to experimental confirmation! First, however, in view of the far-reaching implications of this result, it is worthwhile to reconsider the assumptions about quantum-classical correspondence that are reflected in the Ehrenfest correspondence principle and explore more carefully the alternatives to this correspondence conjecture.

1.4 Quantum Correspondence with Liouville Mechanics

In the preceding discussion I have drawn attention to some similarities between the properties of a time-evolved quantum state and those of a corresponding ensemble of classical trajectories. The general description of the time-evolution of this ensemble is prescribed by the classical Liouville equation. This connection may provide further insight into the problem of identifying the distinctive features of the quantum dynamics that arise under

conditions of chaos in the classical Hamiltonian dynamics. Moreover, in view of the practical and conceptual difficulties that challenge the validity of the Ehrenfest correspondence conjecture (that is, the view that the predictions of quantum mechanics coincide with Newton's laws for macroscpic objects), it is important to determine whether the correspondence between quantum mechanics and classical Liouville mechanics is constrained by similar difficulties in the case of chaotic dynamics.

A useful starting point for investigating the correspondence between these two theories starts with a description of the classical Liouville equation. Since one typically does not have *exact* knowledge of the initial coordinates that describe a physical system, Liouville was interested in describing how this cloud, or ensemble, of *possible* initial coordinates evolves in time. The time-dependence is given by the following partial differential equation [51],

$$\frac{\partial \rho(\mathbf{x}, t)}{\partial t} = \{\rho(\mathbf{x}), H(\mathbf{x})\} \tag{1.19}$$

where $\rho(\mathbf{x}, t)$ is a non-negative distribution function (a probability density), $\mathbf{x}$ are the phase space coordinates, and the symbols $\{\cdot, \cdot\}$ denote the Poisson bracket. A unique solution to the time-dependence requires the specification of an initial boundary condition for the density, *i.e.*, some initial state $\rho(q, p, 0)$. A classical dynamical system is also associated with an invariant (Liouville) measure $\mu(\mathbf{x})$ on the phase space manifold $\mathcal{P}$. Then, at each point in time, one can calculate the ensemble average for an observable $A(\mathbf{x})$ from the prescription,

$$\langle A(\mathbf{x}) \rangle_c = \int_{\mathcal{P}} d\mu(\mathbf{x})\ \rho_c(\mathbf{x})\ A(\mathbf{x}). \tag{1.20}$$

Ballentine *et al.* [7] have shown that, in the generic case of Hamiltonians of the form, $H = p^2/2m + V(q)$, the time-dependence of the classical ensemble averages exhibit a striking similarity to the quantum ones. The Liouville description even includes some of the ostensibly "quantum" corrections to the classical canonical equations of motion. From (1.19) and (1.20) and integrating by parts, one gets,

$$\begin{aligned} \frac{d\langle q \rangle_c}{dt} &= \frac{\langle p \rangle_c}{m} \\ \frac{d\langle p \rangle_c}{dt} &= \langle F(q) \rangle_c. \end{aligned} \tag{1.21}$$

As before, it is useful to expand the force function about the position centroid (of the classical state), which gives,

$$\frac{d\langle q \rangle_c}{dt} = \frac{\langle p \rangle_c}{m}$$

$$\frac{d\langle p\rangle_c}{dt} = F(\langle q\rangle_c) + \frac{\Delta q_c^2}{2}\left.\frac{d^2F(q)}{dq^2}\right|_{q=\langle q\rangle_c} + \dots \tag{1.22}$$

where $\Delta q_c^2 = \langle q^2\rangle_c - \langle q\rangle_c^2$. As noted above for the time-development of the quantum expectation values (1.1), the classical ensmble averages also exibit a first-order "correction" term which is proportional to the state variance and which will lead to deviations from the canonical equations of motion (1.4).

Of course, the quantum and classical Liouville theories do not provide identical theoretical descriptions of the same physical system. There are two independent sources of discrepency: dynamical differences and differences in the initial conditions. The dynamical differences become apparent only when the time-development of the higher-order moments (that is, the additional terms in the expansion (1.3)) are calculated explicitly. These calculations are carried out most easily in the Wigner-Weyl representation of quantum mechanics [93]. The relevent features of this representation are introduced in Appendix B.

The time-dependence of the Wigner quasi-distribution $\rho_W(q,p)$ can be expressed as [71],

$$\frac{d\rho_w(q,p,t)}{dt} = \{H,\rho_w\} + \sum_{n=1}^{\infty}\left(\frac{\hbar}{2}\right)^{2n}\frac{(-1)^n}{(2n+1)!}\frac{\partial^{2n+1}\rho_w}{\partial p^{2n+1}}\frac{\partial^{2n+1}H}{\partial q^{2n+1}} \tag{1.23}$$

where $\{\cdot,\cdot\}$ denotes the classical Poisson bracket. As explained in Appendix B, although the "Moyal terms" contain an explicit proportionality to powers of $\hbar$, these terms are not guaranteed to become vanishingly small in the limit "$\hbar \to 0$" since the momentum derivatives will generally produce factors proportional to $(q/\hbar)$.

The Wigner quasi-distribution is not a unique quantum phase space distribution, and more importantly, may take on negative values. Consequently, it may not be interpreted as a probability density and does not have direct experimental significance. The origin of the dynamical differences between the quantum and classical theories is clearer if we consider differences arising explicitly at the level of observable quantities. As shown in Appendix B, for a general time-independent Weyl-ordered operator, $A(q,p)$, the time-development of the corresponding quantum expectation value $\langle A(q,p)\rangle$, is given by,

$$\frac{d\langle A_w(q,p)\rangle}{dt} = \{H_w,A_w\} + \sum_{n=1}^{\infty}\left(\frac{\hbar}{2}\right)^{2n}\frac{(-1)^{n+1}}{(2n+1)!}\frac{\partial^{2n+1}A}{\partial p^{2n+1}}\frac{\partial^{2n+1}H}{\partial q^{2n+1}}. \tag{1.24}$$

The Moyal corrections to the dynamics for Liouville averages do not arise *explicitly* unless the operator $A(q,p)$ contains at least a cubic power of the momentum. Differences arise *implicitly*, however, even for the low-order moments, since the time-development of the

low-order moments will eventually become sensitive to the Moyal corrections through their dependence on the time-development of the higher moments. The quantum and Liouville time-evolution equations evidently exhibit a much greater degree of similarity than that observed between the quantum equations and Hamilton's equations of motion.

Similary, the Liouville picture provides a much more versatile framework for matching the details of the initial quantum state. Using a Liouville density with non-vanishing support, it is possible to match not only the initial quantum expectation values (associated with the classical dynamical variables), but also the higher-order quantum moments. The "best-case" scenario arises for the coherent states, which are minimum uncertainty states, $\Delta q \Delta p = \hbar/2$. These states are the unique quantum states that are associated with non-negative Wigner functions. Consequently all of the quantum moments (given by Hermitian Weyl-ordered operators) can be matched exactly by those of a classical density. The appropriate classical density is a Gaussian with support concentrated over an area $\Delta q_c \Delta p_c \simeq \hbar$, as expected from the uncertainty principle. Perhaps not surprisingly, this matching may not be carried out to arbitrary precision for a general quantum state. An intuitive way of understanding this is to note that the Wigner quasi-distribution will generally take on negative values, and therefore some of the quantum moments will take on numerical values that cannot be reproduced by a non-negative Liouville density.

These formal observations motivate an alternative interpretation of the requirements of the correspondence principle. This interpretation consists of the conjecture that the the predictions of quantum mechanics should coincide with those of classical Liouville mechanics when the predictions of the latter are experimentally valid. It will sometimes be convenient to refer to this conjecture as the *Liouville* correspondence principle. This is a weaker conjecture than the Ehrenfest correspondence principle, which was stated in the discussion preceding the heuristic formula (1.7).

Ballentine and coworkers have studied the details of this quantum-Liouville correspondence for a few non-integrable systems. Ballentine, Yang, and Zibin [7] compared quantum expectation values and classical ensemble averages for the low-order moments, *e.g.* the dynamical variables and their variances, primarily at early times, that is, in the initial Ehrenfest regime of a few low-dimensional model systems. For fixed system size, the correspondence with Liouville mechanics was shown to be much more accurate, and to last much longer, than the correspondence with a single classical trajectory. They demonstrated a remarkable degree of improved correspondence under conditions of classical chaos.

Ballentine and McRae [11] and Ballentine [12] examined the degree of Liouville correspondence for the Henon-Heiles model. They demonstrated that both the quantum and classical variances grow at an approximately exponential rate, a result obtained previously by Fox and coworkers for different model systems [47, 46]. They also characterised the dynamical behaviour of the quantum-Liouville differences for the dynamical variables and their variances. They determined that, for states initiated from a chaotic region, the quantum-Liouville differences grow exponentially, in the initial Ehrefenst regime, with a characteristic exponent that is larger than the largest Lyapunov exponent.

The duration of the correspondence between quantum mechanics and Liouville mechanics has been considered by Zurek and Paz [96, 98] in the "optimal" case of minimum uncertainty states. Using very general arguments about the nature of the chaotic classical dynamics and the growth of the Moyal corrections in Eq. (1.23), they have estimated that the quantum-Liouville differences should be governed by a break time that scales as,

$$t_b \simeq \frac{1}{\lambda_L} \ln(L\ \Delta p(0)/\hbar) \tag{1.25}$$

where L and $\Delta p(0)$ are defined as in Eqs. (1.5) and (1.18). Casati and Chirikov [23] have argued that (1.25) is not a distinct result, but is essentially the same as the (Ehrenfest) break-time, given by (1.16), that was first developed in Refs. [15, 24]. Although the estimates (1.25) and (1.16) bear a formal similarity, this Introduction makes clear that they are based on distinct correspondence criteria. (The conditions for Liouville and Ehrenfest correspondence are often not clearly distinguished in the literature.)

However, the formal similarity between t_b and t_{Ehr} suggests that the Liouville correspondence principle may also be at risk of breaking down in the case of chaotic macroscopic motion, for systems such as Hyperion, since the break-time scaling exhibited by Eq. (1.25) suggests the possibility of observable quantum-classical differences on an experimentally accessible time-scale [97]. While Zurek has raised the possibility of a *breakdown* of the correspondence principle [99] in this context, he has also suggested that this breakdown is not actually observed because of the "decoherence" effects that result from weak coupling to the ubiquitous environment.

Habib *et al.* [56] have considered the effects of decoherence on the degree of Liouville correspondence at the level of expectation values for low-order moments and also by comparing Wigner quasi-distributions directly with the classical density in study of the Henon-Heiles model. They demonstrated that the degree of correspondence (for fixed $\hbar/\mathcal{J}$) improved

when the effects of a stochastic enviroment (or "decoherence") are taken into account. The positive effects of decoherence on the degree of quantum-Liouville correspondence have been demonstrated in several recent theoretical studies of classically chaotic models [62, 58, 18, 52]. In the case of the kicked rotor model, a suppression of quantum localisation due to environmental noise has been demonstrated *experimentally* in a simulation of the model using trapped cesium atoms subjected to a pulsed laser beam [1]. The "environment" in this case consists of spontaneous emission due to the "vacuum fluctuations." However, Farini *et al.* [37] have shown that the magnitude of the Moyal terms in Eq. (1.23) can remain small even for an isolated system, and therefore the effects of decoherence may not be necessary to recover classical properties.

The scaling of the Liouville break-time estimate (1.25) has been examined by Roncaglia *et al.* [79] in numerical studies of the *anomolous diffusion regime* of the kicked rotor. These authors provided some numerical evidence in support of the scaling with increasing system size expressed in Eq. (1.25) by considering the differences between the quantum expectation values and Liouville ensemble averages for low-order moments, such as $\langle p^2 \rangle$. However, it is important to emphasize that the $\log(\mathcal{J}/\hbar)$ scaling for the Liouville break-time does not hold in the general case. In particular, the quantum-Liouville break-time that arises in the *localisation regime* of the kicked rotor is believed to grow as a small power of the ratio $(\mathcal{J}/\hbar)$ [55], which is more than adequate for correspondence in the macroscopic limit.

These considerations have been outlined in order to motivate the following questions: (1) Under what conditions does the Liouville break-time estimate (1.25) hold? (2) Although environmental noise may improve the degree of quantum-Liouville correspondence, is decoherence necessary for quantum-Liouville correspondence in the macroscopic limit? (3) Can decoherence help restore Ehrenfest correspondence?

The main focus of the work presented in this thesis is to characterize the properties of Liouville and Ehrenfest correspondence, particularly under conditions of classical chaos, for an isolated few degree-of-freedom system. The central challenge of this analysis consists of extrapolating the predictions of quantum theory (and therefore the degree of correspondence) into the macroscopic regime, where direct calculation is of course not feasible in the generic case of a non-integrable system.

This thesis is organised as follows. In Chapter 2 I will describe the quantum and classical versions of the model examined in this thesis. Since the model is novel I will examine the behaviours of the chaotic classical dynamics in some detail. I will also describe the initial

quantum states, which are SU(2) coherent states, and then define a corresponding classical density on the 2-sphere which is a good analog for these states. I show in Appendix A that a perfect match is impossible: no distribution on $\mathcal{S}^2$ can reproduce the moments of the SU(2) coherent states exactly. At the end of Chapter 2 I will describe some of the numerical techniques that were required for the quantum and classical Liouville descriptions of the dynamics.

In Chapter 3 I will examine the characteristics of quantum-Liouville correspondence at the level of the low-order moments. First I will demonstrate that a close correspondence with Liouville mechanics persists well after the Ehrenfest correspondence has broken down. The widths of both the quantum states and the Liouville densities grow exponentially until saturation at the system size. I will then confirm that the quantum-Liouville differences exhibit an initial phase of exponential growth for chaotic states, but also demonstrate that this growth terminates well before the differences reach the system size. I will also show that the Liouville break-time scales according to the estimate Eq. (1.25), but only for the onset of very small quantum-Liouville differences. By "very small" I mean differences that remain a factor $(\hbar/\mathcal{J})$ smaller than the system size. As a result, I argue that decoherence is not necessary for the emergence of these classical properties in the macroscopic limit.

This demonstrated correspondence at the level of the low-order moments still leaves room for significant quantum-Liouville deviations. In Chapter 4 I will examine the degree of correspondence between the quantum and classical probability distributions, emphasizing the details of this correspondence after the states have spread to the system size. In particular, I will show that the initially localised quantum states approach the classical equilibrium on the same relaxation time-scale as the corresponding Liouville density. When the classical Hamiltonian exhibits widespread chaos, the quantum probability distributions approach microcanonical equilibrium configurations. I also demonstrate that the quantum fluctuations away from the classical equilibrium become vanishingly small in the macroscopic limit. These results reinforce the conclusion that quantum-Liouville differences for classical observables become increasingly difficult to detect as the system size increases.

In Chapter 5 I will examine the properties of Ehrenfest correspondence. I will demonstrate that the Ehrenfest differences, in contrast with the quantum-Liouville differences, actually grow to a macroscopic size on the short time-scale (1.18) in the case of chaotic classical dynamics. Moreover, decoherence is unable to restore the *Ehrenfest* correspondence

for these observables. I will conclude that Ehrenfest correspondence may be subject to experimental refutation for some chaotic macroscopic bodies. At the end of Chapter 5 I will address the implications of this result for the correspondence principle and the interpretation of the quantum state.

Chapter 2

Description of the Model

This chapter is taken from Emerson and Ballentine [35].

2.1 The Model

We consider the quantum and classical dynamics generated by a non-integrable model of two interacting spins,

$$H = a(S_z + L_z) + cS_xL_x \sum_{n=-\infty}^{\infty} \delta(t-n) \tag{2.1}$$

where $\mathbf{S} = (S_x, S_y, S_z)$ and $\mathbf{L} = (L_x, L_y, L_z)$. The first two terms in (2.1) correspond to simple rotation of both spins about the z-axis. The sum over coupling terms describes an infinite sequence of δ-function interactions at times $t = n$ for integer n. Each interaction term corresponds to an impulsive rotation of each spin about the x-axis by an angle proportional to the x-component of the other spin.

2.1.1 The Quantum Dynamics

To obtain the quantum dynamics we interpret the Cartesian components of the spins as operators satisfying the usual angular momentum commutation relations,

$$\begin{aligned}
[S_i, S_j] = &\quad i\epsilon_{ijk}S_k \\
[L_i, L_j] = &\quad i\epsilon_{ijk}L_k \\
[J_i, J_j] = &\quad i\epsilon_{ijk}J_k.
\end{aligned}$$

In the above we have set $\hbar = 1$ and introduced the total angular momentum vector $\mathbf{J} = \mathbf{S}+\mathbf{L}$.

The Hamiltonian (2.1) possesses kinematic constants of the motion, $[\mathbf{S}^2, H] = 0$ and $[\mathbf{L}^2, H] = 0$, and the total state vector $|\psi\rangle$ can be represented in a finite Hilbert space of dimension $N = (2s+1) \times (2l+1)$. This space is spanned by the orthonormal vectors $|s, l, m_s, m_l\rangle = |s, m_s\rangle \otimes |l, m_l\rangle$ with $m_s \in \{s, s-1, \ldots, -s\}$ and $m_l \in \{l, l-1, \ldots, -l\}$. These are the joint eigenvectors of the four spin operators

$$\begin{aligned} \mathbf{S}^2|s,l,m_s,m_l\rangle &= s(s+1)|s,l,m_s,m_l\rangle, \\ S_z|s,l,m_s,m_l\rangle &= m_s|s,l,m_s,m_l\rangle, \\ \mathbf{L}^2|s,l,m_s,m_l\rangle &= l(l+1)|s,l,m_s,m_l\rangle, \\ L_z|s,l,m_s,m_l\rangle &= m_l|s,l,m_s,m_l\rangle. \end{aligned} \tag{2.2}$$

The periodic sequence of interactions introduced by the δ-function produces a quantum mapping. The time-evolution for a single iteration, from just before a kick to just before the next, is produced by the unitary transformation,

$$|\psi(n+1)\rangle = F\ |\psi(n)\rangle, \tag{2.3}$$

where F is the single-step Floquet operator,

$$F = \exp\left[-ia(S_z + L_z)\right] \exp\left[-icS_x L_x\right]. \tag{2.4}$$

Since a is a rotation its range is 2π radians. The quantum dynamics are thus specified by two parameters, a and c, and two quantum numbers, s and l.

An explicit representation of the single-step Floquet operator can be obtained in the basis (2.2) by first re-expressing the interaction operator in (2.4) in terms of rotation operators,

$$\begin{aligned} \exp\left[-icS_x \otimes L_x\right] &= \left[R^{(s)}(\theta,\phi) \otimes R^{(l)}(\theta,\phi)\right]\ \exp\left[-icS_z \otimes L_z\right] \\ &\quad \times \left[R^{(s)}(\theta,\phi) \otimes R^{(l)}(\theta,\phi)\right]^{-1}, \end{aligned} \tag{2.5}$$

using polar angle $\theta = \pi/2$ and azimuthal angle $\phi = 0$. Then non-zero off-diagonal terms arise only in the expressions for the rotation matrices, which take the form,

$$\langle j, m'|R^{(j)}(\theta,\phi)|j, m\rangle = \exp(-im'\phi) d^{(j)}_{m',m}(\theta). \tag{2.6}$$

The matrix elements,

$$d^{(j)}_{m',m}(\theta) = \langle j, m'| \exp(-i\theta J_y)|j, m\rangle \tag{2.7}$$

are given explicitly by Wigner's formula [81].

We are interested in studying the different time-domain characteristics of quantum observables when the corresponding classical system exhibits either regular or chaotic dynamics. In order to compare quantum systems with different quantum numbers it is convenient to normalize subsystem observables by the subsystem magnitude $\sqrt{\langle \mathbf{L}^2 \rangle} = \sqrt{l(l+1)}$. We denote such normalized observables with a tilde, where

$$\langle \tilde{L}_z(n) \rangle = \frac{\langle \psi(n) | L_z | \psi(n) \rangle}{\sqrt{l(l+1)}} \tag{2.8}$$

and the normalized variance at time n is defined as,

$$\Delta \tilde{\mathbf{L}}^2(n) = \frac{\langle \mathbf{L}^2 \rangle - \langle \mathbf{L}(n) \rangle^2}{l(l+1)}. \tag{2.9}$$

We are also interested in evaluating the properties of the quantum probability distributions. The probability distribution corresponding to the observable L_z is given by the trace,

$$P_z(m_l) = \mathrm{Tr}\left[\rho^{(l)}(n) | l, m_l \rangle \langle l, m_l | \right] = \langle l, m_l | \rho^{(l)}(n) | l, m_l \rangle, \tag{2.10}$$

where $\rho^{(l)}(n) = \mathrm{Tr}^{(s)} \left[\, |\psi(n)\rangle\langle\psi(n)| \; |s, m_s\rangle\langle s, m_s| \, \right]$ is the reduced state operator for the spin $\mathbf{L}$ at time n and $\mathrm{Tr}^{(s)}$ denotes a trace over the factor space corresponding to the spin $\mathbf{S}$.

2.1.2 Classical Map

For the Hamiltonian (2.1) the corresponding classical equations of motion are obtained by interpreting the angular momentum components as dynamical variables satisfying,

$$\begin{aligned} \{S_i, S_j\} &= \epsilon_{ijk} S_k \\ \{L_i, L_j\} &= \epsilon_{ijk} L_k \\ \{J_i, J_j\} &= \epsilon_{ijk} J_k, \end{aligned}$$

with $\{\cdot, \cdot\}$ denoting the Poisson bracket. The periodic δ-function in the coupling term can be used to define surfaces at $t = n$, for integer n, on which the time-evolution reduces to a stroboscopic mapping,

$$\begin{aligned} \tilde{S}_x^{n+1} &= \tilde{S}_x^n \cos(a) - \left[\tilde{S}_y^n \cos(\gamma r \tilde{L}_x^n) - \tilde{S}_z^n \sin(\gamma r \tilde{L}_x^n) \right] \sin(a), \\ \tilde{S}_y^{n+1} &= \left[\tilde{S}_y^n \cos(\gamma r \tilde{L}_x^n) - \tilde{S}_z^n \sin(\gamma r \tilde{L}_x^n) \right] \cos(a) + \tilde{S}_x^n \sin(a), \end{aligned}$$

$$\begin{aligned}
\tilde{S}_z^{n+1} &= \tilde{S}_z^n \cos(\gamma r \tilde{L}_x^n) + \tilde{S}_y^n \sin(\gamma r \tilde{L}_x^n), \\
\tilde{L}_x^{n+1} &= \tilde{L}_x^n \cos(a) - \left[\tilde{L}_y^n \cos(\gamma \tilde{S}_x^n) - \tilde{L}_z^n \sin(\gamma \tilde{S}_x^n)\right] \sin(a), \\
\tilde{L}_y^{n+1} &= \left[\tilde{L}_y^n \cos(\gamma \tilde{S}_x^n) - \tilde{L}_z^n \sin(\gamma \tilde{S}_x^n)\right] \cos(a) + \tilde{L}_x^n \sin(a), \\
\tilde{L}_z^{n+1} &= \tilde{L}_z^n \cos(\gamma \tilde{S}_x^n) + \tilde{L}_y^n \sin(\gamma \tilde{S}_x^n),
\end{aligned} \tag{2.11}$$

where $\tilde{\mathbf{L}} = \mathbf{L}/|\mathbf{L}|$, $\tilde{\mathbf{S}} = \mathbf{S}/|\mathbf{S}|$ and we have introduced the parameters $\gamma = c|\mathbf{S}|$ and $r = |\mathbf{L}|/|\mathbf{S}|$. The mapping equations (2.11) describe the time-evolution of (2.1) from just before one kick to just before the next.

Since the magnitudes of both spins are conserved, $\{\mathbf{S}^2, H\} = \{\mathbf{L}^2, H\} = 0$, the motion is actually confined to the four-dimensional manifold $\mathcal{P} = \mathcal{S}^2 \times \mathcal{S}^2$, which corresponds to the surfaces of two spheres. This is manifest when the mapping (2.11) is expressed in terms of the four *canonical* coordinates $\mathbf{x} = (S_z, \phi_s, L_z, \phi_l)$, where $\phi_s = \tan(S_y/S_x)$ and $\phi_l = \tan(L_y/L_x)$. We will refer to the mapping (2.11) in canonical form using the shorthand notation $\mathbf{x}^{n+1} = \mathbf{F}(\mathbf{x}^n)$. It is also useful to introduce a complete set of spherical coordinates $\vec{\theta} = (\theta_s, \phi_s, \theta_l, \phi_l)$ where $\theta_s = \cos^{-1}(S_z/|\mathbf{S}|)$ and $\theta_l = \cos^{-1}(L_z/|\mathbf{L}|)$.

The mapping (2.11) on the reduced surface $\mathcal{P}$ enjoys a rather large parameter space; the dynamics are determined from three independent dimensionless parameters: $a \in [0, 2\pi)$, $\gamma \in (-\infty, \infty)$, and $r \geq 1$. The first of these, a, controls the angle of free-field rotation about the z-axis. The parameter $\gamma = c|\mathbf{S}|$ is a dimensionless coupling strength and $r = |\mathbf{L}|/|\mathbf{S}|$ corresponds to the relative magnitude of the two spins.

We are particularly interested in the effect of increasing the coupling strength γ for different fixed values of r. In Fig. 2.1 we plot the dependence of the classical behaviour on these two parameters for the case $a = 5$, which produces typical results. The data in this figure were generated by randomly sampling initial conditions on $\mathcal{P}$, using the invariant measure,

$$d\mu(\mathbf{x}) = d\tilde{S}_z d\phi_s d\tilde{L}_z d\phi_l, \tag{2.12}$$

and then calculating the largest Lyapunov exponent associated with each trajectory. Open circles correspond to regimes where at least 99% of the initial conditions were found to exhibit regular behaviour and crosses correspond to regimes where at least 99% of these randomly sampled initial conditions were found to exhibit chaotic behaviour. Circles with crosses through them (the superposition of both symbols) correspond to regimes with a mixed phase space. For the case $a = 5$ and with r held constant, the scaled coupling

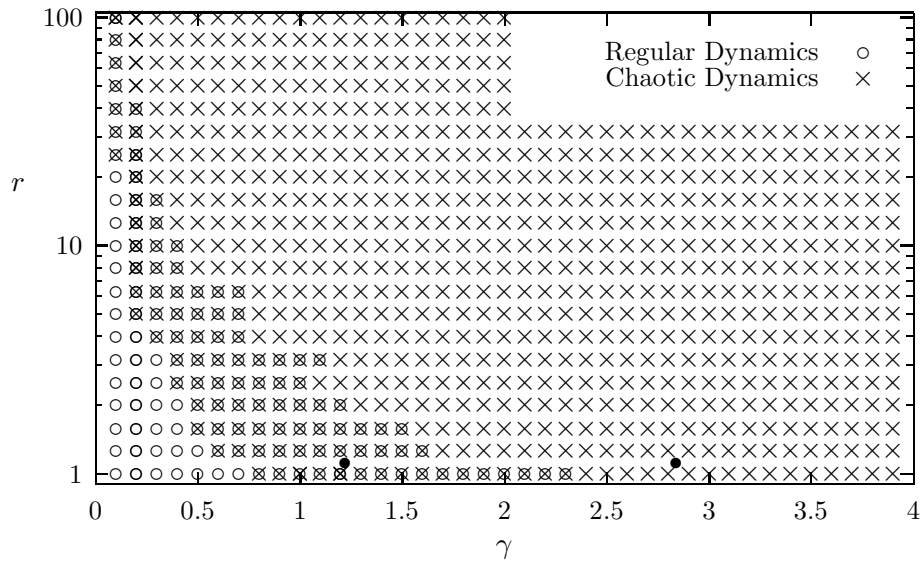

Figure 2.1: Behaviour of the classical mapping for different values of $r = |\mathbf{L}|/|\mathbf{S}|$ and $\gamma = c|\mathbf{S}|$ with $a = 5$. Circles correspond to parameter values for which at least 99% of the surface area $\mathcal{P}$ produces regular dynamics and crosses correspond to parameter values for which the dynamics are at least 99% chaotic. Superpositions of circles and crosses correspond to parameter values which produce a mixed phase space. We investigate quantum-classical correspondence for the parameter values $\gamma = 1.215$ (mixed regime) and $\gamma = 2.835$ (global chaos), with $r = 1.1$, which are indicated by filled circles.

strength γ plays the role of a perturbation parameter: the classical behaviour varies from regular, to mixed, to predominantly chaotic as $|\gamma|$ is increased from zero.

The fixed points of the classical map (2.11) provide useful information about the parameter dependence of the classical behaviour and, more importantly, in the case of mixed regimes, help locate the zones of regular behaviour in the 4-dimensional phase space. We find it sufficient to consider only the four trivial (parameter-independent) fixed points which lie at the poles along the z-axis: two of these points correspond to parallel spins, $(S_z, L_z) = \pm(|\mathbf{S}|, |\mathbf{L}|)$, and the remaining two points correspond to anti-parallel spins, $(S_z, L_z) = (\pm|\mathbf{S}|, \mp|\mathbf{L}|)$.

The stability around these fixed points can be determined from the eigenvalues of the tangent map matrix, $\mathbf{M} = \partial\mathbf{F}/\partial\mathbf{x}$, where all derivatives are evaluated at the fixed point of interest. (It is easiest to derive M using the six *non-canonical* mapping equations (2.11)

since the tangent map for the *canonical* mapping equations exhibits a coordinate system singularity at these fixed points.) The eigenvalues corresponding to the four trivial fixed points are obtained from the characteristic equation,

$$[\xi^2 - 2\xi\cos a + 1]^2 \pm \xi^2\gamma^2 r \sin^2 a = 0, \tag{2.13}$$

with the minus (plus) sign corresponding to the parallel (anti-parallel) cases and I have suppressed the trivial factor $(1-\xi)^2$ which arises since the six equations (2.11) are not independent. For the parallel fixed points the four eigenvalues are

$$\begin{aligned}
\xi^P_{1,2} &= \cos a \pm \frac{1}{2}\sqrt{r\gamma^2\sin^2 a} + \frac{1}{2}\sqrt{\pm 4\cos a\sqrt{\gamma^2 r\sin^2 a} - (\sin^2 a)(4-\gamma^2 r)}, \\
\xi^P_{3,4} &= \cos a \pm \frac{1}{2}\sqrt{r\gamma^2\sin^2 a} - \frac{1}{2}\sqrt{\pm 4\cos a\sqrt{\gamma^2 r\sin^2 a} - (\sin^2 a)(4-\gamma^2 r)},
\end{aligned} \tag{2.14}$$

and the eigenvalues for the anti-parallel cases, ξ^{AP}, are obtained from (2.14) through the substitution $r \to -r$. A fixed point becomes unstable if and only if $|\xi| > 1$ for at least one of the four eigenvalues.

Mixed Phase Space: $\gamma = 1.215$

We are particularly interested in the behaviour of this model when the two spins are comparable in magnitude. Choosing the value $r = 1.1$ (with $a = 5$ as before), we determined by numerical evaluation that the anti-parallel fixed points are unstable for $|\gamma| > 0$. In the case of the parallel fixed points, all four eigenvalues remain on the unit circle, $|\xi^P| = 1$, for $|\gamma| < 1.42$. This stability condition guarantees the presence of regular islands about the parallel fixed points [66]. In Fig. 2.2 we plot the trajectory corresponding to the parameters $a = 5$, $r = 1.1$, $\gamma = 1.215$ and with initial condition $\vec{\theta}(0) = (5^o, 5^o, 5^o, 5^o)$ which locates the trajectory near a stable fixed point of a mixed phase space (see Fig. 2.1.) This trajectory clearly exhibits a periodic pattern which we have confirmed to be regular by computing the associated Lyapunov exponent ($\lambda_L = 0$). In contrast, the trajectory plotted in Fig. 2.3 is launched with the same parameters but with initial condition $\vec{\theta}(0) = (20^o, 40^o, 160^o, 130^o)$, which is close to one of the unstable anti-parallel fixed points. This trajectory explores a much larger portion of the surface of the two spheres in a seemingly random manner. As expected, a computation of the largest associated Lyapunov exponent yields a positive number ($\lambda_L = 0.04$).

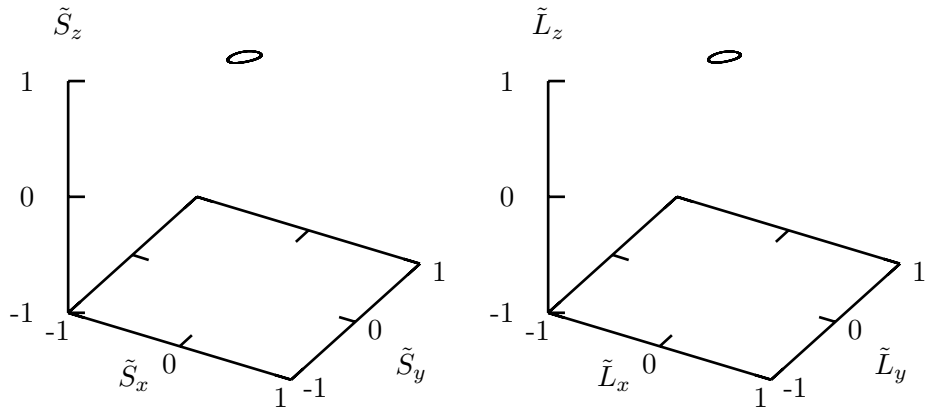

Figure 2.2: Stroboscopic trajectories on the unit sphere launched from a regular zone of the mixed regime with $\gamma = 1.215$, $r = 1.1$, $a = 5$ and $\vec{\theta}(0) = (5^o, 5^o, 5^o, 5^o)$.

Global Chaos: $\gamma = 2.835$

If we increase the coupling strength to the value $\gamma = 2.835$, with $a = 5$ and $r = 1.1$ as before, then all four trivial fixed points become unstable. By randomly sampling $\mathcal{P}$ with 3×10^4 initial conditions we find that less than 0.1% of the kinematically accessible surface $\mathcal{P}$ is covered with regular islands (see Fig. 2.1). This set of parameters produces a connected chaotic zone with largest Lyapunov exponent $\lambda_L = 0.45$. We will refer to this type of regime as one of "global chaos" although the reader should note that our usage of this expression differs slightly from that in Ref. [66].

The Limit $r \gg 1$

Another interesting limit of our model arises when one of the spins is much larger than the other, $r \gg 1$. We expect that in this limit the larger spin ($\mathbf{L}$) will act as a source of essentially external "driving" for the smaller spin ($\mathbf{S}$). Referring to the coupling terms in the mapping (2.11), the "driving" strength, or perturbation upon $\mathbf{S}$ from $\mathbf{L}$, is determined from the product $\gamma r = c|\mathbf{L}|$, which can be quite large, whereas the "back-reaction" strength, or perturbation upon $\mathbf{L}$ from $\mathbf{S}$, is governed only by the scaled coupling strength $\gamma = c|\mathbf{S}|$, which can be quite small. It is interesting to examine whether a dynamical regime exists where the larger system might approach regular behaviour while the smaller 'driven' system

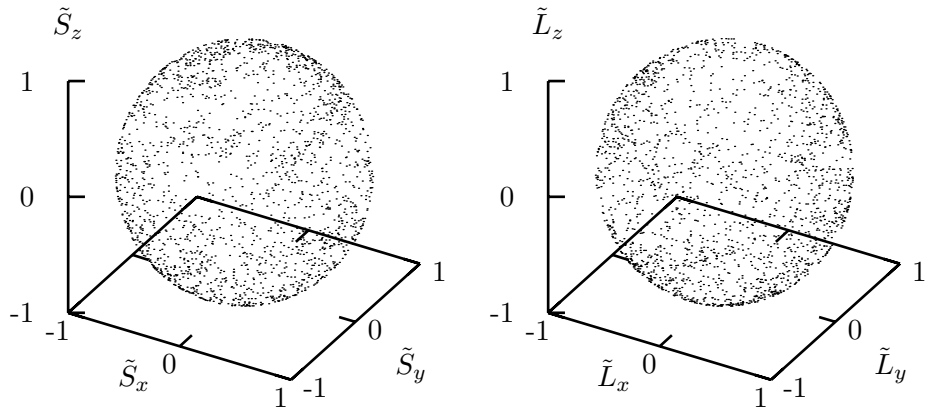

Figure 2.3: Same parameters as Fig. 2.2 but the trajectory is launched from a chaotic zone of the mixed regime with initial condition $\vec{\theta}(0) = (20^o, 40^o, 160^o, 130^o)$.

is still subject to chaotic motion.

In Fig. 2.4 we plot a chaotic trajectory for $r = 100$ with initial condition $\vec{\theta}(0) = (27^o, 27^o, 27^o, 27^o)$ which is located in a chaotic zone ($\lambda_L = 0.026$) of a mixed phase space (with $a = 5$ and $\gamma = 0.06$). Although the small spin wanders chaotically over a large portion of its kinematically accessible shell $\mathcal{S}^2$, the motion of the large spin remains confined to a 'narrow' band. Although the band is narrow relative to the large spin's length, it is not small relative to the smaller spin's length. The trajectories are both plotted on the unit sphere, so the effective area explored by the large spin (relative to the effective area covered by the small spin) scales in proportion to r^2.

2.1.3 The Liouville Dynamics

We are interested in comparing the quantum dynamics generated by (2.3) with the corresponding Liouville dynamics of a classical distribution. The time-evolution of a classical phase space distribution is generated by the partial differential equation,

$$\frac{\partial \rho_c(\mathbf{x}, t)}{\partial t} = -\{\rho_c, H\}, \tag{2.15}$$

where H stands for the Hamiltonian (2.1) and $\mathbf{x} = (S_z, \phi_s, L_z, \phi_l)$.

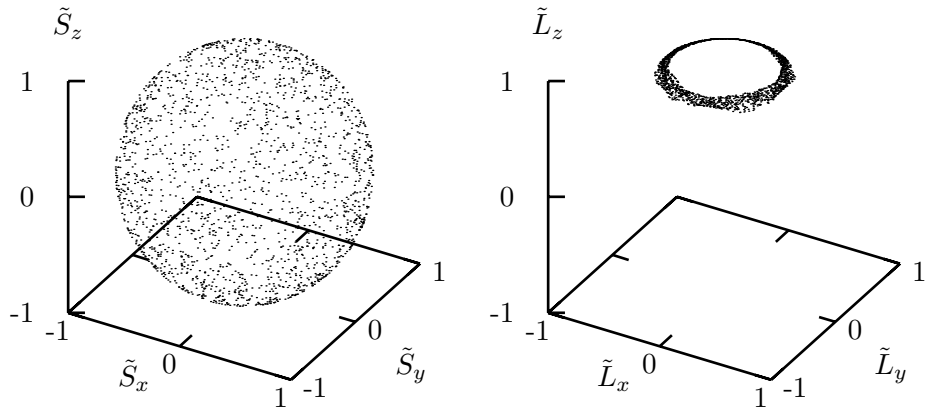

Figure 2.4: A chaotic trajectory for mixed regime parameters $\gamma = 0.06$, $r = 100$, and $a = 5$ with $\vec{\theta}(0) = (27^o, 27^o, 27^o, 27^o)$. The motion of the larger spin appears to remain confined to a narrow band on the surface of the sphere.

The solution to (2.15) can be expressed in the compact form,

$$\rho_c(\mathbf{x}, t) = \int_{\mathcal{P}} \mathrm{d}\mu(\mathbf{y})\ \delta(\mathbf{x} - \mathbf{x}(t, \mathbf{y}))\ \rho_c(\mathbf{y}, 0), \tag{2.16}$$

with measure $d\mu(\mathbf{y})$ given by (2.12). Each time-dependent function $\mathbf{x}(t, \mathbf{y}) \in \mathcal{P}$ is a solution of the equations of motion for (2.1) with initial condition $\mathbf{y} \in \mathcal{P}$. The solution (2.16) simply expresses that Liouville's equation (2.15) describes the dynamics of a classical density $\rho_c(\mathbf{x}, t)$ of points evolving in phase space under the Hamiltonian flow. We exploit this fact to numerically solve (2.15) by randomly generating initial conditions consistent with an initial phase space distribution $\rho_c(\mathbf{x}, 0)$ and then time-evolving each of these initial conditions using the equations of motion (2.11). We then calculate the ensemble averages of dynamical variables,

$$\langle \tilde{L}_z(n) \rangle_c = \int_{\mathcal{P}} \mathrm{d}\mu(\mathbf{x}) \frac{L_z}{|\mathbf{L}|} \rho_c(\mathbf{x}, n). \tag{2.17}$$

by summing over this distribution of trajectories at each time step.

2.1.4 Correspondence Between Quantum and Classical Models

For a quantum system specified by the four numbers $\{a, c, s, l\}$, the corresponding classical parameters $\{a, \gamma, r\}$ may be determined by first defining the classical magnitudes in terms

of the quantum magnitudes,

$$\begin{aligned} |\mathbf{S}|_c &= \sqrt{s(s+1)} \\ |\mathbf{L}|_c &= \sqrt{l(l+1)}, \end{aligned} \tag{2.18}$$

where the quantities on the left hand side are the lengths of the classical spins and those on the right are the quantum numbers. If we set the Hamiltonian coefficients a and c numerically equal for both models, then the remaining two dimensionless classical parameters are determined,

$$\begin{aligned} r &= \sqrt{\frac{l(l+1)}{s(s+1)}} \\ \gamma &= c\sqrt{s(s+1)}. \end{aligned} \tag{2.19}$$

We are interested in extrapolating the behaviour of the quantum dynamics in the limit $s \to \infty$ and $l \to \infty$. This is accomplished by studying sequences of quantum models with increasing s and l chosen such that r and γ are held fixed. Since s and l are restricted to integer (or half-integer) values, the corresponding classical r will actually vary slightly for each member of this sequence, although γ can be matched exactly by varying the quantum parameter c. In the limit $s \to \infty$ and $l \to \infty$ this variation becomes increasingly small since $r = \sqrt{l(l+1)/s(s+1)} \to l/s$. For convenience, the classical r corresponding to each member of the sequence of quantum models is identified by its value in this limit. We have examined the effect of the small variations in the value of r on the classical behaviour and found the variation to be negligible.

2.2 Initial States

2.2.1 Initial Quantum State

We consider *initial* quantum states which are pure and separable,

$$|\psi(0)\rangle = |\psi_s(0)\rangle \otimes |\psi_l(0)\rangle. \tag{2.20}$$

For the initial state of each subsystem we use one of the directed angular momentum states,

$$|\theta, \phi\rangle = R^{(j)}(\theta, \phi)|j, j\rangle, \tag{2.21}$$

which correspond to states of maximum polarization in the direction (θ, ϕ). It has the properties:

$$\begin{aligned} \langle\theta,\phi|J_z|\theta,\phi\rangle &= j\cos\theta \\ \langle\theta,\phi|J_x \pm iJ_y|\theta,\phi\rangle &= je^{\pm i\phi}\sin\theta, \end{aligned} \tag{2.22}$$

where j in this section refers to either l or s.

The states (2.21) are the SU(2) coherent states, which, like their counterparts in the Euclidean phase space, are minimum uncertainty states [72]; the normalized variance of the quadratic operator,

$$\Delta\tilde{\mathbf{J}}^2 = \frac{\langle\theta,\phi|\mathbf{J}^2|\theta,\phi\rangle - \langle\theta,\phi|\mathbf{J}|\theta,\phi\rangle^2}{j(j+1)} = \frac{1}{(j+1)}, \tag{2.23}$$

is minimised for given j and vanishes in the limit $j \to \infty$. The coherent states polarized along the z-axis, $|j,j\rangle$ and $|j,-j\rangle$, also saturate the inequality of the uncertainty relation,

$$\langle J_x^2\rangle\langle J_y^2\rangle \geq \frac{\langle J_z\rangle^2}{4}, \tag{2.24}$$

although this inequality is not saturated for coherent states polarized along other axes.

2.2.2 Initial Classical State and Correspondence in the Macroscopic Limit

We compare the quantum dynamics with that of a classical Liouville density which is chosen to match the initial probability distributions of the quantum coherent state. For quantum systems with a Euclidean phase space it is always possible to construct a classical density with marginal probability distributions that match exactly the corresponding moments of the quantum coherent state. This follows from the fact that the marginal distributions for a coherent state are positive definite Gaussians, and therefore all of the moments can be matched *exactly* by choosing a Gaussian classical density. For the SU(2) coherent state, however, we show in Appendix A that no classical density has marginal distributions that can reproduce even the low order moments of the quantum probability distributions (except in the limit of infinite j). Thus from the outset it is clear that any choice of an initial classical state will exhibit residual discrepancy in matching some of the initial quantum moments.

We have examined the initial state and dynamical quantum-classical correspondence using several different classical distributions. These included the vector model distribution

described in Appendix A and the Gaussian distribution used by Fox and Elston in correspondence studies of the kicked top [46]. For a state polarized along the z-axis we chose the density,

$$\begin{aligned} \rho_c(\theta,\phi)\ \sin\theta d\theta d\phi &= C\exp\left[-\frac{2\sin^2(\frac{\theta}{2}))}{\sigma^2}\right]\sin\theta d\theta d\phi \\ &= C\exp\left[-\frac{(1-\tilde{J}_z)}{\sigma^2}\right]\ d\tilde{J}_z d\phi, \end{aligned} \tag{2.25}$$

with $C = \left[2\pi\sigma^2\left(1-\exp(-2\sigma^{-2})\right)\right]^{-1}$, instead of those previously considered, because it is periodic under 2π rotation. An initial state directed along (θ_o, ϕ_o) is then produced by a rigid body rotation of (2.25) by an angle θ_o about the y-axis followed by rotation with angle ϕ_o about the z-axis.

The variance σ^2 and the magnitude $|\mathbf{J}|_c$ are free parameters of the classical distribution that should be chosen to fit the quantum probabilities as well as possible. It is shown in Appendix A that no classical density has marginal distributions which can match all of the quantum moments, so we concentrate only on matching the lowest order moments. Since the magnitude of the spin is a kinematic constant both classically and quantum mechanically, we choose the squared length of the classical spin to have the correct quantum value,

$$|\mathbf{J}|_c^2 = \langle J_x^2\rangle_c + \langle J_y^2\rangle_c + \langle J_z^2\rangle_c = j(j+1). \tag{2.26}$$

For a state polarized along the z-axis, we have $\langle J_x\rangle = \langle J_y\rangle = 0$ and $\langle J_y^2\rangle = \langle J_x^2\rangle$ for both distributions as a consequence of the axial symmetry. Furthermore, as a consequence of (2.26), we will automatically satisfy the condition,

$$2\langle J_x^2\rangle_c + \langle J_z^2\rangle_c = j(j+1). \tag{2.27}$$

Therefore we only need to consider the classical moments,

$$\langle J_z\rangle_c = |\mathbf{J}|\ G(\sigma^2) \tag{2.28}$$

$$\langle J_x^2\rangle_c = |\mathbf{J}|^2\sigma^2\ G(\sigma^2), \tag{2.29}$$

calculated from the density (2.25) in terms of the remaining free parameter, σ^2, where,

$$G(\sigma^2) = \left[\frac{1+\exp(-2\sigma^{-2})}{1-\exp(-2\sigma^{-2})}\right] - \sigma^2. \tag{2.30}$$

We would like to match both of these classical moments with the corresponding quantum values,

$$\langle J_z \rangle = j, \tag{2.31}$$

$$\langle J_x^2 \rangle = j/2, \tag{2.32}$$

calculated for the coherent state (2.21). However, no choice of σ^2 will satisfy both constraints.

If we choose σ^2 to satisfy (2.31) exactly then we would obtain,

$$\sigma^2 = \frac{1}{2j} - \frac{3}{8j^2} + \mathcal{O}(j^{-3}). \tag{2.33}$$

If we choose σ^2 to satisfy (2.32) exactly then we would obtain,

$$\sigma^2 = \frac{1}{2j} + \frac{1}{4j^2} + \mathcal{O}(j^{-3}). \tag{2.34}$$

(These expansions are most easily derived from the approximation $G(\sigma^2) \simeq 1 - \sigma^2$, which has an exponentially small error for large j.)

We have chosen to compromise between these values by fixing σ^2 so that the ratio $\langle J_z \rangle_c / \langle J_x^2 \rangle_c$ has the correct quantum value. This leads to the choice,

$$\sigma^2 = \frac{1}{2\sqrt{j(j+1)}} = \frac{1}{2j} - \frac{1}{4j^2} + \mathcal{O}(j^{-3}). \tag{2.35}$$

These unavoidable initial differences between the classical and quantum moments will vanish in the "classical" limit. To see this explicitly it is convenient to introduce a measure of the quantum-classical differences,

$$\delta J_z(n) = |\langle J_z(n) \rangle - \langle J_z(n) \rangle_c|, \tag{2.36}$$

defined at time n. For an initial state polarised in direction (θ, ϕ), the choice (2.35) produces the initial difference,

$$\delta J_z(0) = \frac{\cos(\theta)}{8j} + \mathcal{O}(j^{-2}), \tag{2.37}$$

which vanishes as $j \to \infty$.

2.3 Numerical Methods

The time-periodic spin Hamiltonian (2.1) is convenient for numerical study because the time-dependence reduces to a simple mapping and the quantum state vector is confined to a finite dimensional Hilbert space. Consequently we can solve the exact time-evolution equations (2.3) numerically without introducing any artificial truncation of the Hilbert space. The principal source of numerical inaccuracy arises from the numerical evaluation of the matrix elements of the rotation operator $\langle j, m'|R(\theta,\phi)|j,m\rangle = \exp(-i\phi m')d^{(j)}_{m'm}(\theta)$. The rotation operator is required both for the calculation of the initial quantum coherent state, $|\theta,\phi\rangle = R(\theta,\phi)|j, m = j\rangle$, and for the evaluation of the unitary Floquet operator. In order to maximise the precision of our results we calculated the matrix elements $d^{(j)}_{m'm}(\theta) = \langle j, m'|\exp(-i\theta J_y)|j,m\rangle$ using the recursion algorithm of Ref. [21] and then tested the accuracy of our results by introducing controlled numerical errors. For small quantum numbers ($j < 50$) we are able to confirm the correctness of our coded algorithm by comparing these results with those obtained by direct evaluation of Wigner's formula for the matrix elements $d^{(j)}_{m'm}(\theta)$.

The time evolution of the Liouville density was simulated by numerically evaluating between 10^8 and 10^9 classical trajectories with randomly selected initial conditions weighted according to the initial distribution (2.25). Such a large number of trajectories was required in order to keep Monte Carlo errors small enough to resolve the initial normalized quantum-classical differences, which scale as $1/8j^2$, over the range of j values we have examined.

We identified initial conditions of the classical map as chaotic by numerically calculating the largest Lyapunov exponent, λ_L, using the formula,

$$\lambda_L = \frac{1}{N}\sum_{n=1}^{N} \ln d(n) \tag{2.38}$$

where $d(n) = \sum_i |\delta x_i(n)|$, with $d(0) = 1$. The differential $\delta\mathbf{x}(n)$ is a difference vector between adjacent trajectories and thus evolves under the action of the tangent map,

$$\delta\mathbf{x}(n+1) = \mathbf{M}\cdot\delta\mathbf{x}(n), \tag{2.39}$$

where $\mathbf{M}$ is evaluated along some fiducial trajectory [66].

Since we are interested in studying quantum states, and corresponding classical distributions which have non-vanishing support on the sphere, it is also important to get an idea of the size of these regular and chaotic zones. By comparing the size of a given regular or

chaotic zone to the variance of an initial state located within it, we can determine whether most of the state is contained within this zone. However, we can not perform this comparison by direct visual inspection since the relevant phase space is 4-dimensional. One strategy which we used to overcome this difficulty was to calculate the Lyapunov exponent for a large number of randomly sampled initial conditions and then project only those points which are regular (or chaotic) onto the plane spanned by $\tilde{S}_z = \cos\theta_s$ and $\tilde{L}_z = \cos\theta_l$. If the variance of the initial quantum state is located within, and several times smaller than, the dimensions of a zone devoid of any of these points, then the state in question can be safely identified as chaotic (or regular).

Chapter 3

Correspondence for Low Order Moments

This chapter is taken from Emerson and Ballentine [35].

3.1 Introduction

There is considerable interest in the interface between quantum and classical mechanics and the conditions that lead to the emergence of classical behaviour. In order to characterize these conditions, it is important to differentiate two dynamical regimes of quantum-classical correspondence [7]:
(i) Ehrenfest correspondence, in which the centroid of the wave packet approximately follows a classical trajectory; and
(ii) Liouville correspondence, in which the quantum probability distributions are in approximate agreement with those of an appropriately constructed classical ensemble satisfying Liouville's equation.

Regime (i) is relevant only when the width of the quantum state is small compared to the dimensions of the system; if the initial state is not narrow, this regime may be absent. Regime (ii), which generally includes (i), applies to a much broader class of states, and this regime of correspondence may persist well after the Ehrenfest correspondence has broken down. The distinction between regimes (i) and (ii) has not always been made clear in the literature, though the conditions that delimit these two regimes, and in particular their

scaling with system parameters, may be quite different.

The theoretical study of quantum chaos has raised the question of whether the quantum-classical break occurs differently in chaotic states, in states of regular motion, and in mixed phase-space systems. This is well understood only in the case of regime (i). There it is well-known [15, 54, 25] that the time for a minimum-uncertainty wave packet to expand beyond the Ehrenfest regime scales as $\log(\mathcal{J}/\hbar)$ for chaotic states, and as a power of $\mathcal{J}/\hbar$ for regular states, where $\mathcal{J}$ denotes a characteristic system action.

The breakdown of quantum-classical correspondence, in the case of regime (ii), is less well understood, though it has been argued that this regime may also be delimited by a $\log(\mathcal{J}/\hbar)$ break-time in classically chaotic states [96, 56]. Some numerical evidence in support of this conjecture has been reported in a study of the kicked rotor in the *anomolous diffusion* regime [79]. (On the other hand, in the regime of *quantum localization*, the break-time for the kicked rotor seems to scale as $(\mathcal{J}/\hbar)^2$ [55].) Since the $\log(\mathcal{J}/\hbar)$ time scale is rather short, it has been suggested that certain macroscopic objects would be predicted to exhibit non-classical behaviour on observable time scales [97, 99]. These results highlight the importance of investigating the characteristics of quantum-classical correspondence in more detail.

In this paper we study the classical and quantum dynamics of two interacting spins. This model is convenient because the Hilbert space of the quantum system is finite-dimensional, and hence tractable for computations. Spin models have been useful in the past for exploring classical and quantum chaos [54, 38, 4, 5, 6, 78] and our model belongs to a class of spin models which show promise of experimental realization in the near future [69]. The classical limit is approached by taking the magnitude of both spins to be very large relative to $\hbar$, while keeping their ratio fixed. For our model a characteristic system action is given by $\mathcal{J} \simeq \hbar l$, where l is a quantum number, and the classical limit is simply the limit of large quantum numbers, *i.e.* the limit $l \to \infty$.

In the case of the chaotic dynamics for our model, we first show that the widths of both the quantum and classical states grow exponentially at a rate given approximately by the largest Lyapunov exponent (until saturation at the system dimension). We then show that the initially small quantum-classical differences also grow at an exponential rate, with an exponent λ_{qc} that is independent of the quantum numbers and at least twice as large as the largest Lyapunov exponent. We demonstrate how this exponential growth of differences leads to a log break-time rule, $t_b \simeq \lambda_{qc}^{-1} \ln(lp/\hbar)$, delimiting the regime of

Liouville correspondence. The factor p, measured in units of $\hbar$, is some preset tolerance that defines a *break* between the quantum and classical expectation values, but does not scale with the system dimension. However, we also show that this logarithmic rule holds *only if* the tolerance p for quantum-classical differences is chosen extremely small, in particular $p < \mathcal{O}(\hbar)$. For larger values of the tolerance, the break-time does not occur on this log time-scale and may not occur until the recurrence time. In this sense, log break-time rules describing Liouville correspondence are not robust. These results demonstrate that, for chaotic states in the classical limit, quantum observables are described approximately by Liouville ensemble averages well beyond the Ehrenfest time-scale, after which both quantum and classical states relax towards equilibrium configurations. This demonstration of correspondence is obtained for a few degree-of-freedom quantum system of coupled spins that is described by a pure state and subject only to unitary evolution.

3.2 Characteristics of the Quantum and Liouville Dynamics

3.2.1 Mixed Phase Space

We consider the time-development of initial quantum coherent states (2.21) evolved according to the mapping (2.3) using quantum numbers $s = 140$ and $l = 154$ and associated classical parameters $\gamma = 1.215$, $r \simeq 1.1$, and $a = 5$, which produce a mixed phase space (see Fig. 2.1). The classical results are generated by evolving the initial ensemble (2.25) using the mapping (2.11). In Fig. 3.1 we compare the time-dependence of the normalized quantum variance, $\Delta\tilde{\mathbf{L}}^2 = [\langle \mathbf{L}^2 \rangle - \langle \mathbf{L} \rangle^2]/l(l+1)$, with its classical counterpart, $\Delta\tilde{\mathbf{L}}_c^2 = [\langle \mathbf{L}^2 \rangle_c - \langle \mathbf{L} \rangle_c^2]/|\mathbf{L}|^2$. Circles (diamonds) correspond to the dynamics of an initial quantum (classical) state centered at $\vec{\theta}(0) = (20^o, 40^o, 160^o, 130^o)$, which is located in the connected chaotic zone near one of the unstable fixed points of the classical map. Crosses (plus signs) correspond to an initial quantum (classical) state centered on the initial condition $\vec{\theta}(0) = (5^o, 5^o, 5^o, 5^o)$, which is located in the regular zone near one of the stable fixed points. For both initial conditions the quantum and classical results are nearly indistinguishable on the scale of the figure. In the case of the regular initial condition, the quantum variance remains narrow over long times and, like its classical counterpart, exhibits a regular oscillation. In the case of the chaotic initial condition the quantum variance also exhibits a periodic oscillation but this oscillation is superposed on a very rapid, approximately exponential, growth rate. This exponential growth persists until the variance approaches the

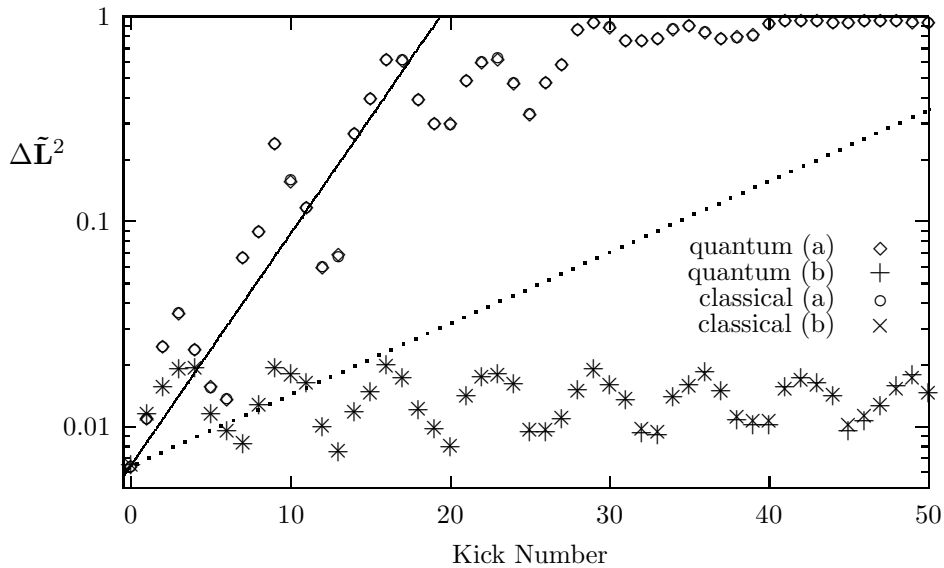

Figure 3.1: Growth of normalized quantum and classical variances in a chaotic zone (a) and a regular zone (b) of the mixed phase space regime $\gamma = 1.215$ and $r \simeq 1.1$ with $l = 154$. Quantum and classical results are nearly indistinguishable on this scale. In the chaotic case, the approximately exponential growth of both variances is governed by a much larger rate, $\lambda_w = 0.13$ (solid line), than that predicted from the largest Lyapunov exponent, $\lambda_L = 0.04$ (dotted line).

system size, that is, when $\Delta\tilde{\mathbf{L}}^2 \simeq 1$. The initial exponential growth of the quantum variance in classically chaotic regimes has been observed previously in several models and appears to be a generic feature of the quantum dynamics; this behaviour of the quantum variance is mimicked very accurately by the variance of an initially well-matched classical distribution [11, 46, 47].

For well-localized states, in the classical case, the exponential growth of the distribution variance in chaotic zones is certainly related to the exponential divergence of the underlying trajectories, a property that characterizes classical chaos. To examine this connection we compare the observed exponential rate of growth of the widths of the classical (and quantum) state with the exponential rate predicted from the classical Lyapunov exponent. For the coherent states the initial variance can be calculated exactly, $\Delta\tilde{\mathbf{L}}^2(0) = 1/(l+1)$. Then,

assuming exponential growth of this initial variance we get,

$$\Delta\tilde{\mathbf{L}}^2(n) \simeq \frac{1}{l}\exp(2\lambda_w n) \qquad \text{for} \quad n < t_{sat}, \tag{3.1}$$

where a factor of 2 is included in the exponent since $\Delta\tilde{\mathbf{L}}^2$ corresponds to a squared length. The dotted line in Fig. 3.1 corresponds to the prediction (3.1) with $\lambda_w = \lambda_L = 0.04$, the value of the largest classical Lyapunov exponent. As can be seen from the figure, the actual growth rate of the classical (and quantum) variance of the chaotic initial state is significantly larger than that predicted using the largest Lyapunov exponent. For comparison purposes we also plot a solid line in Fig. 3.1 corresponding to (3.1) using $\lambda_w = 0.13$, which provides a much closer approximation to the actual growth rate. We find, for a variety of initial conditions in the chaotic zone of this mixed regime, that the actual classical (and quantum) variance growth rate is consistently larger than the simple prediction (3.1) using λ_L for the growth rate. This systematic bias requires some explanation.

As pointed out in Ref. [46], the presence of some discrepancy between λ_w and λ_L can be expected from the fact that the Lyapunov exponent is defined as a geometric mean of the tangent map eigenvalues sampled over the entire connected chaotic zone (corresponding to the infinite time limit $n \to \infty$) whereas the *actual* growth rate of a given distribution over a small number of time-steps will be determined largely by a few eigenvalues of the local tangent map. In mixed regimes these local eigenvalues will vary considerably over the phase space manifold and the product of a few of these eigenvalues can be quite different from the geometric mean over the entire connected zone.

However, we find that the actual growth rate is consistently *larger* than the Lyapunov exponent prediction. It is well known that in mixed regimes the remnant KAM tori can be 'sticky'; these sticky regions can have a significant decreasing effect on a calculation of the Lyapunov exponent. In order to identify an initial condition as chaotic, we specifically choose initial states that are concentrated away from these KAM surfaces (regular islands). Such initial states will then be exposed mainly to the larger local expansion rates found away from these surfaces. This explanation is supported by our observations that, when we choose initial conditions closer to these remnant tori, we find that the growth rate of the variance is significantly reduced. These variance growth rates are still slightly larger than the Lyapunov rate, but this is not surprising since our initial distributions are concentrated over a significant fraction of the phase space and the growth of the distribution is probably more sensitive to contributions from those trajectories subject to large eigenvalues away

from the KAM boundary than those stuck near the boundary. These explanations are further supported by the results of the following section, where we examine a phase space regime that is nearly devoid of regular islands. In these regimes we find that the Lyapunov exponent serves as a much better approximation to the variance growth rate.

3.2.2 Regime of Global Chaos

If we increase the dimensionless coupling strength to $\gamma = 2.835$, with $a = 5$ and $r \simeq 1.1$ as before, then the classical flow is predominantly chaotic on the surface $\mathcal{P}$ (see Fig. 2.1). Under these conditions we expect that generic initial classical distributions (with non-zero support) will spread to cover the full surface $\mathcal{P}$ and then quickly relax close to microcanonical equilibrium. We find that the initially localised quantum states also exhibit these generic features when the quantum map is governed by parameters that produce these conditions classically.

For the non-autonomous Hamiltonian system (2.11) the total energy is not conserved, but the two invariants of motion, $\mathbf{L}^2$ and $\mathbf{S}^2$, confine the dynamics to the 4-dimensional manifold $\mathcal{P} = \mathcal{S}^2 \times \mathcal{S}^2$, which is the surface of two spheres. The corresponding microcanonical distribution is a constant on this surface, with measure (2.12), and zero elsewhere. From this distribution we can calculate microcanonical equilibrium values for low order moments, where, for example, $\{L_z\} = (4\pi)^{-2} \int_{\mathcal{P}} L_z d\mu = 0$ and $\{\Delta \mathbf{L}^2\} = \{\mathbf{L}^2\} - \{\mathbf{L}\}^2 = |\mathbf{L}|^2$. The symbols $\{\cdot\}$ denote a microcanonical average.

To give a sense of the accuracy of the correspondence between the classical ensemble and the quantum dynamics in Fig. 3.2, we show a direct comparison of the dynamics of the quantum expectation value $\langle \tilde{L}_z \rangle$ with $l = 154$ and the classical distribution average $\langle \tilde{L}_z \rangle_c$ for an initial coherent state and corresponding classical distribution centered at $\vec{\theta} = (45^o, 70^o, 135^o, 70^o)$. To guide the eye in this figure we have drawn lines connecting the stroboscopic points of the mapping equations. The quantum expectation value exhibits essentially the same dynamics as the classical Liouville average, not only at early times, that is, in the initial Ehrenfest regime [7, 57], but for times well into the equilibrium regime where the classical moment $\langle L_z \rangle$ has relaxed close to the microcanonical equilibrium value $\{L_z\} = 0$. We have also provided results for a single trajectory launched from the same initial condition in order to emphasize the qualitatively distinct behaviour it exhibits.

In Fig. 3.3 we show the exponential growth of the normalized quantum and classical variances on a semilog plot for the same set of parameters and quantum numbers. Numerical

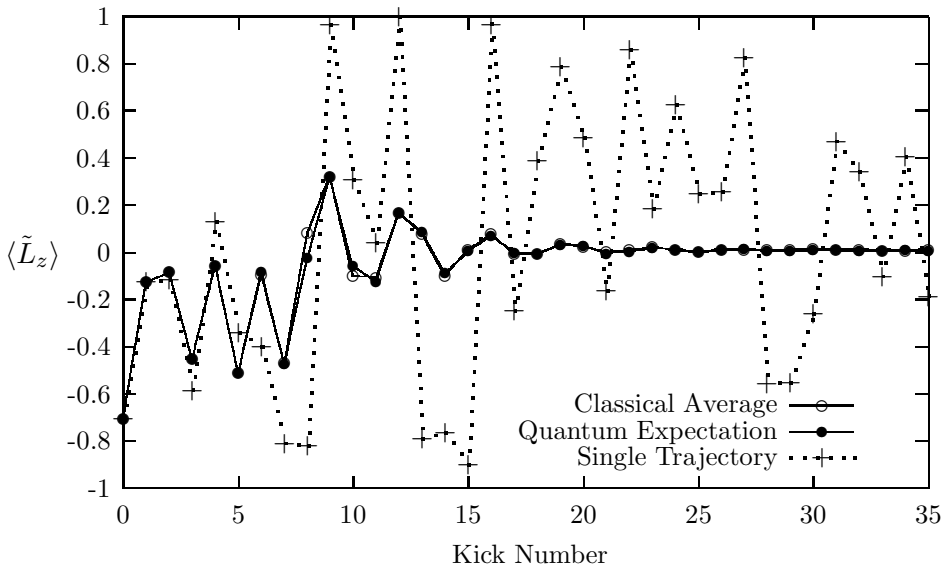

Figure 3.2: Comparison of quantum expectation value and corresponding classical average $\langle L_z \rangle_c$ in the regime of global chaos $\gamma = 2.835$ and $r \simeq 1.1$ with $l = 154$ and initial condition $\vec{\theta}_o = (45^o, 70^o, 135^o, 70^o)$. The points of the stroboscopic map are connected with lines to guide the eye. The quantum expectation value and the Liouville average exhibit esentially the same rate of relaxation to microcanonical equilibrium, a behaviour which is qualitatively distinct from that of the single trajectory.

data for (a) correspond to initial condition $\vec{\theta}(0) = (20^o, 40^o, 160^o, 130^o)$ and those for (b) correspond to $\vec{\theta}(0) = (45^o, 70^o, 135^o, 70^o)$. As in the mixed regime case, the quantum-classical differences are nearly imperceptible on the scale of the figure, and the differences between the quantum and classical variance growth rates are many orders of magnitude smaller than the small differences in the growth rate arising from the different initial conditions.

In contrast with the mixed regime case, in this regime of global chaos the prediction (3.1) with $\lambda_w = \lambda_L = 0.45$ now serves as a much better approximation to the exponential growth rate of the quantum variance, and associated relaxation rate of the quantum and classical states. In this regime the exponent λ_w is also much larger than in the mixed regime case due to the stronger degree of classical chaos. As a result, the initially localised quantum and classical distributions saturate at system size much sooner.

It is useful to apply (3.1) to estimate the time-scale at which the quantum (and classical) distributions saturate at system size. From the condition $\Delta\tilde{\mathbf{L}}^2(t_{sat}) \simeq 1$ and using (3.1) we

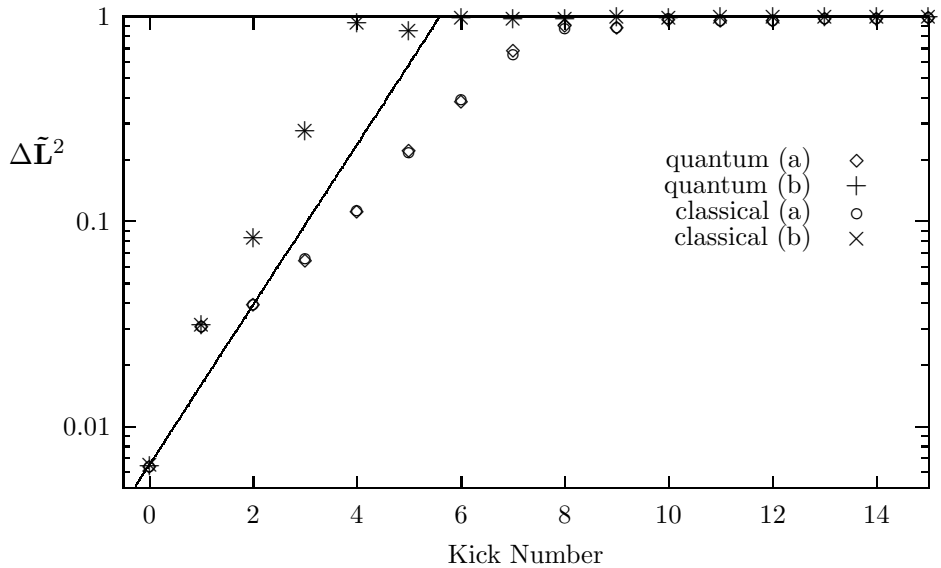

Figure 3.3: Growth of normalized quantum and classical variances in the regime of global chaos, $\gamma = 2.835$ and $r \simeq 1.1$ with l=154, for the two initial conditions cited in the text. Quantum-classical differences are nearly imperceptible on this scale. In this regime the largest Lyapunov exponent $\lambda_L = 0.45$ provides a much better estimate of the initial variance growth rate.

obtain,

$$t_{sat} \simeq (2\lambda_w)^{-1} \ln(l) \tag{3.2}$$

which serves as an estimate of this characteristic time-scale. In the regimes for which the full surface $\mathcal{P}$ is predominately chaotic, we find that the actual exponential growth rate of the width of the quantum state, λ_w, is well approximated by the largest Lyapunov exponent λ_L. For $a = 5$ and $r = 1.1$, the approximation $\lambda_w \simeq \lambda_L$ holds for coupling strengths $\gamma > 2$, for which more than 99% of the surface $\mathcal{P}$ is covered by one connected chaotic zone (see Fig. 2.1).

By comparing the quantum probability distribution to its classical counterpart, we can learn much more about the relaxation properties of the quantum dynamics. In order to compare each m_l value of the quantum distribution, $P_z(m_l)$, with a corresponding piece of the continuous classical marginal probability distribution,

$$P_c(L_z) = \iiint d\tilde{S}_z d\phi_s d\phi_l \; \rho_c(\theta_s, \phi_s, \theta_l, \phi_l), \tag{3.3}$$

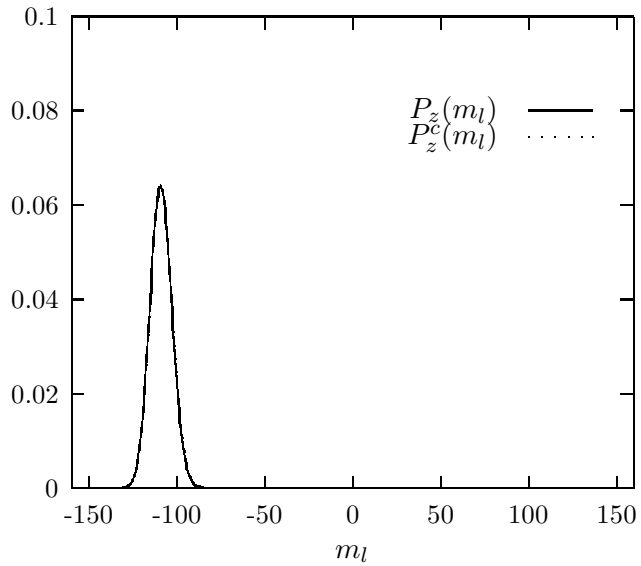

Figure 3.4: Initial probability distributions for L_z for $\vec{\theta}(0) = (45^o, 70^o, 135^o, 70^o)$ with $l = 154$. The quantum and classical distributions are indistinguishable on the scale of the figure.

we discretize the latter into $2j + 1$ bins of width $\hbar = 1$. This procedure produces a discrete classical probability distribution $P_z^c(m_l)$ that prescribes the probability of finding the spin component L_z in the interval $[m_l + 1/2, m_l - 1/2]$ along the z-axis.

To illustrate the time-development of these distributions we compare the quantum and classical probability distributions for three successive values of the kick number n, using the same quantum numbers and initial condition as in Fig. 3.2. In Fig. 3.4 the initial quantum and classical states are both well-localised and nearly indistinguishable on the scale of the figure. At time $n = 6 \simeq t_{sat}$, shown in Fig. 3.5, both distributions have grown to fill the accessible phase space. It is at this time that the most significant quantum-classical discrepancies appear.

For times greater than t_{sat}, however, these emergent quantum-classical discrepencies do not continue to grow, since both distributions begin relaxing towards equilibrium distributions. Since the dynamics are confined to a *compact* phase space, and in this parameter regime the remnant KAM tori fill a negligibly small fraction of the kinematicaly accessible phase space, we might expect the classical equilibrium distribution to be very close to

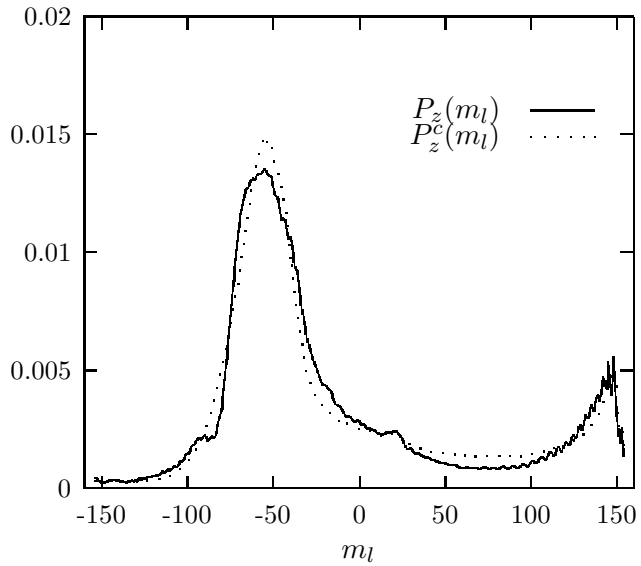

Figure 3.5: Same as Fig. 3.4 but the states have evolved to $n = 6$ in the regime of global chaos $\gamma = 2.835$ and $r \simeq 1.1$. Both the quantum and classical distribution have spread to system dimension and exhibit their largest differences on this saturation time-scale.

the microcanonical distribution. Indeed such relaxation close to microcanonical equilibrium is apparent for both the quantum and the classical distribution at very early times, as demonstrated in Fig. 3.6, corresponding to $n = 15$.

Thus the signature of a classically hyperbolic flow, namely, the exponential relaxation of an arbitrary distribution (with non-zero measure) to microcanonical equilibrium [30], holds to good approximation in this model in a regime of global chaos. More suprisingly, this classical signature is manifest also in the dynamics of the quantum distribution. In the quantum case, however, as can be seen in Fig. 3.6, the probability distribution is subject to small irreducible time-dependent fluctuations about the classical equilibrium. We examine these quantum fluctuations in detail Chapter 4.

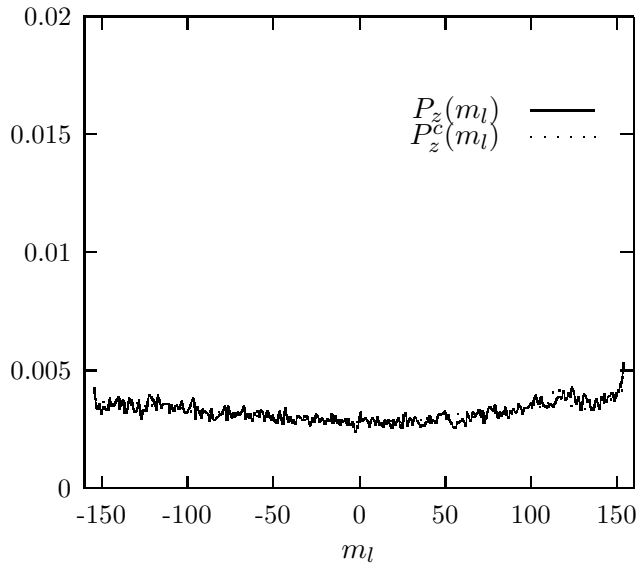

Figure 3.6: Same as Fig. 3.5, but for $n = 15$. Both quantum and classical distributions have relaxed close to the microcanonical equilibrium.

3.3 Time-Domain Characteristics of Quantum-Classical Differences

We consider the time dependence of quantum-classical differences defined along the z-axis of the spin $\mathbf{L}$,

$$\delta L_z(n) = |\langle L_z(n)\rangle - \langle L_z(n)\rangle_c|, \tag{3.4}$$

at the stroboscopic times $t = n$. In Fig. 3.7 we compare the time-dependence of $\delta L_z(n)$ on a semi-log plot for a chaotic state (filled circles), with $\vec{\theta}(0) = (20^o, 40^o, 160^o, 130^o)$, and a regular state (open circles), $\vec{\theta}(0) = (5^o, 5^o, 5^o, 5^o)$, evolved using the same mixed regime parameters ($\gamma = 1.215$ and $r \simeq 1.1$) and quantum numbers ($l = 154$) as in Fig. 3.1.

We are interested in the behaviour of the upper envelope of the data in Fig. 3.7. For the regular case, the upper envelope of the quantum-classical differences grows very slowly, as some polynomial function of time. For the chaotic case, on the other hand, at early times the difference measure (3.4) grows exponentially until saturation around $n = 15$, which is well before reaching system dimension, $|\mathbf{L}| \simeq l = 154$. After this time, which we denote t^*, the quantum-classical differences exhibit no definite growth, and fluctuate about the

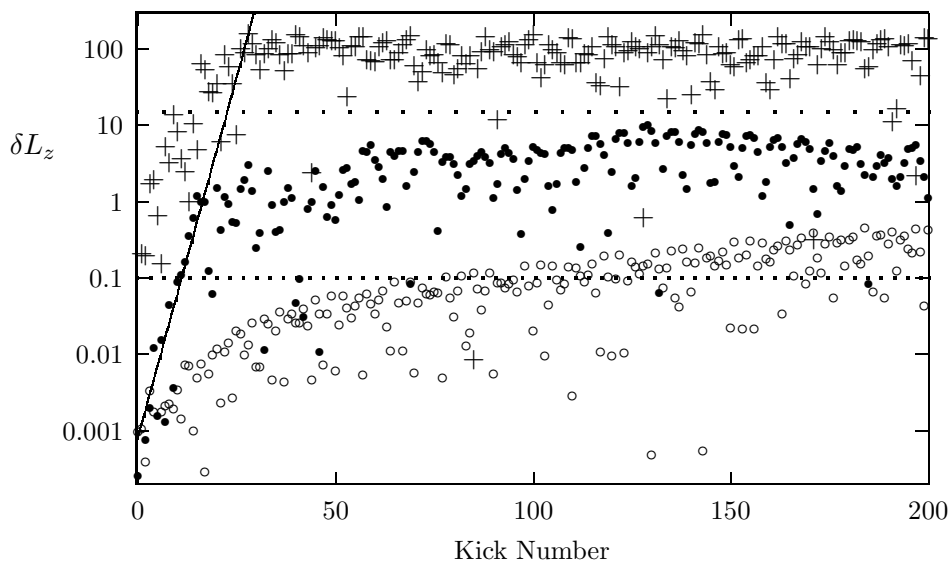

Figure 3.7: Time-dependence of quantum-classical differences in a regular zone (open circles) and a chaotic zone (filled circles) of mixed regime ($\gamma = 1.215$ and $r \simeq 1.1$) with $l = 154$. For the chaotic state, $\delta L_z = |\langle L_z \rangle - \langle L_z \rangle_c|$ is contrasted with the Ehrenfest difference $|\langle L_z \rangle - L_z|$ between the quantum expectation value and a single trajectory (plus signs), which grows until saturation at system dimension. The solid line corresponds to (3.5) using $\lambda_{qc} = 0.43$. The horizontal lines indicate two different values of the difference tolerance p which may be used to determine the break-time; for $p = 0.1$ (dotted line) t_b occurs on a logarithmic time-scale, but for $p = 15.4$ (sparse dotted line) t_b is not defined over numerically accessible time-scales.

equilibrium value $\delta L_z \sim 1 \ll |\mathbf{L}|$. In Fig. 3.7 we also include data for the time-dependence of the Ehrenfest difference $|\langle L_z \rangle - L_z|$, which is defined as the difference between the quantum expectation value and the dynamical variable of a single trajectory initially centered on the quantum state. In contrast to δL_z, the rapid growth of the Ehrenfest difference continues until saturation at the system dimension.

In Fig. 3.8 we compare the time-dependence of the quantum-classical differences in the case of the chaotic initial condition $\vec{\theta}(0) = (20^o, 40^o, 160^o, 130^o)$ for quantum numbers $l = 22$ (filled circles) and $l = 220$ (open circles), using the same parameters as in Fig. 3.7. This demonstrates the remarkable fact that the exponential growth terminates when the difference measure reaches an essentially fixed magnitude ($\delta L_z \sim 1$ as for the case $l = 154$),

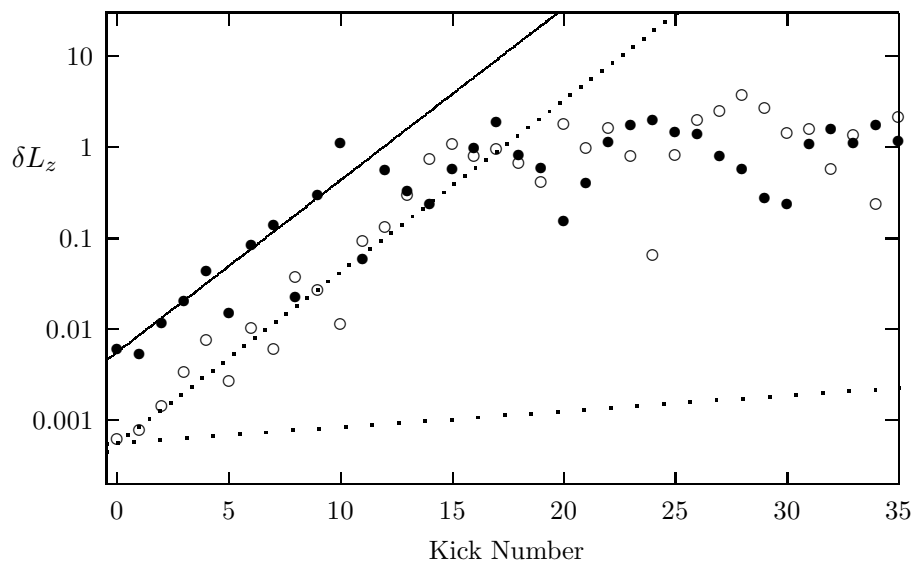

Figure 3.8: Growth of the quantum-classical difference δL_z in the chaotic zone of a mixed regime, $\gamma = 1.215$ and $r \simeq 1.1$, with $l = 22$ (filled circles) and $l = 220$ (open circles). For $l = 220$ the exponential growth rate (3.5) is plotted using the classical Lyapunov exponent, $\lambda_L = 0.04$ (sparse dotted line), and for both l values (3.5) is plotted using the exponent $\lambda_{qc} = 0.43$ (solid line for $l = 22$, dotted line for $l = 220$), which is obtained from a fit of (3.6) to the corresponding break-time data in Fig. 3.10.

although the system dimension differs by an order of magnitude in the two cases.

In Fig. 3.9 we consider the growth of the quantum-classical difference measure $\delta L_z(n)$ in a regime of global chaos, for $l = 154$, and using the same set of parameters as those examined in Fig. 3.3 ($\gamma = 2.835$ and $r \simeq 1.1$). Again the upper envelope of the difference measure $\delta L_z(n)$ exhibits exponential growth at early times, though in this regime of global chaos the exponential growth persists only for a very short duration before saturation at $t^* \simeq 6$. The initial condition $\vec{\theta}(0) = (20^o, 40^o, 160^o, 130^o)$ is a typical case (filled circles), where, as seen for the mixed regime parameters, the magnitude of the difference at the end of the exponential growth phase saturates at the value $\delta L_z(t^*) \simeq 1$, which does not scale with the system dimension (see Fig. 3.11). The initial condition $\vec{\theta}(0) = (45^o, 70^o, 135^o, 70^o)$ (open circles) leads to an anomolously large deviation at the end of the exponential growth phase, $\delta L_z(t^*) \simeq 10$, though still small relative to the system dimension $|\mathbf{L}| \simeq 154$. This deviation is transient however, and at later times the magnitude of quantum-classical differences

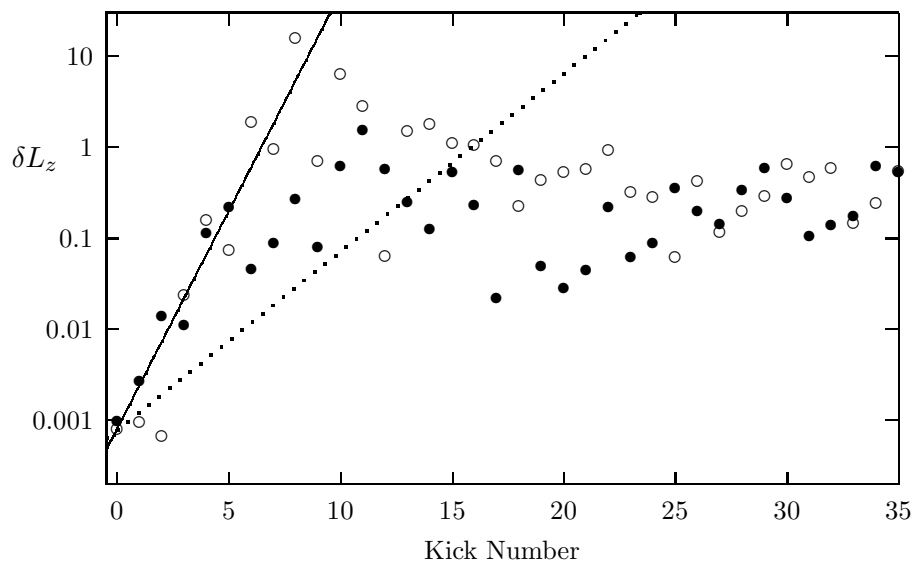

Figure 3.9: Growth of quantum-classical differences in the regime of global chaos, $\gamma = 2.835$ and $r \simeq 1.1$, with $l = 154$, for the two initial conditions cited in text. The exponential growth rate (3.5) is plotted using the classical Lyapunov exponent, $\lambda_L = 0.45$ (dotted line), and the exponent $\lambda_{qc} = 1.1$ (solid line), which is obtained from a fit of (3.6) to the corresponding break-time data in Fig. 3.10.

fluctuates about the equilibrium value $\delta L_z \sim 1$. The quantum-classical differences are a factor of $1/l$ smaller than typical differences between the quantum expectation value and the single trajectory, which are of order system dimension (see Fig. 3.2) as in the mixed regime case.

In all cases where the initial quantum and classical states are launched from a chaotic zone we find that the initial time-dependence of quantum-classical differences compares favorably with the exponential growth ansatz,

$$\delta L_z(n) \simeq \frac{1}{8l} \exp(\lambda_{qc} n) \qquad \text{for} \quad n < t^*, \tag{3.5}$$

where the exponent λ_{qc} is a new exponent subject to numerical measurement [11]. Since contributions from the initial differences in other mismatched moments will generally mix under the dynamical flow, it is appropriate to consider an effective initial difference for the prefactor in (3.5). The prefactor $1/8l$ is obtained by accounting for the initial contributions from the 3 cartesian components, $[\delta^2 L_x(0) + \delta^2 L_y(0) + \delta^2 L_z(0)]^{1/2} = 1/8l$.

We are interested in whether the Lyapunov exponent λ_L is a good approximation to λ_{qc}. In Fig. 3.8 we plot (3.5) with $\lambda_{qc} = \lambda_L = 0.04$ (dotted line) for $l = 220$. Clearly the largest Lyapunov exponent severly underestimates the exponential growth rate of the quantum-classical differences, in this case by more than an order of magnitude. The growth rate of the state width, $\lambda_w = 0.13$, is also several times smaller than the initial growth rate of the quantum-classical differences. In the case of Fig. 3.9, corresponding to a regime of global chaos with a much larger Lyapunov exponent, we plot (3.5) with $\lambda_{qc} = \lambda_L = 0.45$ (dotted line), demonstrating that, in this regime too the largest Lyapunov exponent underestimates the initial growth rate of the quantum-classical difference measure $\delta L_z(n)$.

We also find, from inspection of our results, that the time t^* at which the exponential growth (3.5) terminates can be estimated from t_{sat}, the time-scale on which the distributions saturate at or near system size (3.2). In the case of the chaotic initial condition of Fig. 3.1, for which $\gamma = 1.215$, visual inspection of the figure suggests that $t_{sat} \simeq 18$. This should be compared with Fig. 3.7, where the exponential growth of $\delta L_z(n)$ ends rather abruptly at $t^* \simeq 15$. In Fig. 3.3, corresponding to a regime of global chaos ($\gamma = 2.835$), the variance growth saturates much earlier, around $t_{sat} \simeq 6$ for both initial conditions. From Fig. 3.9 it is apparent that in this regime $t^* \simeq 6$. As we increase γ further, we find that the exponential growth phase of quantum-classical differences $\delta L_z(n)$ is shortened, lasting only until the corresponding quantum and classical distributions saturate at system size. For $\gamma \simeq 12$, with $\lambda_L \simeq 1.65$, the chaos is sufficiently strong that the initial coherent state for $l = 154$ spreads to cover $\mathcal{P}$ within a single time-step. Similarly the initial difference measure $\delta L_z(0) \simeq 0.001$ grows to the magnitude $\delta L_z(1) \simeq 1$ within a single time-step and subsequently fluctuates about that equilibrium value. We have also inspected the variation of t^* with the quantum numbers and found it to be consistent with the logarithmic dependence of t_{sat} in (3.2).

3.4 Correspondence Scaling in the Macroscopic Limit

We have assumed in (3.5) that the exponent λ_{qc} is independent of the quantum numbers. A convenient way of confirming this, and also estimating the numerical value of λ_{qc}, is by means of a break-time measure. The break-time is determined from the time $t_b(l, p)$ at which quantum-classical differences exceed some tolerance p, which does not scale with the system size for each quantum model. The classical parameters and initial condition are held

fixed. Setting $\delta L_z(t_b) = p$ in (3.5), we obtain t_b in terms of p, l and λ_{qc},

$$t_b \simeq \lambda_{qc}^{-1} \ln(8\, p\, l) \qquad \textit{provided} \qquad p < \mathcal{O}(1). \tag{3.6}$$

The restriction $p < \mathcal{O}(1)$, which plays a crucial role in limiting the robustness of the break-time measure (3.6), is explained and motivated further below.

The explicit form we have obtained for the argument of the logarithm in (3.6) is a direct result of our estimate that the initial quantum-classical differences arising from the Cartesian components of the spin provide the dominant contribution to the prefactor of the exponential growth ansatz (3.5). Differences in the mismatched higher order moments, as well as intrinsic differences between the quantum dynamics and classical dynamics, may also contribute to this effective prefactor. We have checked that the initial value $\delta L_z(0) \simeq 1/8l$ is an adequate estimate by comparing the intercept of the quantum-classical data on a semilog plot with the prefactor of (3.5) for a variety of l values (see *e.g.* Fig. 3.8).

In Fig. 3.10 we examine the scaling of the break-time for l values ranging from 11 to 220 and with fixed tolerance $p = 0.1$. The break-time can assume only the integer values $t = n$ and thus the data exhibits a step-wise behaviour. For the mixed regime parameters, $\gamma = 1.215$ and $r \simeq 1.1$ (filled circles), with initial condition $\vec{\theta}(0) = (20^o, 40^o, 160^o, 130^o)$, a non-linear least squares fit to (3.6) gives $\lambda_{qc} = 0.43$. This fit result is plotted in the figure as a solid line. The close agreement between the data and the fit provides good evidence that the quantum-classical exponent λ_{qc} is independent of the quantum numbers. To check this result against the time-dependent $\delta L_z(n)$ data, we have plotted the exponential curve (3.5) with $\lambda_{qc} = 0.43$ in Fig. 3.7 using a solid line and in Fig. 3.8 using a solid line for $l = 22$ and a dotted line for $l = 220$. The exponent obtained from fitting (3.6) serves as an excellent approximation to the initial exponential growth (3.5) of the quantum-classical differences in each case.

In Fig. 3.10 we also plot break-time results for the global chaos case $\gamma = 2.835$ and $r \simeq 1.1$ (open circles) with initial condition $\vec{\theta}(0) = (45^o, 70^o, 135^o, 70^o)$. In this regime the quantum-classical differences grow much more rapidly and, consequently, the break-time is very short and remains nearly constant over this range of computationally accessible quantum numbers. Due to this limited variation, in this regime we can not confirm (3.6), although the data are consistent with the predicted logarithmic dependence on l. Moreover, the break-time results provide an effective method for estimating λ_{qc} if we assume that (3.6) holds. The same fit procedure as detailed above yields the quantum-classical exponent

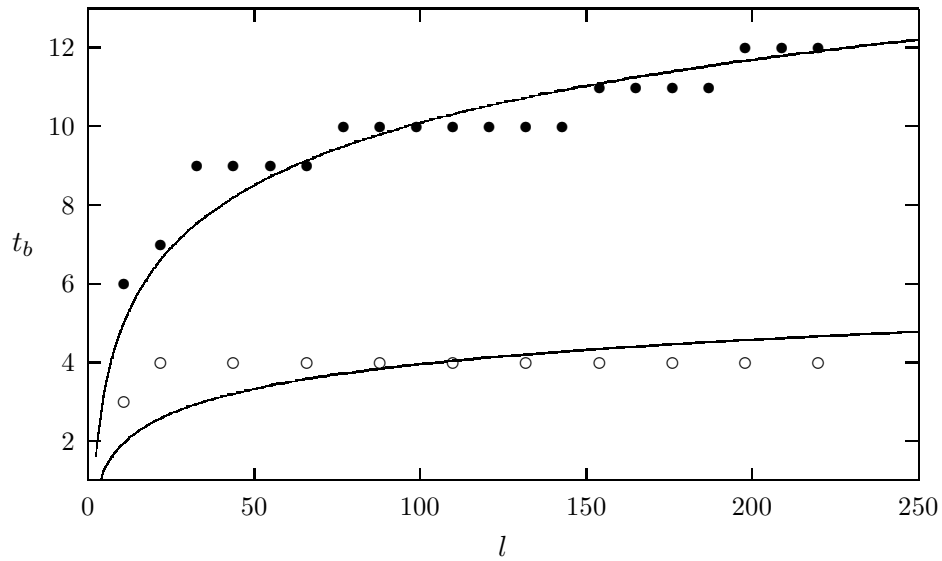

Figure 3.10: Scaling of the break-time using tolerance $p = 0.1$ as a function of increasing quantum number for the mixed regime parameters $\gamma = 1.215$ and $r \simeq 1.1$ with $\vec{\theta}(0) = (20^o, 40^o, 160^o, 130^o)$ (filled circles) and for the global chaos parameters $\gamma = 2.835$ and $r \simeq 1.1$ with $\vec{\theta}(0) = (45^o, 70^o, 135^o, 70^o)$ (open circles). We also plot the results of fits to the log rule (3.6), which produced exponents $\lambda_{qc} = 0.43$ for $\gamma = 1.215$ and $\lambda_{qc} = 1.1$ for $\gamma = 2.835$.

$\lambda_{qc} = 1.1$. This fit result is plotted in Fig. 3.10 as a solid line. More importantly, the exponential curve (3.5), plotted with fit result $\lambda_{qc} = 1.1$, can be seen to provide very good agreement with the initial growth rate of Fig. 3.9 for either initial condition, as expected.

In the mixed regime ($\gamma = 1.215$), the quantum-classical exponent $\lambda_{qc} = 0.43$ is an order of magnitude greater than the largest Lyapunov exponent $\lambda_L = 0.04$ and about three times larger than the growth rate of the width $\lambda_w = 0.13$. In the regime of global chaos ($\gamma = 2.835$) the quantum-classical exponent $\lambda_{qc} = 1.1$ is a little more than twice as large as the largest Lyapunov exponent $\lambda_L = 0.45$.

The condition $p < \mathcal{O}(1)$ is a very restrictive limitation on the domain of application of the log break-time (3.6) and it is worthwhile to explain its significance. In the mixed regime case of Fig. 3.7, with $l = 154$, we have plotted the tolerance values $p = 0.1$ (dotted line) and $p = 15.4$ (sparse dotted line). The tolerance $p = 0.1$ is exceeded at $t = 11$, while the quantum-classical differences are still growing exponentially, leading to a log break-time

for this tolerance value. For the tolerance $p = 15.4 \ll |\mathbf{L}|$, on the other hand, the break-time does not occur on a measurable time-scale, whereas according to the logarithmic rule (3.6), with $l = 154$ and $\lambda_{qc} = 0.43$, we should expect a rather short break-time $t_b \simeq 23$. Consequently the break-time (3.6), applied to delimiting the end of the Liouville regime, is not a robust measure of quantum-classical correspondence.

Our definition of the break-time (3.6) requires holding the tolerance p fixed as the system size increases (and not as a fraction of the system dimension as in [54]) when comparing systems with different quantum numbers. Had we chosen to compare systems using a fixed relative tolerance, f, then the break-time would be of the form $t_b \simeq \lambda_{qc}^{-1} \ln(8\ f\ l^2)$ and subject to the restriction $f < \mathcal{O}(1/l)$. Since $f \to 0$ in the classical limit, this form emphasizes that the log break-time applies only to differences that are vanishing fraction of the system dimension in that limit.

Although we have provided numerical evidence (in Fig. 3.8) of one mixed regime case in which the largest quantum-classical differences occuring at the end of the exponential growth period remain essentially constant for varying quantum numbers, $\delta L_z(t^*) \sim \mathcal{O}(1)$, we find that this behaviour represents the typical case for all parameters and initial conditions which produce chaos classically. To demonstrate this behaviour we consider the scaling (with increasing quantum numbers) of the maximum values attained by $\delta L_z(n)$ over the first 200 kicks, δL_z^{max}. Since $t^* \ll 200$ over the range of l values examined, the quantity δL_z^{max} is a rigorous upper bound for $\delta L_z(t^*)$.

In Fig. 3.11 we compare δL_z^{max} for the two initial conditions of Fig. 3.9 and using the global chaos parameters ($\gamma = 2.835$, $r \simeq 1.1$). The filled circles in Fig. 3.11 correspond to the initial condition $\vec{\theta}(0) = (20^o, 40^o, 160^o, 130^o)$. As in the mixed regime, the maximum deviations exhibit little or no scaling with increasing quantum number. This is the typical behaviour that we have observed for a variety of different initial conditions and parameter values. These results motivate the generic rule,

$$\frac{\delta L_z(t^*)}{\sqrt{l(l+1)}} \leq \frac{\delta L_z^{max}}{\sqrt{l(l+1)}} \sim \mathcal{O}(1/l). \tag{3.7}$$

Thus the magnitude of quantum-classical differences reached at the end of the exponential growth regime, expressed as a fraction of the system dimension, approaches zero in the classical limit.

However, for a few combinations of parameters and initial conditions we do observe a 'transient' discrepancy peak occuring at $t \simeq t^*$ that exceeds $\mathcal{O}(1)$. This peak is quickly

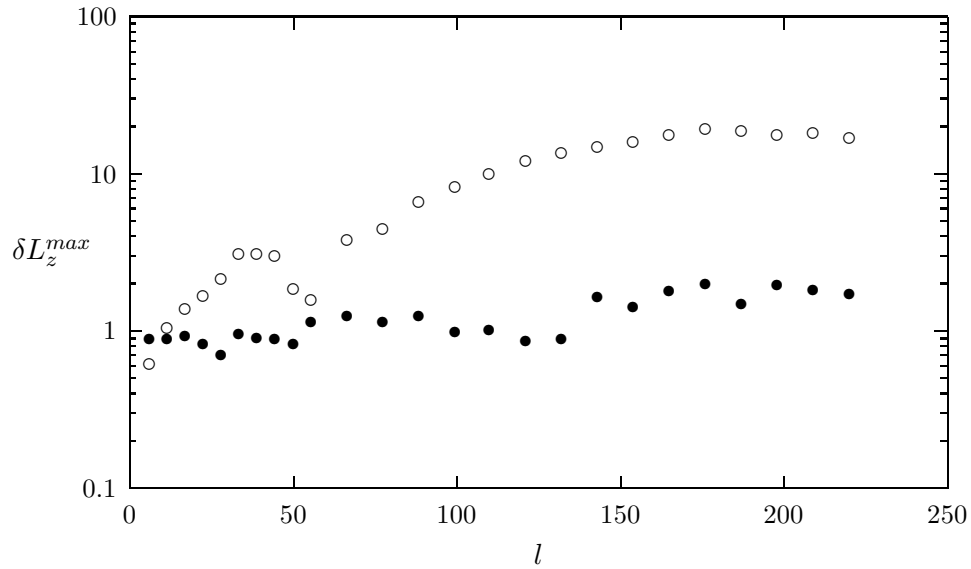

Figure 3.11: Maximum quantum-classical difference occuring over the first 200 kicks in the regime of global chaos ($\gamma = 2.835$, $r \simeq 1.1$) plotted against increasing quantum number. These maximum values provide an upper bound on $\delta L_z(t^*)$ for each l. The data corresponding to the initial condition $\vec{\theta}(0) = (20^o, 40^o, 160^o, 130^o)$ (filled circles) represent a typical case in which the maximum quantum-classical differences do not vary significantly with l. The large deviations observed for the initial condition $\vec{\theta}(0) = (45^o, 70^o, 135^o, 70^o)$ (open circles) are an exceptional case, with maximum differences growing rapidly for small quantum numbers but tending asymptotically toward independence of l. These curves provide an upper bound on the tolerance values p for which the break-time measure scales logarithmically with l.

smoothed away by the subsequent relaxation of the quantum and classical distributions. This peak is apparent in Fig. 3.9 (open circles), corresponding to the most conspicuous case that we have identified. This case is apparent as a small deviation in the normalized data of Fig. 3.2. The scaling of the magnitude of this peak with increasing l is plotted with open circles in Fig. 3.11. The magnitude of the peak initially increases rapidly but appears to become asymptotically independent of l. The other case that we have observed occurs for the classical parameters $\gamma = 2.025$, with $r \simeq 1.1$ and $a = 5$, and with initial condition $\vec{\theta}(0) = (20^o, 40^o, 160^o, 130^o)$. We do not understand the mechanism leading to such transient peaks, although they are of considerable interest since they provide the most prominent examples of quantum-classical discrepancy that we have observed.

3.5 Discussion

In this study of a non-integrable model of two interacting spins we have characterized the correspondence between quantum expectation values and classical ensemble averages for intially localised states. We have demonstrated that in chaotic states the quantum-classical differences initially grow exponentially with an exponent λ_{qc} that is consistently larger than the largest Lyapunov exponent. In a study of the moments of the Henon-Heiles system, Ballentine and McRae [11, 12] have also shown that quantum-classical differences in chaotic states grow at an exponential rate with an exponent larger than the largest Lyapunov exponent. This exponential behaviour appears to be a generic feature of the short-time dynamics of quantum-classical differences in chaotic states.

Since we have studied a spin system, we have been able to solve the quantum problem without truncation of the Hilbert space, subject only to numerical roundoff, and thus we are able to observe the dynamics of the quantum-classical differences well beyond the Ehrenfest regime. We have shown that the exponential growth phase of the quantum-classical differences terminates well before these differences have reached system dimension. We find that the time-scale at which this occurs can be estimated from the time-scale at which the distribution widths approach the system dimension, $t_{sat} \simeq (2\lambda_w)^{-1} \ln(l)$ for initial minimum uncertainty states. Due to the close correspondence in the growth rates of the quantum and classical distributions, this time-scale can be estimated from the classical physics alone. This is useful because the computational complexity of the problem does not grow with the system action in the classical case. Moreover, we find that the exponent λ_w can be approximated by the largest Lyapunov exponent when the kinematic surface is predominantly chaotic.

We have demonstrated that the exponent λ_{qc} governing the initial growth rate of the quantum-classical differences is independent of the quantum numbers, and that the effective prefactor to this exponential growth decreases as $1/l$. These results imply that a log break-time rule (3.6) delimits the dynamical regime of Liouville correspondence. However, the exponential growth of quantum-classical differences persists only for short times and small differences, and thus this log break-time rule applies only in a similarly restricted domain. In particular, we have found that the magnitude of the differences occuring at the end of the initial exponential growth phase does not scale with the system dimension. A typical magnitude for these differences, relative to the system dimension, is $\mathcal{O}(1/l)$. Therefore, $\log(l)$

break-time rules characterizing the end of the Liouville regime are not robust, since they apply to quantum-classical differences only in a restricted domain, *i.e.* to relative differences that are smaller than $\mathcal{O}(1/l)$.

This restricted domain effect does not arise for the better known log break-time rules describing the end of the Ehrenfest regime [7, 15, 54]. The Ehrenfest log break-time remains robust for arbitrarily large tolerances since the corresponding differences grow roughly exponentially until saturation at the system dimension [46, 47]. Consequently, a $\log(l)$ break-time indeed implies a *breakdown* of Ehrenfest correspondence. However, the logarithmic break-time rule characterizing the end of the Liouville regime does not imply a breakdown of Liouville correspondence because it does not apply to the observation of quantum-classical discrepancies larger than $\mathcal{O}(1/l)$. The appearance of residual $\mathcal{O}(1/l)$ quantum-classical discrepancies in the description of a macroscopic body is, of course, consistent with quantum mechanics having a proper classical limit.

We have found, however, that for certain exceptional combinations of parameters and initial conditions there are relative quantum-classical differences occuring at the end of the exponential growth phase that can be larger than $\mathcal{O}(1/l)$, though still much smaller than the system dimension. In absolute terms, these transient peaks seem to grow with the system dimension for small quantum numbers but become asymptotically independent of the system dimension for larger quantum numbers. Therefore, even in these least favorable cases, the *fractional* differences between quantum and classical dynamics approach zero in the limit $l \to \infty$. This vanishing of fractional differences is sufficient to ensure a classical limit for our model.

Finally, contrary to the results found in the present model, it has been suggested that a log break-time delimiting the Liouville regime implies that certain isolated macroscopic bodies in chaotic motion should exhibit non-classical behaviour on observable time scales. However, since such non-classical behaviour is not observed in the chaotic motion of macroscopic bodies, it is argued that the observed classical behaviour emerges from quantum mechanics only when the quantum description is expanded to include interactions with the many degrees-of-freedom of the ubiquitous environment [97, 99]. (This effect, called decoherence, rapidly evolves a pure system state into a mixture that is essentially devoid of non-classical properties.) However, in our model the classical behaviour emerges in the macroscopic limit of an isolated few degree-of-freedom quantum system that is described by a pure state and subject only to unitary evolution. Quantum-classical correspondence at

both early and late times arises in spite of the log break-time because this break-time rule applies only when the quantum-classical difference threshold is chosen smaller than $\mathcal{O}(\hbar)$. In this sense we find that the decoherence effects of the environment are not necessary for correspondence in the macroscopic limit. Of course the effect of decoherence may be experimentally significant in the quantum and mesoscopic domains, but it is not required *as a matter of principle* to ensure a classical limit.

Chapter 4

Correspondence for the Probability Distributions

This chapter is taken from Emerson and Ballentine [36].

4.1 Introduction

The study of chaos in quantum dynamics has led to differing views on the conditions required for demonstrating quantum-classical correspondence [7, 56]. Moreover, the criteria by which this correspondence should be measured have also been a subject of some controversy [96, 23, 97]. While much of the earlier work on this topic is concerned with characterizing the degree of correspondence between quantum expectation values and classical dynamical variables [15, 48, 54], the more recent approach is to focus on differences between the properties of quantum states and associated classical phase space densities evolved according to Liouville's equation [7, 57, 46, 79, 11, 35].

Several authors have examined quantum-classical correspondence by considering the effects of interactions with a stochastic environment [50, 58, 52], a process sometimes called *decoherence*. While this process may improve the degree of quantum-classical correspondence for fixed quantum numbers, it has been further suggested that the limit of large quantum numbers is inadequate for correspondence, and that decoherence *must* be taken into account to generate classical appearances from quantum theory; this view has been

argued to apply even in the case of macroscopic bodies that are described initially by well-localised states, provided their classical motion is chaotic [97, 98, 99]. In this chapter we examine how the degree of correspondence with Liouville dynamics scales specifically in the limit of *large* quantum numbers. This "classical limit" is distinct from a "thermodynamic limit", that is, a limit involving *many* quantum numbers.

The degree of Liouville correspondence has been characterized previously by studying the differences between the means and variances of the dynamical variables [7, 57, 79, 11, 35, 12]. This involves a comparison of quantum expectation values and classical ensemble averages. However, these low-order moments give only crude information about the differences between the quantum and classical states. Specifically, the quantum state may exhibit coarse structure which differs significantly from the classical state although the means and variances (for some simple observabes) are nearly the same for the quantum and classical states. Moreover, much of the previous work was concerned with correspondence at early times, or more precisely, in the Ehrenfest regime when the states are narrow compared to system dimensions [11, 35].

Another approach is to identify quantum-classical differences with differences between the Wigner quasi-distribution and the classical phase space density [56]. This approach is objectionable because the Wigner quasi-distribution may take on negative values and therefore may not be interpreted as a "classically observable" phase space distribution. It is possible to consider instead smoothed quantum phase space distributions, but in this case the residual quantum-classical differences still do not have clear experimental significance.

In this chapter, we characterize the degree of quantum-classical correspondence by comparing quantum probability distributions for dynamical variables with the corresponding classical marginal distributions for these dynamical variables. These are well-defined classical observables that describe the distribution of outcomes upon measurement of the given dynamical variable. We are interested in the differences that arise on a *fine* scale and therefore characterize the typical quantum-classical deviations that arise in bins of width $\hbar$.

The dynamics are generated by the model of interacting spins described in Chapter 2. The Hilbert space is finite dimensional so no artificial truncation of the state is required. The quantum time-evolution is unitary and the classical motion is volume-preserving (symplectic). In the case of classically chaotic motion, we follow initially localised states until they have evolved well beyond the relaxation time-scale of the classical density. Throughout the chapter we emphasize that the *quantum* signatures of chaos that appear in the quantum

distributions are the same as those that appear in the marginal classical distributions. In particular, the quantum relaxation rates can be accurately estimated from the Liouville dynamics of an approximately matching initial phase space density. This purely classical approximation is surprisingly accurate even for small quantum numbers, but may be most useful for the theoretical description of mesoscopic systems since the purely classical calculations do not scale with the quantum numbers.

The quantum and classical probability distributions remain close even after the states have spread to the system dimension. Specifically, in mixed regimes, the quantum distributions exhibit an equilibrium shape that reflects the details of the classical KAM surfaces. When the classical manifold is predominantly chaotic, the quantum and classical states relax close to the microcanonical state. However, in both of these chaotic regimes the equilibrium quantum distributions exhibit characteristic fluctuations away from the classical ones. We demonstrate that the standard deviation of these quantum-classical differences becomes vanishingly small in the classical limit, $\mathcal{J}/\hbar \to \infty$, where $\mathcal{J}$ is a characteristic system action.

4.2 Dynamical Behaviour of Probability Distributions

In the case of a classical mixing system, initial densities with non-zero measure are expected to spread in an increasingly uniform manner throughout the accessible phase space. The term *uniform* is meant to apply specifically in a coarse-grained sense. For some simple maps, such as the baker's map, it is possible to show that this rate of relaxation to the equilibrium configuration occurs exponentially with time [30].

The spin map we consider (2.11) is not *mixing* on the accessible classical manifold $\mathcal{P}$, but has *mixed* dynamics: depending on the system parameters, the surface $\mathcal{P}$ can generally be decomposed into regions of regular dynamics and a connected region of chaotic dynamics [35]. In parameter regimes that are predominantly chaotic, we expect behaviour on $\mathcal{P}$ that approximates that of a mixing system. In particular, initially localised Liouville densities should relax close towards the microcanonical measure at an exponential rate, on average. In this section we demonstrate that these signatures of chaos are exhibited also by the quantum dynamics. Most striking is the degree of similarity between the quantum and classical behaviours even in regimes with classically mixed dynamics.

We are interested in the behaviour of quantum probability distributions that are associated with measurements of classical dynamical variables. The quantum probability

distribution associated with the classical observable L_z is given by,

$$P_{L_z}(m_l) = \langle\psi(n)|\ R_{l,m_l}\ |\psi(n)\rangle = \mathrm{Tr}\left[\ |l,m_l\rangle\langle l,m_l|\rho^{(l)}(n)\ \right], \tag{4.1}$$

where,

$$R_{l,m_l} = 1_s \otimes |l,m_l\rangle\langle l,m_l| \tag{4.2}$$

is a projection operator onto the eigenstates of L_z, and

$$\rho^{(l)}(n) = \mathrm{Tr}^{(s)}\left[\ |\psi(n)\rangle\langle\psi(n)|\ \right], \tag{4.3}$$

is the reduced state operator for the spin $\mathbf{L}$ at time n and $\mathrm{Tr}^{(s)}$ denotes a trace over the factor space $\mathcal{H}_s$. We have written out the explicit expression (4.1) to emphasize that the probability of obtaining each m_l value is associated with a projector onto a subspace of the *factor* space $\mathcal{H}_l$.

For reasons related to this fact (which we will make clear in later sections), we are also interested in examining the probability distributions associated with components of the *total* angular momentum $\mathbf{J} = \mathbf{S} + \mathbf{L}$. The probability of obtaining a given m_j value upon measurement of J_z is given by,

$$P_{J_z}(m_j) = \sum_{m_s} |\langle\psi(n)|s,l,m_s,m_j - m_s\rangle|^2, \tag{4.4}$$

where $|s,l,m_s,m_j - m_s\rangle$ is an element of the orthonormal basis (2.2). The probability $P_{J_z}(m_j)$ is associated with a projector onto a subspace of the *full* Hilbert space $\mathcal{H}$. The dimension of each subspace is given by the number of pairs (m_s, m_l) that yield a given value of $m_j = m_s + m_l$.

The classical probability distributions associated with dynamical variables are obtained by partial integration over the accessible phase space. In the case of L_z, the continuous marginal distribution is given by,

$$P(L_z) = \int\int\int dS_z d\phi_s d\phi_l\ \rho_c(S_z, \phi_s, L_z, \phi_l), \tag{4.5}$$

where for notational convenience we have suppressed reference to the time-dependence. The marginal probability distribution for the total spin component J_z is obtained by integration subject to the constraint $S_z + L_z = J_z$,

$$P(J_z) = \int\int\int\int dS_z d\phi_s dL_z d\phi_l\ \rho_c(S_z, \phi_s, L_z, \phi_l)\ \delta(S_z + L_z - J_z). \tag{4.6}$$

These classical distributions are continuous, though their quantum counter-parts are intrinsically discrete. To construct a meaningful quantum-classical comparison it is useful to discretize the classical distrbutions by integrating the continuous probabilities over intervals of width $\hbar = 1$ centered on the quantum eigenvalues. In the case of the component L_z, the quantum probability $P_{L_z}(m_l)$ is then associated with the classical probability of finding L_z in the interval $[m_l - 1/2, m_l + 1/2]$. This is given by

$$P^c_{L_z}(m_l) = \int_{m_l-1/2}^{m_l+1/2} P(L_z). \tag{4.7}$$

Similarly, in the case of J_z, we compare each quantum $P_{J_z}(m_j)$ with the *discrete classical* probability,

$$P^c_{J_z}(m_j) = \int_{m_j-1/2}^{m_j+1/2} P(J_z). \tag{4.8}$$

In the following discussion of the numerical results we will emphasize that, for chaotic states, the steady-state shape of the quantum and classical distributions should be compared with the marginal distributions derived from the microcanonical state. Our model is non-autonomous, but the spin magnitudes are conserved. The appropriate *classical* microcanonical measure is a constant on the accessible manifold $\mathcal{P} = S^2 \times S^2$. This follows from the usual equilibrium hypothesis that all accessible microstates are equiprobable, where equiprobability is defined with respect to the invariant measure (2.12). This microcanonical density projected onto the L_z-axis produces the discrete, flat distribution,

$$P^{mc}_{L_z}(m_l) = (2l+1)^{-1}. \tag{4.9}$$

However, projected along J_z, the microcanonical distribution is not flat, but has a tent-shape,

$$\begin{aligned} P^{mc}_{J_z}(m_j) &= \frac{l+s+1-|m_j|}{(2s+1)(2l+1)} \quad \text{for} \quad |m_j| \geq l-s \\ &= \frac{1}{2l+1} \quad \text{for} \quad |m_j| \leq l-s. \end{aligned} \tag{4.10}$$

In quantum mechanics, the equiprobability hypothesis implies that the appropriate microcanonical state is an equal-weight mixture. This microcanonical state, sometimes called a random state, is proportional to the identity in the full Hilbert space $\mathcal{H} = \mathcal{H}_s \otimes \mathcal{H}_l$. It produces the same projected microcanonical distributions, *i.e.* (4.9) for L_z and (4.10) for J_z, as the classical microcanonical state.

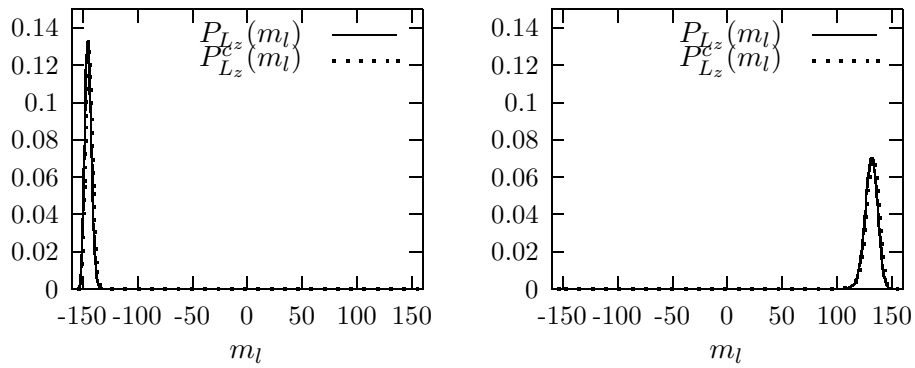

Figure 4.1: Quantum and classical probability distributions for L_z with $l = 154$ in chaotic zone of mixed regime ($\gamma = 1.215, r = 1.1, a = 5$). The dots are visible because they are shifted to the right by half of their width. The figure on the left is the initial state ($n = 0$) and that on the right is at time-step $n = 6$.

4.2.1 Mixed Regime Chaos

We consider first a classical parameter regime ($\gamma = 1.215$, $r = 1.1$, and $a = 5$) for which the kinematically accessible phase space $\mathcal{P}$ is highly mixed. The chaotic region appears to be connected (all chaotic initial conditions have the same largest Lyapunov exponent $\lambda_L = 0.04$) and covers about half of the kinematic surface. A projection of only the chaotic initial conditions onto the plane spanned by S_z and L_z reveals large regular islands surrounding the stable parallel fixed points $(\pm S_z, \pm L_z)$, with chaotic regions spreading out from the unstable anti-parallel fixed points $(\pm S_z, \mp L_z)$. A similar projection of the regular initial conditions shows points not only clustered about the parallel fixed points but also spread along the axis $\tilde{S}_z = \tilde{L}_z$.

We now consider the time-evolution of quantum and classical states concentrated in the chaotic zone near one of the unstable anti-parallel fixed points, with initial centroids directed along $\theta(0) = (20^o, 40^o, 160^o, 130^o)$. The quantum dynamics are calculated using quantum numbers $s = 140$ and $l = 154$. As shown in Fig. 4.1, at early times both the quantum distribution $P_{L_z}(m_l)$ (solid line) and the corresponding classical distribution $P^c_{L_z}(m_l)$ (dots) remain well-localised. Their initial differences are not distinguishable on the scale of the figures. (The dots are shifted to the right by half of their width.) By time-step $n = 20$ both quantum and classical distributions have broadened to the system dimension and begin to

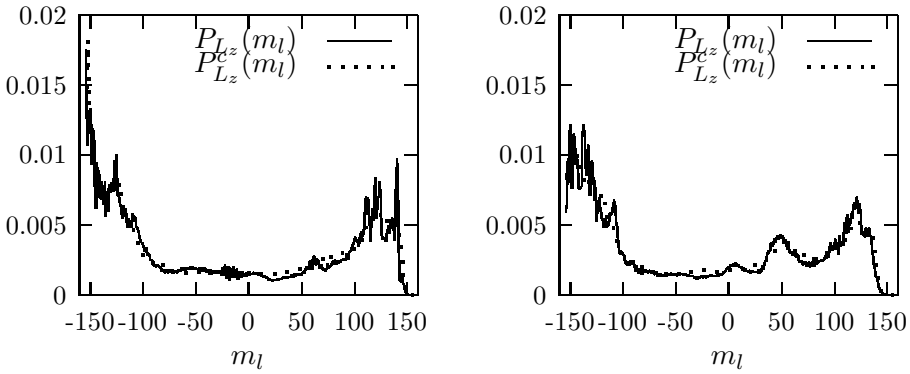

Figure 4.2: Same as Fig. 4.1 but for time-steps $n = 99$ on the left and $n = 100$ on the right. Both quantum and classical distributions have reached the system dimension and are relaxing towards equilibrium.

exhibit noticeable differences. As shown in Fig. 4.2, around $n = 100$ the distributions have begun to settle close to an equilibrium shape. In Fig. 4.3 the successive time steps $n = 199$ and $n = 200$ show that, although both the quantum and classical distributions have relaxed very close to the same equilibrium distribution, the quantum distribution exhibits rapidly oscillating fluctuations about the classical steady-state.

Both the quantum and classical equilibrium distributions (projected along L_z) show significant deviation from the microcanonical distribution (4.9). This is also true of the distribution projected along L_x, which has a different non-uniform equilibrium distribution than that observed when projecting onto L_z (see the left box of Fig. 4.4). Uniform marginal distributions would be expected if the classical mapping was mixing, in which case arbitrary initial densities (with non-vanishing measure) would relax to the microcanonical distribution. Since the accessible kinematic surface has large KAM surfaces in this parameter regime, the coarse-grained *classical* equilibrium distributions are not expected to be flat. An unexpected feature of the results is the observation that the shape of the equilibrium *quantum* distributions so accurately reflects the details of the KAM structure in the classical phase space. This feature is most striking in the case of the distributions projected along J_z (see the right box in Fig. 4.4). The steady-state quantum and classical probability distributions $P_{J_z}(m_j)$ and $P^c_{J_z}(m_j)$ are both sharply peaked about $m_j = 0$. This equilibrium shape is much more sharply peaked than the tent-shape of the projected *microcanonical* distribution, $P^{mc}_{J_z}(m_j)$, given by (4.10) and also plotted in the right box in Fig. 4.4. The

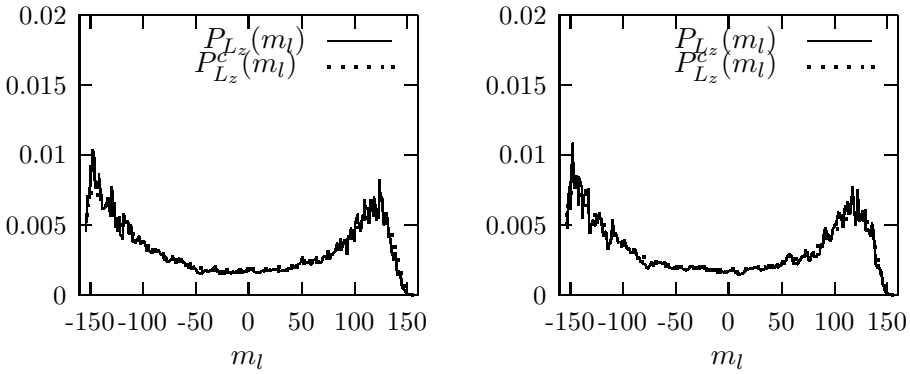

Figure 4.3: Same as Fig. 4.1 but for $n = 199$ on the left and $n = 200$ on the right. The quantum distribution is fluctuating about a classical steady-state.

important point is that the additional localization of the *quantum* distribution can be understood from a standard fixed-point analysis of the *classical* map [35]: the presence of KAM surfaces arising due to the stability of the parallel fixed points prevents the chaotic classical spins from aligning in parallel along the z-axis. Most remarkably, we find that the steady-state quantum distributions accurately reproduce this parameter-dependent structure of the mixed classical phase space even for much smaller quantum numbers. We examine how the accuracy of this correspondence scales with the quantum numbers in section 4.5.

4.2.2 Regime of Global Chaos

If we hold $a = 5$ and $r = 1.1$ fixed and increase the coupling strength to the value $\gamma = 2.835$, then all four of the fixed points mentioned above become unstable [35]. Under these conditions less than 0.1% of the surface $\mathcal{P}$ is covered with regular islands; the remainder of the surface produces a connected chaotic zone with largest Lyapunov exponent $\lambda_L = 0.45$. We will sometimes refer to this parameter regime as one of *global chaos* since the kinematically accessible phase space is predominantly chaotic.

The dynamics of the classical and quantum distributions are much simpler in this regime. We find that initially localised distributions, launched from arbitrary initial conditions, relax to the microcanonical distribution on a very short time-scale. To demonstrate this, we consider the dynamics of an initial quantum state with $s = 140$ and $l = 154$, and a corresponding classical density, launched from $\theta(0) = (20^o, 40^o, 160^o, 130^o)$. Though the initial

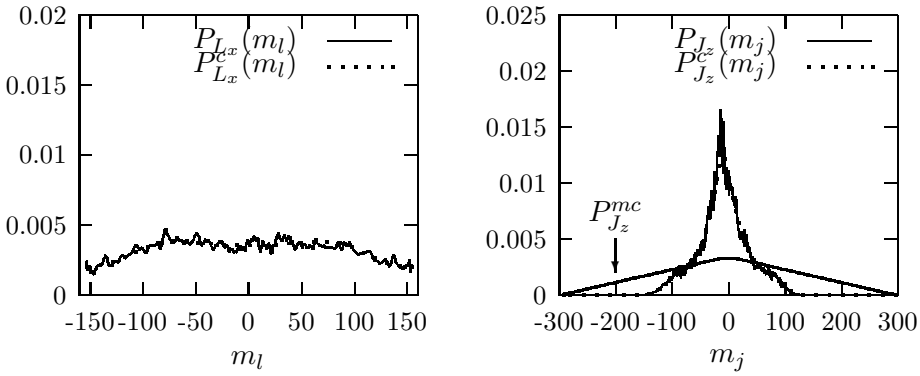

Figure 4.4: Same as in the previous figure, but for $P_{L_x}(m_l)$ on the left and $P_{J_z}(m_j)$ on the right, at time-step $n = 200$. Both $P_{J_z}(m_j)$ and $P^c_{J_z}(m_j)$ are localised relative to the projected microcanonical distribution $P^{mc}_{J_z}(m_j)$.

distributions are the same as in the mixed regime, by time-step $n \simeq 6$ the quantum and classical distributions have already spread to the system dimension and begin to exhibit noticeable differences. By time-step $n \simeq 12$ both distributions have relaxed very close to the microcanonical distributions. We plot the equilibrium quantum and classical projected distributions $P_{L_z}(m_j)$ and $P_{J_z}(m_j)$ in Fig. 4.5 for time-step $n = 50$. The projected *classical* distributions are nearly indistinguishable from the microcanonical forms, $P^{mc}_{L_z}(m_j)$ and $P^{mc}_{L_z}(m_j)$, and the *quantum* distributions again exhibit small fluctuations about the classical distributions. We have found that these equilibrium quantum-classical differences asymptote to a non-vanishing minimum when the measure of KAM surfaces becomes negligible. These minimum quantum fluctuations reflect characteristic deviations from the microcanonical state that arise because the equilibrium quantum state is a sequence of pure states, whereas the microcanonical state corresponds to a random mixture.

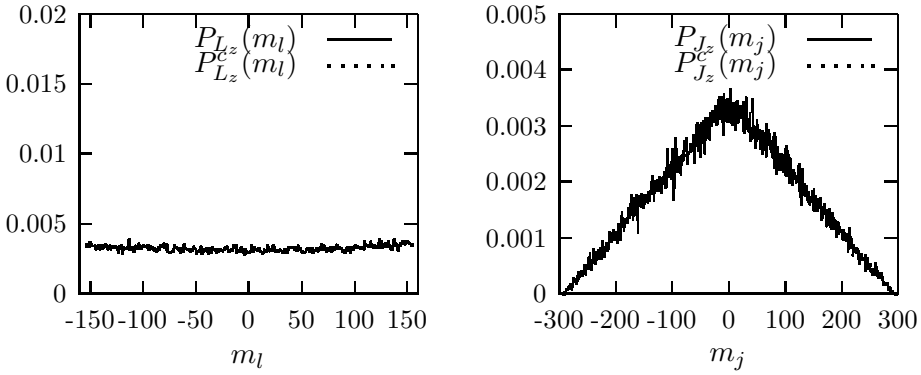

Figure 4.5: The equilibrium shapes of $P_{L_z}(m_l)$ and $P_{J_z}(m_j)$ at time-step $n = 50$ with $l = 154$ for a state launched in the global chaos regime ($\gamma = 2.835, r = 1.1, a = 5$). The quantum distributions exhibit small rapidly oscillating fluctuations about the projected microcanonical distributions. The classical distributions are not visible since the points lie within the fluctuating quantum data.

4.3 Rates of Relaxation to Equilibrium

In order to characterize the time-scale of relaxation to equilibrium it is convenient to study the time-dependence of a scalar measure that is sensitive to deviations from the equilibrium state. A conventional indicator of this rate of approach to equilibrium is the coarse-grained entropy,

$$H = -\sum_i P_i \ln P_i. \tag{4.11}$$

Here the $\{P_i\}$ stand for the quantum probabilities associated with projectors onto some basis of microstates (*e.g.* the projected distributions discussed in the previous section). The sum (4.11) is a standard measure of the information contained in a probability distribution and is sometimes called the Shannon entropy.

The Shannon entropy has a number of useful properties. First, unlike the von Neumann entropy $\mathrm{T}r[\rho \ln \rho]$, the Shannon entropy is basis-dependent. It reduces to the von Neumann entropy if the 'chosen' basis diagonalizes the state operator. However, this basis, or, more precisely, the set of projectors onto the (time-dependent) spectral decomposition of the state operator, does not necessarily correspond to a set of classically meaningful observables. Our main interest is to examine correspondence at the level of classical dynamical variables, so we consider probabilty distributions associated with projectors onto the eigenstates of classically well-defined operators. The classical counterparts to these probability distributions are associated with some fixed partioning of the phase space into cells of width $\hbar$ along the axes of the associated dynamical variable.

Second, whereas the von Neuman entropy of the total system is constant in time ($\mathrm{T}r[\rho \ln \rho] = 0$ since $\rho = |\psi\rangle\langle\psi|$), the basis-dependent Shannon entropy may have time-dependence even if the quantum state is pure. Thus (4.11) may be applied to examine the rate of relaxation of either *pure* or *mixed* quantum states. It is in this sense that we use the term *relaxation*, although the time-evolution is unitary in the quantum model (and volume-preserving in the classical model).

Given some fixed partioning of the phase space, if a classical state remains evenly spread through the phase space cells it occupies, and spreads through the phase-space exponentially with time, then an entropy like (4.11) should grow linearly with time. In this section we show that this argument holds approximately also for quantum states launched from a classically chaotic region of phase space. The actual rate of relaxation of the quantum states is accurately predicted by the classical entropy even for small quantum numbers.

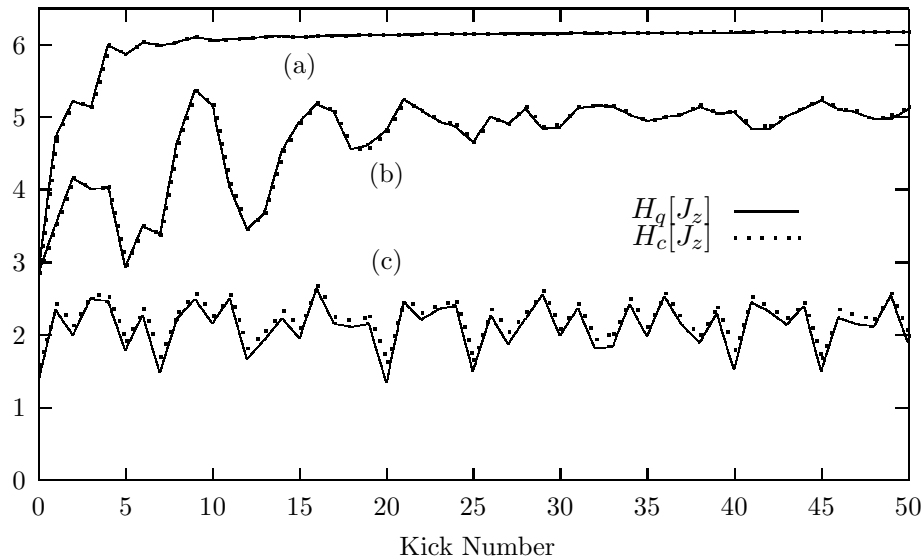

Figure 4.6: Comparison of the quantum and classical entropies $H[J_z] = -\sum_{m_j} P_{J_z}(m_j) \log P_{J_z}(m_j)$ for $s = 140$ and $l = 154$ in (a) regime of global chaos ($\gamma = 2.835$); (b) chaotic zone of the mixed regime ($\gamma = 1.215$); (c) regular zone of the mixed regime ($\gamma = 1.215$).

We demonstrate this behaviour by first considering the quantum entropy $H_q[J_z]$ of the probabilities associated with the eigenvalues m_j of J_z, *i.e.* the probabilities defined in (4.4). The corresponding classical entropy, $H_c[J_z]$, is calculated using the discrete classical probabilities (4.8). In Fig. 4.6 we compare the time-development of the quantum and classical entropies using quantum numbers $s = 140$ and $l = 154$. For these quantum numbers, the microcanonical (*i.e.* maximum) value of the entropy is $H^{mc}[J_z] = 6.2$. In case (c), corresponding to a regular zone of the mixed regime ($\theta(0) = (5^o, 5^o, 5^o, 5^o)$,$\gamma = 1.215$), we actually see the greatest amount of difference between the quantum ($H_q[J_z]$) and classical ($H_c[J_z]$) entropies. H_q exhibits a quasi-periodic oscillation about its initial value whereas for H_c these oscillations eventually dampen. For smaller quantum numbers, and thus broader initial states, H_c dampens much more rapidly although H_q continues to exhibit a pronounced quasi-periodic behaviour. In case (b), with initial centroid $\theta(0) = (20^o, 40^o, 160^o, 130^o)$ set in a chaotic region of the equally mixed regime, both H_q and H_c oscillate about an initially

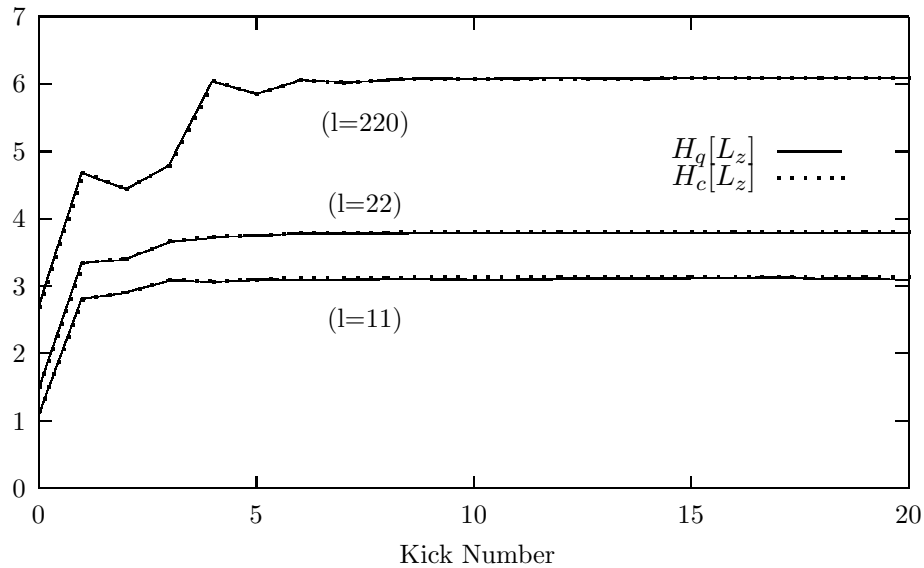

Figure 4.7: Comparison of the quantum and classical subsystem entropies $H[L_z] = -\sum_{m_j} P_{L_z}(m_l) \ln P_{L_z}(m_l)$ for increasing system sizes in the global chaos regime of Fig. 4.6.

increasing average before relaxing towards a constant value that lies well below the microcanonical maximum $H^{mc}[J_z] = 6.2$. This saturation away from the maximum is expected in the classical model since a large fraction of the kinematic surface is covered with regular islands and remains inaccessible. In case (a), corresponding to the regime of global chaos ($\gamma = 2.835$) and with the same initial state as (b), the entropies are nearly identical. Both grow much more quickly than in the mixed regime case, roughly linearly, until saturating very near the maximum value.

The quantum entropy is very well approximated by its classical counterpart also for smaller quantum numbers. In Fig. 4.7 we display the growth rates of the quantum and classical entropies of the probabilty distributions associated with the observable L_z for three sizes of quantum system ($l = 11$, $l = 22$, $l = 220$) using the same parameters and initial condition as for data-set (a) in Fig. 4.6. In each case the quantum entropy is essentially identical to the corresponding classical entropy. The initial rate of growth is similar in each case, roughly linear, and of order the Lyapunov exponent, $\lambda_L = 0.45$.

These results extend previous work demonstrating that the widths of quantum states

grow exponentially with time, on average, until saturation at the system dimension [46, 11, 35]. Modulo the small quantum fluctuations, for both quantum and classical models we find that the subsequent relaxation to an equilibrium configuration occurs on the time-scale,

$$t_{rel} \sim t_{sat} + \mathcal{O}(\lambda_L^{-1}), \tag{4.12}$$

where $t_{sat} \simeq \lambda_w^{-1} \ln l$ estimates the time it takes the initial coherent state to reach the system dimension. The exponent λ_w is the exponent governing the growth rate of the state width [35]. The last term $\mathcal{O}(\lambda_L^{-1})$ approximates the additional time-required for the state to become more or less uniformly spread over the accessible phase space. In predominantly chaotic regimes we have found that $\lambda_w \simeq \lambda_L$, though in mixed regimes λ_w is generally a few times larger than the largest Lyapunov exponent.

4.4 Time-dependence of Quantum-Classical Differences

Before examing the scaling of quantum-classical differences with increasing quantum numbers, it is useful to determine first their time-domain characteristics under the different types of classical behviour. Previous work has shown that quantum-classical differences for low-order moments, though initially small, grow exponentially with time when the classical motion is chaotic [11, 12] until the states approach the system size [35]. On this saturation time-scale those quantum-classical differences reach their maximum magnitude, but surprisingly this maximum was small, $\mathcal{O}(\hbar)$. More specifically, it did not scale with the quantum numbers. Of course, two distributions can be altogether different even when the differences between their means and variances are quite small, and therefore it is useful to examine the differences between the quantum and classical states in a more sensitive way.

In this section we examine the time-dependence of bin-wise deviations between the quantum and classical probability distributions. For the observable L_z this indicator takes the form,

$$\sigma[L_z] = \sqrt{\frac{1}{(2l+1)} \sum_{m_l=-l}^{l} [P_{L_z}(m_l) - P^c_{L_z}(m_l)]^2}. \tag{4.13}$$

This standard deviation estimates typical quantum-classical differences on the scale of $\hbar$ along the L_z-axis. Each interval is centered on a quantum eigenvalue. The $P^c_{L_z}(m_l)$ correspond to a measurement, or coarse-graining, of the classical density on an extremely fine-scale.

In Fig. 4.8 we examine the time dependence of $\sigma[L_z]$ for the same three classical sets of parameters and initial conditions displayed in Fig. 4.6. The initial value of $\sigma[L_z]$ is generally not zero since it is not possible to match all the marginal distributions exactly in the case of the SU(2) coherent states [35]. The actual magnitude of the initial discrepancy depends on the angle between the axis of measurement, *e.g.* L_z, and the direction of polarization of the initial state. For both chaotic states the differences initially decrease from their angle-dependent value and then increase until saturation at a steady-state value. This steady-state value is reached much later in the mixed regime (upper solid line), than in the global chaos regime (lower solid line). It occurs on the time-scale, t_{rel}, on which the underlying distributions have reached their steady-state configurations (modulo the quantum fluctuations).

As shown in Fig. 4.8, the quantum-classical differences are actually largest for the regular

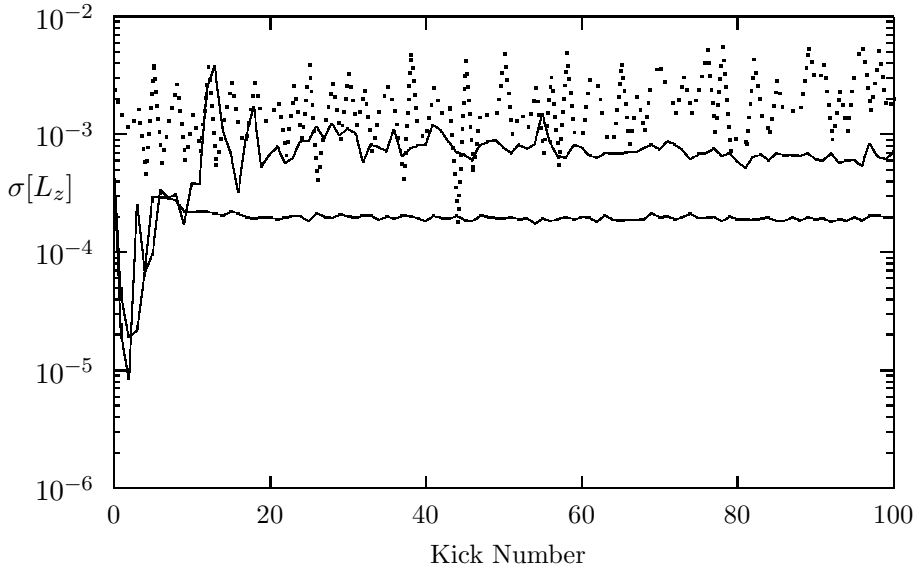

Figure 4.8: Time dependence of the standard deviation $\sigma[L_z]$ of quantum-classical differences (4.13) for states launched from a regular zone (dotted line) of the mixed regime ($\gamma = 1.215$), from a chaotic zone of the same mixed regime (middle solid line), and from the regime of global chaos (lower solid line,$\gamma = 2.835$). The initial discrepancy is relatively large, but quickly decreases, and then increases until reaching an asymptotic equilibrium value. This occurs more slowly for the mixed regime case, for which the asymptotic value is also larger. In all cases $s = 140$ and $l = 154$.

state (dotted line) of the mixed regime ($\gamma = 1.215$) at both early and late times (relative to the relaxation time-scale). The steady-state magnitude of the differences for the global chaos regime ($\gamma = 2.835$) is significantly smaller than the typical magnitude for the mixed regime. However, for larger values of the classical perturbation strength γ, this average steady-state magnitude does not decrease further (with the quantum numbers held fixed) but has reached a non-vanishing minimum. The magnitude of the minimum steady-state fluctuations, $\sigma_{L_z} \simeq 2 \times 10^{-4}$, should be compared with a typical magnitude of the quantum and classical distributions, $P_{L_z}(m_l) \simeq 3 \times 10^{-3}$. In the following section we examine how these fluctuations scale with increasing quantum numbers.

Above we have considered quantum-classical differences for observables (projectors onto subspaces) associated with the factor space $\mathcal{H}_l$. In this factor space the state is initially pure but becomes mixed as a result of dynamical interacions with the other subsystem. It

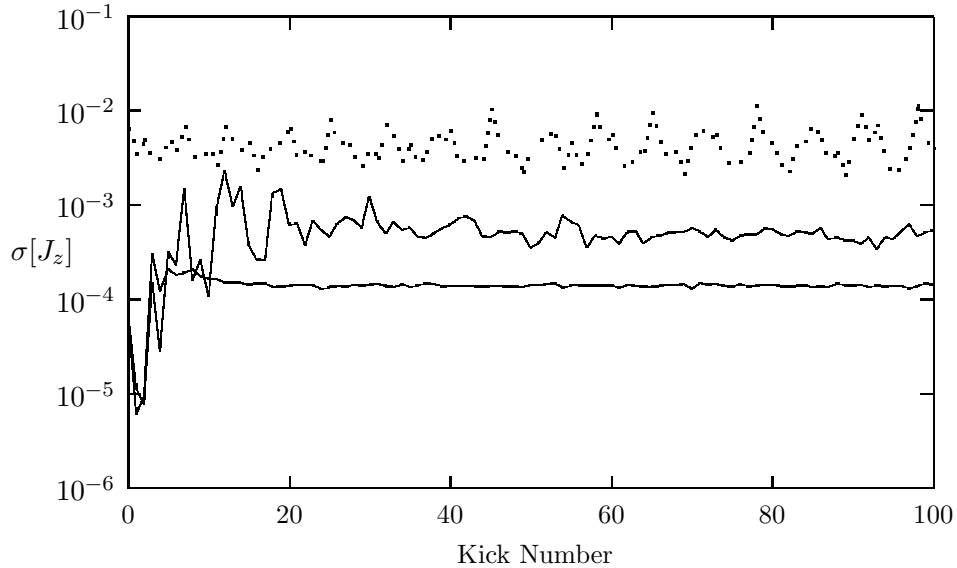

Figure 4.9: Same as Fig. 4.8 but for the standard deviation of quantum-classical differences of the total angular momentum, $\sigma[J_z]$, given by (4.14).

is interesting to check if the dynamical behaviours of the differences are an artefact of this dynamical mixing. Therefore we consider also bin-wise quantum-classical differences for an observable ($J_z = S_z + L_z$) that acts non-trivially on the full Hilbert space $\mathcal{H} = \mathcal{H}_s \otimes \mathcal{H}_l$. The quantum state in the full Hilbert space remains pure throughout the time-evolution. We construct the same standard deviation of the bin-wise differences between the quantum and classical probability distributions as above,

$$\sigma[J_z] = \sqrt{\frac{1}{[2(s+l)+1)]} \sum_{m_j} [P_{J_z}(m_j) - P^c_{J_z}(m_j)]^2}, \tag{4.14}$$

where $m_j \in \{l+s, l+s-1, \ldots, -(l+s)\}$. In Fig. 4.9 we compare $\sigma[J_z]$ in the same three classical regimes examined in Fig. 4.8. Once again the regular state (dotted line) exhibits the largest quantum-classical differences, and the differences for both chaotic states (middle and lower solid line) grow to a steady-state value on the time-scale at which the underlying distributions relax to their equilibrium configurations. As above, the average value of the differences for $\gamma = 2.835$ (lower solid line) correspond to a non-vanishing minimum, that is, the average value does not noticeably decrease for larger values of γ. The minimum quantum

fluctuations are again small when compared with the average height of the probability distribution, $[2(s+l)+1]^{-1} \simeq 2 \times 10^{-3}$.

For $\gamma \simeq 2.835$, the measure of regular islands is already very close to zero and the classical system is nearly ergodic on $\mathcal{P}$. Similarly, the quantum state is no longer constrained by any invariant classical structures but spreads *almost* evenly about the accessible Hilbert space. We find that the standard deviations of the quantum fluctuations that account for the equilibrium quantum-classical differences approach a non-vanishing minimum as the classical dynamics approach ergodicity on $\mathcal{P}$. These equilibrium differences can not vanish (for fixed quantum numbers) because the total quantum state remains pure under the unitary dynamics, whereas the microcanonical equilibrium corresponds to an equal-weight mixture.

4.5 Correspondence in the Classical Limit

We now turn to an examination of the classical limit, $\mathcal{J}/\hbar \to \infty$, where $\mathcal{J}$ is characteristic system action. Since the quantum-classical differences grow to their largest values once the states have spread to the system size and subsequently fluctuate about this magnitude, we will examine the scaling of the differences in this late time-domain, that is, when the states have relaxed close to their equilibrum configurations. Moreover, these scaling results will then complement previous work that has focussed on correspondence at early times [35], in the Ehrenfest regime when the states are narrow relative to the system dimensions.

We wish to determine if the standard deviation of the quantum-classical differences (defined in the previous section) decreases in magnitude with increasing quantum numbers. When comparing models with increasing quantum numbers, we hold the width of each probability bin fixed (at $\hbar = 1$). Since the number of bins will increase with the quantum number, it follows that the height of the probability distribution in a given bin will also decrease. Consequently, we construct a scale-independent, or relative, measure of the bin-wise quantum fluctuations by taking the ratio of the standard deviation to the average value of the probability distribution. For the observable L_z this takes the form,

$$R[L_z(n)] = \frac{\sigma[L_z(n)]}{\overline{P}_{L_z}} = N_l \, \sigma[L_z(n)]. \tag{4.15}$$

where the average value $\overline{P}_{L_z} = 1/(2l+1) = 1/N_l$. If this relative measure approaches zero in the classical limit then the quantum probabilty distribution converges to the corresponding classical one in that limit.

In Fig. 4.10 we consider typical equilibrium values of $R[L_z(n)]$ plotted against $1/\sqrt{N_l}$. We study the scaling using N_l because it is equal to the dimension of the factor space $\mathcal{H}_l$ and it is also proportional to the subsystem size $N_l \simeq 2|\mathbf{L}|$. We first consider a state launched in the global chaos regime ($\gamma = 2.835$, $r = 1.1$), with initial condition $\theta(0) = (45^o, 70^o, 135^o, 70^o)$. The scatter of plus signs for each $N_l = 2l + 1$ value corresponds to time-steps n such that $41 \leq n \leq 50$. These time-step values are chosen because they occur well after the relaxation time $t_{rel} \simeq 6$. In this regime the data exhibits very little scatter. A least-squares fit to the curve $R = A/\sqrt{N_l} + B$ yields a value for the intercept B that is consistent with zero ($B = 0.001 \pm 0.001$) and a slope of order unity ($A = 1.032 \pm 0.02$). An intercept consistent with zero implies that quantum-classical differences vanish in the classical limit, *i.e.* $P_{L_z}(m_l) \to P^c_{L_z}(m_l)$ as $l \to \infty$. This result is especially remarkable since

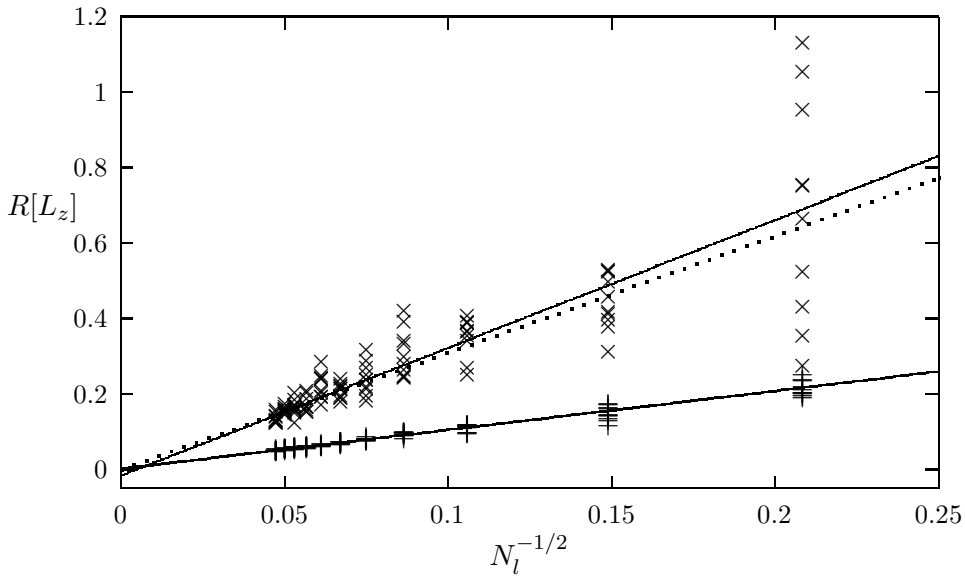

Figure 4.10: Scaling of relative quantum-classical differences (4.15 in the equilibrum time-domain versus increasing system size. Scatter of crosses corresponds to time-steps $191 \leq n \leq 200$, for a state launched in the chaotic zone of the mixed regime ($\gamma = 1.215$). Scatter of plus signs corresponds to time-steps $41 \leq n \leq 50$, for a state launched in the global chaos regime. Data sets in both of these regimes are consistent with the scaling law $R \simeq {N_l}^{-1/2}$, where $N_l = 2l + 1$.

we have considered the differences that arise given classical measurements which resolve the observable L_z with the rather extraordinary precision of $\hbar = 1$.

We next consider a state launched from the chaotic zone of the mixed regime ($\gamma = 1.215$, $r = 1.1$) with $\theta(0) = (20^o, 40^o, 160^o, 130^o)$. The scatter of crosses in Fig. 4.10 corresponds to time-steps $191 \leq n \leq 200$ n, again chosen well after the relaxation time t_{rel} for the range of quantum numbers considered. The scatter of quantum-classical differences at each N_l value is much more significant in this regime in which the equilibrium distributions reflect a much more complex phase space structure. However, the relative differences exhibit, on average, a similar dependence on the quantum numbers as in the predominantly chaotic regime. In this regime a least-squares fit to the curve $R = A/{N_l}^{1/2} + B$ yields a slope of order unity ($A = 3.39 \pm 0.15$) but a negative value for the intercept ($B = -0.017 \pm 0.009$) within two-standard deviations of zero. A negative intercept is not physically meaningful (since R is a positive definite quantity) and we assume it arises as a consequence of the statistical

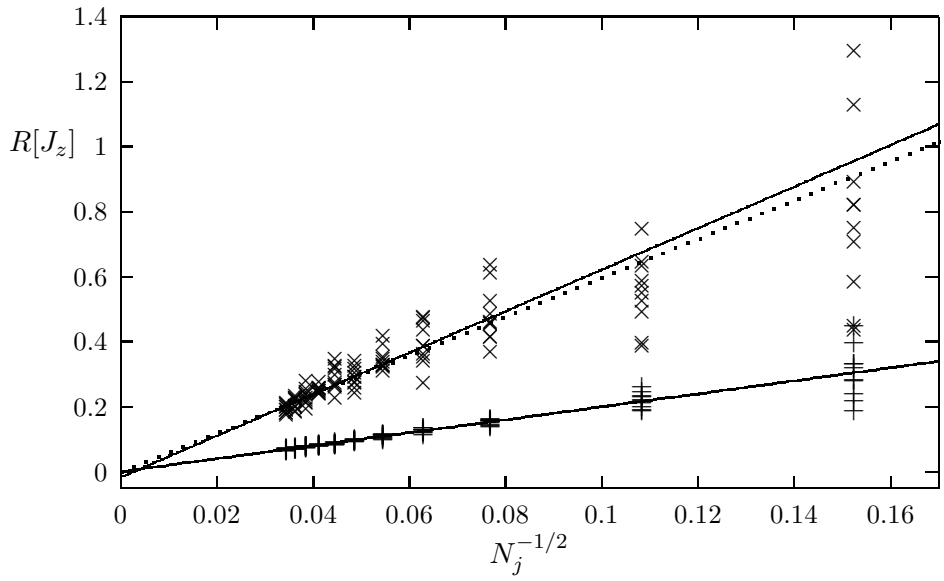

Figure 4.11: Same as Fig. 4.10 but using $R[J_z]$, as given by (4.16). Data sets in both types of chaotic regime are consistent with the scaling law $R \simeq {N_j}^{-1/2}$, where $N_j = 2(l+s)+1$.

scatter in the data. Also plotted is the curve $R = C/N_l^{1/2}$, with slope $C = 3.09 \pm 0.04$ also determined from a least-squares fit. Both fits are good, with reduced χ^2 values of order unity.

As we noted in the last section, the subsystem states do not remain pure, because of dynamically induced entanglement between the subsystems. Since the subsystem state (4.3) in the factor space $\mathcal{H}_l$ is not pure, but highly mixed in the equilibrium time-domain, it is possible that the scaling with N_l that we observe is related to the purity-loss from this entanglement. Consequently, it is useful to examine the scaling of the quantum-classical differences for the total spin J_z. The operator J_z acts non-trivially in the full Hilbert space $\mathcal{H}$. In this Hilbert space the system is described by a pure state vector at all times. In Fig. 4.11 we consider the scaling of the ratio,

$$R[J_z(n)] = \frac{\sigma[J_z(n)]}{\overline{P}_{J_z}} = N_j\ \sigma[J_z(n)], \tag{4.16}$$

where $\overline{P}_{J_z} = [2(s+l)+1]^{-1} = N_j^{-1}$ is the average value of either distribution, versus the dimension N_j. Here N_j is the number of subspaces associated with distinct eigenvalues (m_j) of the quantum operator (J_z). In contrast with N_l, N_j is not equal to the dimension of the

corresponding Hilbert space, though it is a measure of the system size since $N_j \simeq 2|\mathbf{J}|$. The parameters and initial conditions shown in Fig. 4.11 are the same as in Fig. 4.10. The same fit procedure as above, but applied to the function $R = A/N_j^{1/2} + B$, yields a value for B that is again consistent with zero ($B = 0.00038 \pm 0.0016$) and a positive slope of order unity ($A = 2.00 \pm 0.04$) in the predominantly chaotic regime (scatter of plus signs). Thus the relative standard deviation for J_z also decreases as the square of the quantum numbers and fits to an intercept that is consistent with zero. This implies that the fluctuating quantum distributions approach the classical equilibrium, even for a few degree-of-freedom system, which is described at all times by a pure state. In a chaotic state of the mixed regime (scatter of crosses), the fluctuations are larger, and the same fit procedure as above gives ($B = -0.016 \pm 0.012$, $A = 6.4 \pm 0.3$), where the negative value for B lies within two standard deviations of zero and is presumed to result from the statistical scatter of the data. Also plotted is the equation $R = C/N_j^{1/2}$, with $C = 5.97 \pm 0.06$ determined from a least-squares fit. The fits to both equations are good, with reduced χ^2 values of order unity.

4.6 Discussion

We have shown that, in classically chaotic regimes, initially localised quantum states relax to an equilibrium configuration that reflects the details of the classical phase-space structure. We find a remarkable degree of correspondence between the quantum and classical relaxation rates, even for small quantum numbers. Moreover, contrary to results obtained for the low-order moments [11, 35], the degree of difference between the probability distributions is actually smaller for the chaotic states than the regular states.

The equilibrium quantum distributions exhibit small rapidly oscillating fluctuations about the coarse-grained classical equilibrium. As the measure of regular islands on the classical manifold approaches zero, the quantum and classical equilibrium configurations approach their microcanonical forms, and the quantum fluctuations about the classical equilibrum approach a non-vanishing minimum. This minimum arises because we consider total quantum states that are pure, whereas the microcanonical configuration is produced by an equal-weight mixture.

For the distributions associated with the subsystem observable $\mathbf{L}$, the standard deviation of these differences, relative to the average value, decreases as $N_l^{-1/2}$, where $N_l = 2l + 1 \simeq 2|\mathbf{L}|$ is the dimension of the factor space, and becomes vanishingly small in the limit of large quantum numbers (*i.e.* large spins). These results suggest that correspondence with classical Liouville mechanics emerges in the classical limit for time-scales much longer than the Ehrenfest time.

A great deal of recent work has emphasized that the loss of purity resulting from interactions with a quantum environment removes characteristic quantum effects and improves the degree of quantum-classical correspondence [58, 56, 52]. While this is certainly the case for small quantum systems, it has been further argued that these *decoherence* effects must be taken into consideration to see the emergence of classical properties from quantum mechanics, even in the limit of large quantum numbers, if the classical motion is chaotic [97, 99].

Since our model is comprised of interacting subsystems, initially separable pure states become entangled dynamically; the subsystem states (in each factor space) do not remain pure but become mixed. This entanglement process has an effect that is analogous to the process of decoherence. Hence one might suspect that the emergent classical behaviour that we have observed for the properties of the subsystem $\mathbf{L}$ may be strictly the result of

a "decoherence" effect arising from entanglement with the other subsystem. To address this possibility, we have considered also the quantum-classical differences that arise in the probability distributions for a total system observable, J_z. In this case the quantum observables are projectors onto subspaces of the full Hilbert space, rather than merely a factor space. The quantum state in this full Hilbert space is not subject to any entanglement or decoherence and remains pure throughout the unitary time-evolution. We have found that the scale-independent standard deviations for these quantum-classical differences decrease as $1/\sqrt{N_j}$, where $N_j = 2(s+l)+1 \simeq 2|\mathbf{J}|$ is a measure of the system size and $N = (2s+1)(2l+1)$ is the dimension of the Hilbert space. The bin-wise quantum-classical differences become increasingly difficult to observe, in the limit of large quantum numbers, even for system observables that are isolated from the effects of decoherence. In this sense the process of decoherence is not *necessary* to produce quantum-classical correspondence in the classical limit.

Chapter 5

Breakdown of Ehrenfest Correspondence

5.1 Introduction

The quantum-classical correspondence principle expresses the view that the predictions of classical mechanics must emerge from quantum mechanics in the macroscopic limit. A typical statement of this principle is given by Messiah [67]: "In the limit $\hbar \to 0$, the laws of Quantum Mechanics must reduce to those of Classical Mechanics." Here the expression "$\hbar \to 0$" is shorthand notation for the limit where the characteristic system action is much larger than Planck's constant. Quantum-classical correspondence is *required* in the macroscopic limit if classical mechanics provides a valid approximation to the observed phenomena in this limit, whereas quantum mechanics provides correct predictions on all action scales. In order to test whether this principle holds in relevant physical situations, it is necessary to make more precise statements about which classical theory of mechanics, or, put differently, which classical properties, should be expected to emerge from the underlying quantum description. In this context, it is useful to introduce and distinguish two different interpretations of the quantum-classical correspondence principle.

The first of these, which I shall call *Ehrenfest correspondence*, is the claim that the phase space *trajectories* described by Hamilton's equations of motion are required to emerge from quantum mechanics in the macroscopic limit. This approach to characterizing correspondence was originally devised by Ehrenfest [33] and forms the basis for most textbook

discussions of the correspondence principle [65, 81, 68, 88, 67]. For a generic Hamiltonian system of the form $H = p^2/2m + V(q)$, this theorem states that the time-dependence of the expectation values $\langle q(t)\rangle = \langle\psi(t)|q|\psi(t)\rangle$ and $\langle p(t)\rangle = \langle\psi(t)|p|\psi(t)\rangle$, in an arbitrary quantum state $\psi(t)$, is prescribed by the differential equations,

$$\begin{aligned} \frac{d\langle q(t)\rangle}{dt} &= \frac{\langle p(t)\rangle}{m} \\ \frac{d\langle p(t)\rangle}{dt} &= \langle F(q)\rangle. \end{aligned} \tag{5.1}$$

If the quantum state is sufficiently well-localised, then the approximation,

$$\langle F(q)\rangle \simeq F(\langle q\rangle) \tag{5.2}$$

holds, and the differential equations for the quantum expectation values are then well approximated by Hamilton's equations of motion [51]. A clear statement of this interpretation of the correspondence principle is articulated by Merzbacher [68]: "We require that the classical motion of a particle be approximated by the average behaviour of a wave packet with a fairly sharp peak and as precise a momentum as the uncertainty principle permits and that the expectation values of the dynamical variables, calculated for such a wave packet, satisfy the laws of classical mechanics."

The second interpretation of the correspondence principle, which I will refer to as *Liouville correspondence*, is the weaker proposition that only the statistical properties of Liouville mechanics are required to emerge from the quantum description in the macroscopic limit. This view may be characterized by the condition that the quantum expectation values, $\langle A(q,p)\rangle$, for classically well-defined observables, should approach classical ensemble averages for the associated dynamical variables, $\langle A(q,p)\rangle_c$. In this correspondence picture, the classical ensemble averages are calculated from the prescription,

$$\langle A\rangle_c = \int dq \int dp A(q,p)\rho_c(q,p,t) \tag{5.3}$$

where the classical density, $\rho_c(q,p)$, describes the possible configurations for a system with incompletely specifed phase space coordinates. This density evolves with time according to the Liouville equation,

$$\frac{\partial\rho(q,p,t)}{\partial t} = \{\rho(q,p,t), H\} \tag{5.4}$$

where $\{\cdot,\cdot\}$ is the Poission bracket. In the previous chapters I have examined the characteristics of Liouville correspondence in considerable detail. I have demonstrated, for the model

system described in Chapter 2, that the statistical properties of Liouville mechanics emerge from quantum mechanics with a degree of approximation that improves as the system action increases. In particular, I examined this correspondence for quantum expectation values and classical ensemble averages associated with the system dynamical variables, their variances, and characteristic functions defined over extremely small intervals along the phase space axes corresponding to these variables. Even for the chaotic states of the model, the differences between quantum and Liouville mechanics for these observables have been shown to become vanishingly small in the limit "$\hbar \to 0$" over physically relevant time-scales. Most significantly, the correspondence with Liouville mechanics remained valid not just at early times (for well-localised quantum states), but also at late time (well after the width of the quantum state had grown to the system size). The conditions of Liouville correspondence are therefore satisfied in the macroscopic limit, in the sense that the observables of quantum mechanics are well approximated by the statistical predictions of classical Liouville mechanics, over physically accessible time-scales, even in the case of chaotic motion.

In this chapter I will demonstrate that the conditions of Ehrenfest correspondence may not be satisfied in the macroscopic limit when the classical motion is chaotic. In particular, I will argue that Ehrenfest correspondence may fail on physically relevant time-scales for some chaotic macroscopic systems, and, therefore, that quantum mechanics may be unable to describe the observable, deterministic motion of some macroscopic bodies. The implications of this result for the interpretation of the quantum state will be drawn out in the discussion at the end of this chapter.

This chaper is organized as follows. First I will present a theoretical argument indicating that the presence of chaos in general Hamiltonian models leads to macroscopic differences on a time-scale that grows only logarithmically with increasing system action. Specifically, I will show the quantum state centroids deviate from the predicted Newtonian trajectory in an experimentally observable manner. This time-scale may be experimentally accessible for some real macroscopic systems, leading to an observable breakdown of Ehrenfest correspondence. I will then illustrate the features of this general argument in the specific case of the coupled spin system described in Chapter 2. This example will also clarify how, contrary to a recent claim in the literature [99], the effects of decoherence are unable to restore this anticipated breakdown of Ehrenfest correspondence. In the discusssion I will explain how, on the assumption that individual macroscopic systems conserve energy and remain well-localised over experimentally verifiable time-scales, this argument leads to the

conclusion that quantum mechanics is unable to provide a valid description of macroscopic dynamics, and is therefore not a complete theory.

5.2 Ehrenfest Correspondence Conditions

The conditions for Ehrenfest correspondence are summarised succinctly by Messiah [67]: "In order that this picture be satisfactory, it is necessary that: (a) the mean values follow the classical laws of motion to a good approximation; (b) the dimension of the wave packet be small with respect to the characteristic dimensions of the problem, and that they remain small in the course of time." It is useful to formulate these requirements as mathematical conditions.

Let $\mathbf{x}_c = (q_c^1, \ldots, q_c^N, p_c^1, \ldots, p_c^N)$, denote the $2N$ phase space coordinates of an N degree of freedom system, let $\langle \mathbf{x} \rangle = \langle \psi(t) | \mathbf{x} | \psi(t) \rangle$ denote the corresponding quantum expectation values, and let $\xi^i = (\langle x^i \rangle - x_c^i)$ stand for the Ehrenfest differences. Further, let χ^i denote some prescribed set of thresholds that characterize adequate agreement between the quantum and classical predictions (e.g., determined by the resolution of the experiment measurements), and let t_{obs} stand for a characteristic time-scale over which the system may be subject to experimental observation. I will use $\mathcal{J}$ to denote a characteristic action of a physical system, with the *macroscopic* limit characterized by a very large value of the system action relative to Planck's constant, $\mathcal{J}/\hbar >> 1$. In order for Newtonian trajectories to emerge from the quantum description, the Ehrenfest differences must remain small relative to the prescribed threshold,

$$|\xi^i(t)| = |\langle x^i \rangle - x_c^i| < \chi^i \quad \text{for} \quad t < t_{obs} \quad \text{and} \quad \mathcal{J}/\hbar >> 1. \tag{5.5}$$

For a generic Hamiltonian system, this is only possible if the quantum state remains sufficiently well-localised,

$$\Delta x^i < \chi^i \quad \text{for} \quad t < t_{obs} \quad \text{and} \quad \mathcal{J}/\hbar >> 1, \tag{5.6}$$

where for notational convenience I have used the same tolerance thresholds χ^i for the quantum state widths $\Delta x^i = [\langle (x^i)^2 \rangle - \langle x^i \rangle^2]^{1/2}$ as for the Ehrenfest differences. These Ehrenfest conditions may be taken to define the proposition that quantum mechanics can describe the deterministic motion of a single macroscopic system, to within some prescribed accuracy and over physically observable time-scales, through the centroids of a well-localised state. I will

now show that these Ehrenfest conditions may *break down* on physically relevant time-scales for macroscopic bodies that are subject to classically chaotic dynamics.

5.3 The Ehrenfest Break-Time

Let the Ehrenfest break-time, t_{Ehr}, be defined as the shortest time upon which one of the Ehrenfest differences ξ^i grows larger than one of the thresholds in Eq. (5.5). The question under consideration is whether $t_{Ehr} < t_{obs}$ holds in relevant macroscopic situations.

A simple argument suffices to estimate how the time-scale t_{Ehr} grows with with increasing system action $\mathcal{J}$. In the general case of an autonomous classical flow, the time-dependence of the $2N$ phase space variables are prescibed by the following set of first-order differential equations,

$$\frac{d\mathbf{x}_c}{dt} = \{\mathbf{x}_c, H\} = \mathbf{F}(\mathbf{x}_c). \tag{5.7}$$

where $\{\cdot,\cdot\}$ is the Poisson bracket and H stands for the Hamiltonian. The time-evolution of the corresponding Heisenberg operators, $\mathbf{x}_q$, is given by the same set of differential equations,

$$\frac{d\mathbf{x}_q}{dt} = \frac{i}{\hbar}[x_q, H] = \mathbf{F}(\mathbf{x}_q), \tag{5.8}$$

where $[\cdot,\cdot]$ denotes the commutator for two operators. Expanding the function $\mathbf{F}(x_q)$ about the *classical* trajectory, $\mathbf{x}_c$, gives,

$$\frac{d\mathbf{x}_q}{dt} = \mathbf{F}(\mathbf{x}_c) + (x_q^i - x_c^i)\frac{\partial \mathbf{F}}{\partial x_q^i} + O([x_q^i - x_c^i]^2). \tag{5.9}$$

Taking the expectation value of both sides it follows that,

$$\frac{d\xi}{dt} = \xi \frac{\partial \mathbf{F}}{\partial x^i}|_{x^i = x_c^i} + O(\xi^2). \tag{5.10}$$

While the quantum-classical differences remain sufficiently small,

$$\xi^j \xi^k \frac{\partial^2 F^i}{\partial x_j \partial x_k} << \frac{\partial F^i}{\partial x^l}\xi^l, \tag{5.11}$$

the higher-order terms in the expansion (5.9) remain negligible, and the growth of the Ehrenfest differences is governed by the matrix,

$$M_{ij} = \frac{\partial F_i}{\partial x^j}, \tag{5.12}$$

which is just the classical tangent map. The time-dependent eigenvalues of this matrix, evaluated along a fiducial trajectory, determine the stability of the classical flow. Consequently, in the case of classically *regular* motion, the quantum-classical differences will grow at most as a small power of time,

$$\xi(t) \simeq \xi_o t^{\alpha}, \tag{5.13}$$

where $\alpha \simeq 1$. On the other hand, in classically chaotic regions, the local flow will exhibit expansion along some directions and contraction along others, and the very definition of the classical Lyapunov exponents [66] entails that the quantum-classical differences should grow, on average, exponentially with time,

$$\xi(t) \simeq \xi_o \exp(\lambda_L t), \tag{5.14}$$

where λ_L is the largest Lyapunov exponent. I have used the symbol ξ_o to denote the non-vanishing difference that will immediately arise between the quantum expectation values and classical dynamical variables due to the presence of a non-zero quantum-state width in either position or momentum [7]. Since χ^i denotes the threshold that defines a break between the quantum and classical predictions, it follows that this break arises on the time-scale,

$$t_{Ehr} \sim \lambda_L^{-1} \ln(\chi^i/\xi_o^i). \tag{5.15}$$

The result (5.15) can be expressed in a slightly more useful form. The "classical limit" of quantum mechanics corresponds to a sequence of quantum models that describe physical systems with increasing size (e.g., increasing quantum numbers), but with other parameters adjusted so that each model of this sequence is associated with the same classical system. The duration of the correspondence between the quantum and classical expectation values is *optimized* if the initial states are always chosen to be minimum uncertainty states (i.e., the initial variances are not increased in proportion to the system size but held fixed), whereas the break thresholds χ^i are always chosen as *fixed fraction* of the characteristic system size for each model in this sequence. Under these conditions, the ratio (χ^i/ξ_o^i) will scale as a power of the ratio $(\mathcal{J}/\hbar)$, where $\mathcal{J}$ is a characteristic system action, and the break between the quantum and classical theories arises on the time-scale,

$$t_{Ehr} \sim \lambda_L^{-1} \ln(\mathcal{J}/\hbar), \tag{5.16}$$

which estimates the optimal duration of *Ehrenfest* correspondence for chaotic systems. The time-scale (5.16) has been derived previously for a number of specific model systems [15, 16,

17, 95, 24, 48, 54] through a variety of different techniques. Although some of these authors have interpreted the break-time (5.16) as a time-scale during which "classical" behaviour emerges from the quantum description [95, 25, 48, 54, 22], this interpretation is imprecise [7, 35, 36], and I will refer to (5.16) specifically as the *Ehrenfest* break-time since it is defined as the time-scale during which the *Ehrenfest* correspondence conditions (5.5) remain valid.

5.4 The Breakdown of Ehrenfest Correspondence

Some authors have maintained that the break-time scaling in Eq. (5.16) is compatible with the requirement of quantum-classical correspondence since $t_{Ehr} \to \infty$ as "$\hbar \to 0$" [95, 25, 22]. Of course, for real physical systems $\hbar$ is a constant, and the relevant question is whether (5.16) is sufficiently long to accomodate the Ehrenfest correspondence conditions for all chaotic macroscopic systems. Assuming the thresholds χ^i designate macroscopically observable differences, then the ratio (χ^i/ξ^i_o) is, of course, enormous. However, Zurek and Paz [97, 99] have noted that the factor $\log(\mathcal{J}/\hbar)$, appearing in the break-time expression (5.16), may be quite small for some macroscopic systems, even ones with astronomically large values of the ratio $(\mathcal{J}/\hbar)$, since this ratio appears as an argument inside the logarithm. Consequently, the Ehrenfest break-time may be short compared to actual time-scales of observation. As an explicit example, these authors consider Hyperion, a moon of Saturn which is believed to exhibit a chaotic tumble [94, 20]. They estimate the upper bound $t \simeq 20$ years for the onset of a massive discrepency between the quantum and classical predictions.

Zurek [99] has suggested that such a short break-time raises the possibility of an observable breakdown of the correspondence principle for classically chaotic systems. Although I will demonstrate below that macroscopic chaotic motion certainly raises the possibility of an observable breakdown of the *Ehrenfest correspondence conditions*, it is important to emphasize that these situations do not suggest a breakdown of the correspondence principle, since the possibility of observing macroscopic differences between quantum mechanics and classical Liouville mechanics appears to be extremely remote [35, 36]. In the following section I will draw out some of the implicit assumptions of this breakdown argument that will help clarify this distinction.

5.5 Macroscopic Deviations and Kinematic Constraints

The argument leading to (5.14) leaves room for significant deviations from the exponential growth rate over short times, since the Lyapunov exponent is strictly defined as an average taken in the limit $t \to \infty$. However, the exponential growth rate (5.14) and the $\log(\mathcal{J}/\hbar)$ break-time should hold with a degree of approximation that improves as the initial difference ξ_o decreases relative to the characteristic system size. A more critical assumption of the breakdown argument is that Eq. (5.16) describes the onset of *macroscopic* Ehrenfest differences. This follows only if the exponential growth rule (5.14) remains valid until the Ehrenfest differences grow to a significant fraction of the system size. But it is clear that the exponential growth of the Ehrenfest differences must eventually become invalidated. For example, in the case of bounded systems, Eq. (5.14) can remain valid at most until the differences grow to the size of the accessible phase space, at which time the growth will completely saturate. Although from the condition (5.11) it appears that any characteristic threshold at which this growth rate terminates may be expected to scale with the system size, in the absence of a rigorous argument, it is necessary to confirm this expectation through explicit calculation in specific model systems. Moreover, for any given system, it is necessary to determine if the Ehrenfest differences grow to a sufficiently large fraction of the system size that these differences become larger than the resolution of the macroscopic measurements.

It may be objected that, even if the Ehrenfest differences grow to a macroscopic size on a physically relevant time-scale, these differences may not be experimentally significant as a result of the extreme sensitivity to initial conditions exhibited by the chaotic classical dynamics. Let $\Delta q(0)\Delta p(0) \neq 0$ denote the non-vanishing area of phase space from which the classical trajectory is known to have originated. From a purely classical point of view, at some later time t, it will be impossible to predict the location of the classical trajectory to within an area smaller than $\Delta q(t)\Delta p(t) \simeq \Delta q(0)\Delta p(0)\exp(2\lambda_L t)$ as a result of the exponential growth of the imprecision in the initial phase space coordinates. It is therefore impossible to experimentally confirm the Newtonian prediction with a precision better than $\Delta q(0)\Delta p(0)\exp(2\lambda_L t)$. However, according to (5.14), the Ehrenfest differences are expected to grow at the exponential rate, $\xi_q\xi_p \simeq \xi_q(0)\xi_p(0)\exp(2\lambda_L t)$, which is the same rate of growth governing the imprecision of the classical prediction. Therefore the correctness of the classical (Newtonian) theory may not be experimentally confirmed with a precision that

is smaller than the Ehrenfest differences. According to this objection, even if the predictions of the quantum and classical theories are macroscopically different, these differences are experimentally indistiguishable, and the theoretical prediction of a macroscopic discrepancy does not indicate an observable breakdown of the Ehrenfest correspondence principle.

However, this practical objection may be overcome by considering certain kinematic constraints satisfied by the classical dynamical variables. For an autonomous system with energy $E(\mathbf{q}, \mathbf{p})$, although a prediction of the classical dynamical variables $\mathbf{q}(t)$ and $\mathbf{p}(t)$ remains subject to an exponentially growing imprecision, these variables must satisfy the time-independent constraint $E(\mathbf{q}, \mathbf{p}) = E_o$, since the energy is a constant of the motion. Consequently, at any given time, the experimentally measured values of the coordinates, $\mathbf{q}_m(t) \pm \delta_q$ and $\mathbf{p}_m(t) \pm \delta_p$, are predicted to satisfy the constraint $E(\mathbf{q}_m(t), \mathbf{p}_m(t)) = E_o$ on the basis of the classical theory.

On the basis of the quantum theory, the expectation value of the energy $\langle E(\mathbf{q}, \mathbf{p})\rangle = E_o$ is also a constant of the motion since the energy operator commutes with the Hamiltonian. However, the quantum mechanical prediction for the time-dependence of the function $E(\langle \mathbf{q}(t)\rangle, \langle \mathbf{p}(t)\rangle)$ is not subject to the same constraint as the classical function, and may exhibit macroscopic deviations from that constraint. Consequently, if one can show that the quantum prediction $E(\langle \mathbf{q}(t)\rangle, \langle \mathbf{p}(t)\rangle)$ differs from the classical prediction $E(\mathbf{q}(t), \mathbf{p}(t)) = E_o$ by a macroscopically large magnitude, then experimental observation of the phase space coordinates (with adequate precision) will distinguish the predictions of quantum theory from those of the classical (Newtonian) theory. If the function $E(\mathbf{q}, \mathbf{p})$ is reasonably well-behaved, then a set of macroscopically large Ehrenfest differences, arising on the time-scale t_{Ehr}, should lead to a macroscopically large deviation between the quantum prediction, $E(\langle \mathbf{q}(t_{Ehr})\rangle, \langle \mathbf{p}(t_{Ehr})\rangle)$, and the classical one, $E(\mathbf{q}(t_{Ehr}), \mathbf{p}(t_{Ehr})) = E_o$. This argument may be generalized to the case of a non-autonomous system provided the system possesses any constant of the motion, $I(\mathbf{q}, \mathbf{p})$, i.e., a function that satisfies,

$$\frac{dI(\mathbf{q}, \mathbf{p})}{dt} = \{I(\mathbf{q}, \mathbf{p}), H(\mathbf{q}, \mathbf{p}, t)\} = 0. \tag{5.17}$$

5.6 Case Study: Coupled Spins

I will examine these features of Ehrenfest correspondence by explicit calculation of the quantum and classical dynamics for the model of nonlinearly coupled spins described in

Chapter 2,

$$H = a(S_z + L_z) + cS_x L_x \sum_n \delta(t - \tau n). \tag{5.18}$$

The key feature of the theoretical argument of section 5.4 that must be checked by explicit calculation is whether the exponential growth of the Ehrenfest differences persists until reaching a magnitude that scales with the system size.

I will consider this correspondence in the predominantly chaotic regime associated with the classical parameters $\gamma = 2.835, r = 1.1$, and $a = 5$, and with largest classical Lyapunov exponent $\lambda_L = 0.45$. The quantum dynamics are calculated using an initial coherent state centered at $\vec{\theta}(0) = (20^o, 40^o, 160^o, 130^o)$. The initial Ehrenfest differences may be set to zero if the classical initial conditions are set equal to the initial quantum state centroids,

$$|\mathbf{L}(0)| = |\langle \mathbf{L}(0) \rangle| = l. \tag{5.19}$$

In the case of the coordinate L_z, the time-dependence of the Ehrenfest difference,

$$\xi_{L_i}(t) = \langle L_i(t) \rangle - L_i(t), \tag{5.20}$$

is plotted in Fig. 5.1 for quantum numbers $l = 22$ and $l = 220$ on a semi-log scale. The upper envelope of the Ehrenfest differences indeed corresponds to approximately exponential growth, as expected from Eq. (5.14). More importantly, this exponential growth persists until saturation at the system size that is associated with each quantum model. The system sizes corresponding to $l = 22$ and $l = 220$ are indicated by the horizontal solid lines in the figure. These results are consistent with the general picture of the chaotic quantum dynamics developed in Chapters 3 and 4, where it was shown that the expectation values of dynamical variables approach their microcanonical equilibrium values, e.g., $\langle L_z \rangle \to 0$, on the saturation time-scale.

As explained in section 5.5, even macroscopic values of Ehrenfest differences in the coordinates, such as (5.20), arising on a physically accessible time-scale, do not automatically imply the possibility of an observable (experimentally significant) breakdown of correspondence, due to the exponential loss of precision that characterizes the chaotic classical dynamics. This objection may be overcome by considering the constraints imposed on the dynamics by the classical constant of the motion. For the model (5.18), the magnitudes of the subsystem spins provide the required constants of the motion,

$$\frac{d\mathbf{L}^2}{dt} = \{\mathbf{L}^2, H\} = 0,$$

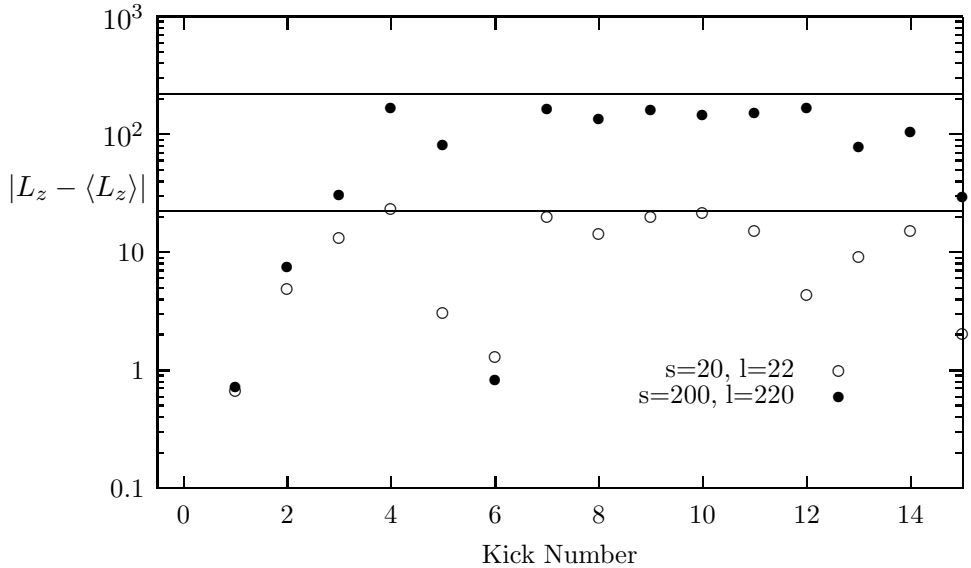

Figure 5.1: The time-development of the Ehrefest differences for L_z for classical parameters $\gamma = 2.835$, $r = 1.1$ and $a = 5$ for which the phase space is predominantly chaotic. Open circles correspond to quantum numbers $(s, l) = (20, 22)$ and filled circle correspond to $(s, l) = (200, 220)$. In both cases the approximately exponential growth of the Ehrenfest differences persists until saturation at the system size $|\mathbf{L}|$, indicated by horizontal lines.

$$\frac{d\mathbf{S}^2}{dt} = \{\mathbf{S}^2, H\} = 0. \tag{5.21}$$

As a result of these constant functions, the time-dependent spin components are subject to the time-independent contraints,

$$\begin{aligned} L_x^2(t) + L_y^2(t) + L_z^2(t) &= |\mathbf{L}|^2 \\ S_x^2(t) + S_y^2(t) + S_z^2(t) &= |\mathbf{S}|^2 \end{aligned} \tag{5.22}$$

In addition, the magnitude of the total system angular momentum, though time-dependent, is subject to the constraint,

$$\mathbf{L}^2 + \mathbf{S}^2 - 2|\mathbf{L}||\mathbf{S}| < \mathbf{J}^2 < \mathbf{L}^2 + \mathbf{S}^2 + 2|\mathbf{L}||\mathbf{S}|. \tag{5.23}$$

In the case of the quantum model, the expectation values of the operators $\mathbf{L}^2$ and $\mathbf{S}^2$ are conserved, but the associated quadratic functions,

$$\langle \mathbf{L} \rangle^2 = \langle L_x(t) \rangle^2 + \langle L_y(t) \rangle^2 + \langle L_z(t) \rangle^2,$$

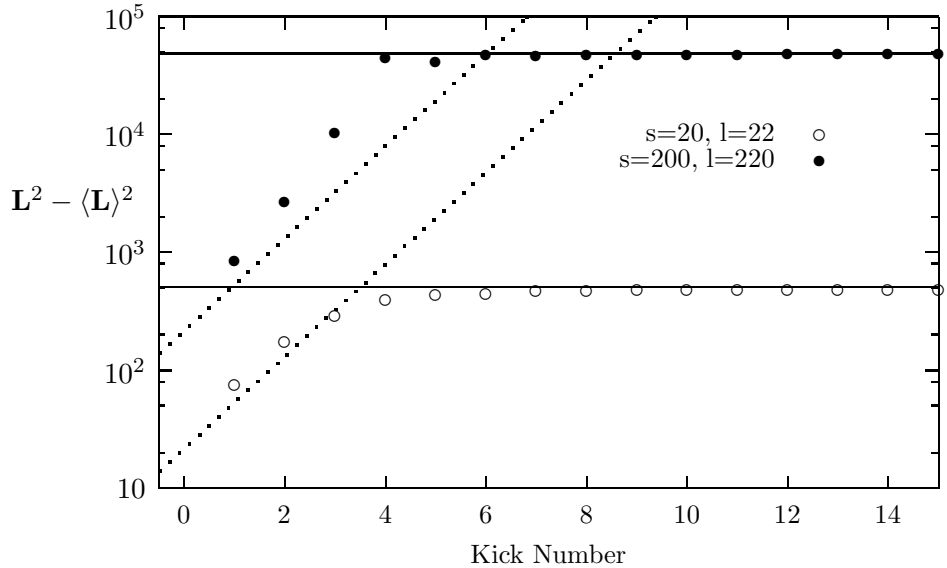

Figure 5.2: The time-development of the differences between the classical constant of the motion $\mathbf{L}^2 = l^2$ and the quantum prediction for $\langle L \rangle^2$ for the same classical parameters as in Fig. 5.1. The data are compared to an exponential growth rate given by twice the classical Lyapunov exponent, $\lambda_L = 0.45$. Open circles correspond to quantum numbers $(s, l) = (20, 22)$ and filled circle correspond to $(s, l) = (200, 220)$. In both cases the exponential growth of the Ehrenfest differences persists until saturation at the maximum possible value $\mathbf{L}^2$, indicated by horizontal lines.

$$\langle \mathbf{S} \rangle^2 \quad = \quad \langle S_x(t) \rangle^2 + \langle S_y(t) \rangle^2 + \langle S_z(t) \rangle^2, \tag{5.24}$$

are not conserved quantities. Similary, the magnitude of the total angular momentum,

$$\langle \mathbf{J} \rangle^2 = \langle J_x \rangle^2 + \langle J_y \rangle^2 + \langle J_z \rangle^2, \tag{5.25}$$

is not bounded by the classical constraint (5.23).

In Fig. 5.2 the time-dependent differences $\mathbf{L}^2 - \langle \mathbf{L} \rangle^2$ are plotted for $l = 22$ and $l = 220$. The growth of these differences is approximately exponential, and governed by a rate that appears to be independent of the system size. This growth may be estimated on the basis of the analytical argument predicting exponential growth (5.14) for the Ehrenfest differences for the coordinates, $\xi = \mathbf{L} - \langle \mathbf{L} \rangle$. Writing $\mathbf{L}(n) = \langle \mathbf{L}(n) \rangle + \xi(n)$ and squaring both sides gives,

$$\mathbf{L}^2 - \langle \mathbf{L} \rangle^2 = \xi^2 - 2\xi \cdot \langle \mathbf{L} \rangle. \tag{5.26}$$

Since $\xi^2(n) \simeq \xi_o^2 \exp(2\lambda_L n)$ grows very rapidly, and assuming the second term in (5.26) may therefore be neglected for large n, it follows that

$$\mathbf{L}^2 - \langle \mathbf{L} \rangle^2 \sim \xi_o^2 \exp(2\lambda_L n). \tag{5.27}$$

An alternative approach to characterizing the growth rate for the Ehrenfest difference $\mathbf{L}^2 - \langle \mathbf{L} \rangle^2$ follows from comparison with the numerically measured exponential rate of growth of the quantum variance (3.1). The magnitude of quantum variance $(\Delta \mathbf{L})^2$ provides a good approximation to the time-dependent Ehrenfest difference, $\mathbf{L}^2 - \langle \mathbf{L} \rangle^2$, for large l, that is,

$$(\Delta \mathbf{L})^2 \simeq \mathbf{L}^2 - \langle \mathbf{L} \rangle^2, \tag{5.28}$$

since,

$$\mathbf{L^2} = l^2 \simeq \langle \mathbf{L}^2 \rangle = l(l+1), \tag{5.29}$$

where quantities on the left correspond to the classical magnitude of the spin and those on the right to the quantum magnitude. Therefore, from (5.28) and (3.1), it may be expected that the Ehrenfest differences for the quadratic functions grow according to,

$$\mathbf{L}^2 - \langle \mathbf{L} \rangle^2 \simeq l \exp(2\lambda_w n), \tag{5.30}$$

where $\lambda_w \simeq \lambda_L$ in regimes of predominantly chaotic dynamics (as shown in Chapter 3). This estimate of the growth rate is the same as (5.27) obtained on the basis of the analytical argument leading to (5.14), but also provides an estimate of the prefactor $\xi_o^2 \simeq l$. The exponential rate (5.30) is plotted in Fig. 5.2, for $l = 22$ and $l = 220$, with $\lambda_w = \lambda_L = 0.45$, which slightly underestimates the growth rate of the data.

The most important feature of the data in Fig. 5.2 is that this exponential growth of these observable Ehrenfest differences does not saturate until the differences reach the magnitude of the corresponding classical constant of the motion $\mathbf{L}^2$. The classical magnitudes $\mathbf{L}^2 = 484$ and $\mathbf{L}^2 \simeq 48400$, for $\mathbf{L} = 22$ and $\mathbf{L} = 220$, respectively, are plotted as solid lines in Fig. 5.2. These are the maximum values that may be expected on purely kinematic grounds, since,

$$0 \leq |\langle \mathbf{L} \rangle^2 - \mathbf{L}^2| \leq \mathbf{L}^2. \tag{5.31}$$

The break-time for the experimentally observable differences $\mathbf{L}^2 - \langle \mathbf{L} \rangle^2$ is determined numerically from the earliest time at which these differences exceed a fraction f of the classical magnitude, i.e., the condition,

$$|\mathbf{L}^2 - \langle \mathbf{L} \rangle^2| > f\mathbf{L}^2. \tag{5.32}$$

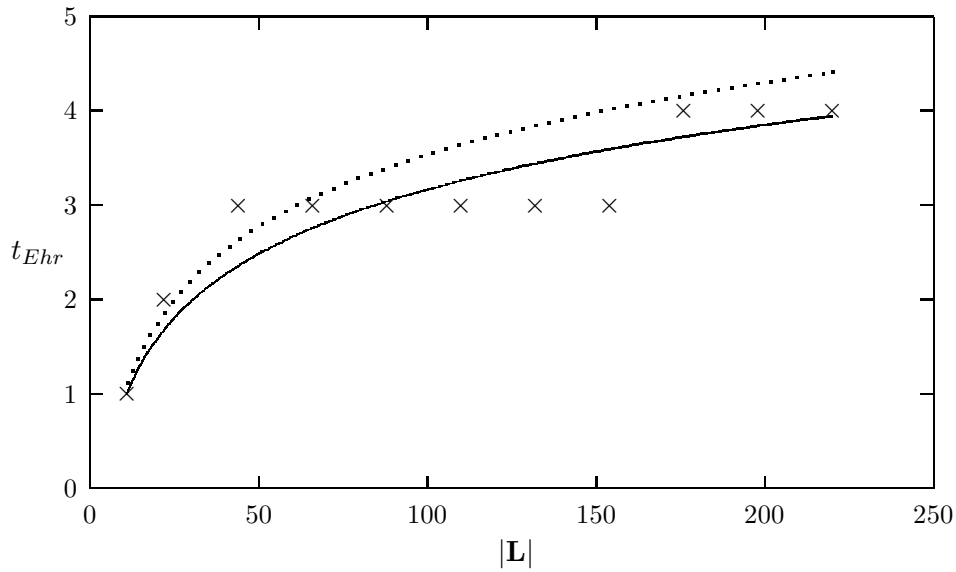

Figure 5.3: The break time obtained by the condition (5.32), using a threshold $f\mathbf{L}^2 = 0.25\mathbf{L}^2$, plotted against quantum number l ranging from 11 to 220. The data are obtained using the same classical parameters as in Fig. 5.2 and initial condition $\vec{\theta} = 20^o, 40^o, 160^o, 130^o$). The solid line corresponds to Eq. 5.33 with exponent $\lambda = 0.51$ obtained by a least-squares fit. The dotted line corresponds to Eq. 5.33 using the largest Lyapunov exponent $\lambda_L = 0.45$.

This calculated break-time is plotted against increasing system size, using $f = 0.25$, in Fig. (5.3). The numerical data exhibit a step-wise behaviour since the time, n, is confined to integer values. This scaling behaviour of the break time may be estimated by setting the LHS of the analytical prediction (5.30) equal to the threshold $f\mathbf{L}^2$, and solving for the time, to give,

$$t_{Ehr} \simeq 1/(2\lambda_w)\log(f\mathbf{L}). \tag{5.33}$$

This curve is plotted in Fig. 5.3 using $\lambda_w = \lambda_L = 0.45$ (dotted line), which slightly overestimates the break-time results. A least squares fit to (5.33) gives $\lambda_w = 0.51$, which provides an excellent fit to the data (solid line). The scaling demonstrated by the break-time data in this figure corresponds to that of a typical initial coherent state evolved under parameters that produce a predominantly chaotic classical phase space. These results explicitly confirm that the $\log(\mathcal{J}/\hbar)$ dependence of the Ehrenfest break-time holds even for *experimentally observable* differences that have grown to a significant fraction of the relevant

classical magnitude.

5.7 Discussion

The argument outlined above should apply to a wide variety of chaotic systems. In particular, the quantum expectation values may be experimentally distinguished from the classical coordinates on the short time-scale (5.16) provided the classical model admits a constant of the motion which is some "reasonable" function of the coordinates. For example, the differences between the quantum and classical predictions for any polynomial function of the coordinates should grow exponentially as long as the differences between the coordinates are themselves subject to exponential growth.

Though I have considered this problem in a specific model system, there is also evidence in other model systems that the break-time (5.16) should apply to Ehrenfest differences of order the system size when the phase space is predominantly chaotic. Fox and coworkers [47, 46] have shown that the quantum variances in the kicked top and the kicked rotor grow at an approximately exponential rate which subsides only when the variances have reached the system size. By virtue of the connection between the quantum variance and the time-development of the expectation values expressed in (1.1), it follows that these systems will also exhibit Ehrenfest differences of order the system size on the time-scale (5.16). Unfortunately, these authors have not explicitly reported how their results scale with increasing system size.

5.7.1 Liouville Correspondence Does Not Breakdown

In section 5.4 I emphasized that the possibility of a breakdown of the correspondence principle was based on demonstrating that *macroscopic* quantum-classical differences arose on an experimentally accessible time-scale. While I have provided evidence above that this is indeed the case for the Ehrenfest differences, the magnitude of which grow to the system size on the short time-scale (5.16), I have also demonstrated, in Chapters 3 and 4, that the quantum-Liouville differences that arise on this short time-scale do not scale with the system size. In particular, in Chapter 3 it was shown that the Liouville break-time grows logarithmically with the system size only when applied to differences that remain a factor $(\hbar/\mathcal{J})$ smaller than the system size. The presence of such small quantum-classical differences in the description of a macroscopic body is not an indication of a *breakdown* of the

correspondence principle, since this principle requires only approximate agreement between the quantum and classical theories in the macroscopic limit.

5.7.2 Can Decoherence Restore Ehrenfest Correspondence?

In the model that I have considered, each spin is a subsystem of a larger, isolated system. The time-evolution of each subsystem may be described, in general, by some non-unitary map as a result of the interactions with the other subsystem. The initial coherent state for each subsystem rapidly evolves into a nearly random mixture. These properties may be considered to arise as a result of the "decoherence" provided from interactions with the other subsystem. The important point is that the quantum environment provided by the other system only serves to increase the state width of each subsystem, and therefore actually leads to a faster breakdown of the Ehrenfest conjecture (5.5), but certainly does not help to preserve that conjecture. Since I have formulated a statement of the correspondence problem specifically in terms of the conjecture (5.5), as a constraint on the system coordinates, these results demonstrate explicitly that decoherence considerations do not circumvent the breakdown of Ehrenfest correspondence.

5.7.3 Consequences for Interpretation of the Quantum State

As explained in the Introduction, the inapplicability of the conjecture (5.5) to the class of chaotic macroscopic bodies, does not entail a failure of the correspondence principle, but a failure of a particular interpretation of the correspondence principle. This view is reinforced by noting that the conjecture (5.5) is not implied by Born's postulate, $P(q) = |\psi(q)|^2$, but consists of an independent assumption. (However, Born's postulate, combined with the assumption (5.6), does entail (5.5).)

The Ehrenfest correspondence conditions, (5.5) and (5.6), are motivated by a particular interpretation of the quantum formalism, namely, the view that quantum mechanics can provide a complete description of an individual physical system. Here it is useful to distinguish between two different interpretations of the quantum state [3]:

(i) a pure state provides a complete and exhaustive description of an individual system; and,

(ii) a pure state provides a description of certain statistical properties of an ensemble of similarly prepared systems.

The results of Chapters 3 and 4 provide strong evidence in support of interpretation (ii), whereas the argument of the present chapter suggests the possibility of experimentally refuting interpretation (i).

5.8 Is Quantum Mechanics Complete?

According to the general argument provided in the Introduction, the quantum expectation values may be expected to deviate from the Newtonian coordinates on a time-scale that may be short compared to physically relevant time-scales for a wide class of chaotic macroscopic systems. If one is tempted to maintain that the quantum expectation values actually describe the dynamics of a single chaotic macroscopic system, as suggested by the Ehrenfest Correspondence conjecture (5.5), then one is lead to the implausible view that significant deviations from classical energy conservation should be expected to arise, very rapidly, in the case of chaotic macroscopic systems. Since something as fundamental as energy conservation for an isolated system is likely to be confirmed under a wide variety of experimental conditions, it is natural to assume that it is the "expectation value trajectory" predicted from the conjecture (5.5), rather than the Newtonian trajectory, that will be experimentally invalidated.

On the assumption that individual macroscopic systems do not violate energy conservation on the time-scale (5.16), the argument outlined in this chapter leads to the conclusion that quantum mechanics is unable to provide a complete description of the motion of individual macroscopic systems. Therefore, quantum theory does not provide a complete description of reality. This is the conclusion derived by Einstein, Podolsky, and Rosen (EPR) a long time ago in a very different way [34]. In order to derive their conclusion EPR adopted the following principle [34]:

A necessary condition for a complete theory is that "every element of physical reality must have a counterpart in the physical theory."

In this chapter I have argued that the coordinates of macroscopic chaotic systems are not correctly described by the quantum expectation values since the latter deviate from these coordinates in a physically implausible and experimentally significant manner. But since this interpretative framework for quantum theory fails to provide a complete description of

macroscopic physical reality, is there then any physical interpretation of quantum theory that can meet the challenge of providing a complete and correct description of the chaotic dynamics of individual macroscopic bodies?

Appendix A

Nonclassical Moments for SU(2) Coherent States

Ideally we would like to construct an initial classical density that reproduces all of the moments of the initial quantum coherent states. This is possible in a Euclidean phase space, in which case all Weyl-ordered moments of the coherent state can be matched exactly by the moments of a Gaussian classical distribution. However, below we prove that no classical density $\rho_c(\theta, \phi)$ that describes an ensemble of spins of fixed length $|\mathbf{J}|$ can be constructed with marginal distributions that match those of the SU(2) coherent states (2.21). Specifically, we consider the set of distributions on $\mathcal{S}^2$ with continuous independent variables $\theta \in [0, \pi]$ and $\phi \in [0, 2\pi)$, measure $d\mu = \sin\theta d\theta d\phi$, and subject to the usual normalization,

$$\int_{\mathcal{S}^2} d\mu \; \rho_c(\theta, \phi) = 1. \tag{A.1}$$

For convenience we choose the coherent state to be polarized along the positive z-axis, $\rho = |j, j\rangle\langle j, j|$. This state is axially symmetric: rotations about the z-axis by an arbitrary angle ϕ leave the state operator invariant. Consequently we require axially symmetry of the corresponding classical distribution,

$$\rho_c(\theta, \phi) = \rho_c(\theta). \tag{A.2}$$

We use the expectation of the quadratic operator, $\langle \mathbf{J}^2 \rangle = j(j+1)$, to fix the length of the classical spins,

$$|\mathbf{J}| = \sqrt{\langle J^2 \rangle_c} = \sqrt{j(j+1)}. \tag{A.3}$$

Furthermore, the coherent state $|j,j\rangle$ is an eigenstate of J_z with moments along the z-axis given by $\langle J_z^n\rangle = j^n$ for integer n. Therefore we require that the classical distribution produces the moments,

$$\langle J_z^n\rangle_c = j^n. \tag{A.4}$$

These requirements are satisfied by the δ-function distribution,

$$\rho_v(\theta) = \frac{\delta(\theta-\theta_o)}{2\pi\sin\theta_o}, \tag{A.5}$$

where $\cos\theta_o = j/|\mathbf{J}|$ defines θ_o. This distribution is the familiar vector model of the old quantum theory corresponding to the intersection of a cone with the surface of the sphere.

However, in order to derive an inconsistency between the quantum and classical moments we do not need to assume that the classical distribution is given explicitly by (A.5); we only need to make use of the the azimuthal invariance condition (A.2), the length condition (A.3), and the first two even moments of (A.4).

First we calculate some of the quantum coherent state moments along the x-axis (or any axis orthogonal to z),

$$\begin{aligned}
\langle J_x^m\rangle &= 0 \quad \text{for odd } m \\
\langle J_x^2\rangle &= j/2 \\
\langle J_x^4\rangle &= 3j^2/4 - j/4.
\end{aligned}$$

In the classical case, these moments are of the form,

$$\langle J_x^m\rangle_c = \int dJ_z \int d\phi \rho_c(\theta)|\mathbf{J}|^m \cos^m(\phi)\sin^m(\theta). \tag{A.6}$$

For m odd the integral over ϕ vanishes, as required for correspondence with the odd quantum moments. For m even we can evaluate (A.6) by expressing the r.h.s. as a linear combination of the z-axis moments (A.4) of equal and lower order. For $m=2$ this requires substituting $\sin^2(\theta) = 1-\cos^2(\theta)$ into (A.6) and then integrating over ϕ to obtain

$$\begin{aligned}
\langle J_x^2\rangle_c &= \pi\int dJ_z\rho_c(\theta)|\mathbf{J}|^2 - \pi\int dJ_z\rho_c(\theta)|\mathbf{J}|^2\cos^2(\theta) \\
&= |\mathbf{J}|/2 - \langle J_z^2\rangle/2.
\end{aligned}$$

Since $\langle J_z^2\rangle$ is determined by (A.4) and the length is fixed from (A.3) we can deduce the classical value without knowing $\rho(\theta)$,

$$\langle J_x^2\rangle_c = j/2. \tag{A.7}$$

This agrees with the value of corresponding quantum moment. For $m = 4$, however, by a similar procedure we deduce

$$\langle J_x^4 \rangle_c = 3j^2/8, \tag{A.8}$$

that differs from the quantum moment $\langle J_x^4 \rangle$ by the factor,

$$\delta J_x^4 = |\langle J_x^4 \rangle - \langle J_x^4 \rangle_c| = |3j^2/8 - j/4|, \tag{A.9}$$

concluding our proof that no classical distribution on $\mathcal{S}^2$ can reproduce the quantum moments.

Appendix B

Wigner-Weyl Representation of Quantum Mechanics

The Wigner function is constructed from a quantum state operator ρ through the transform [91, 93],

$$\rho_w(q,p,t) = \frac{1}{2\pi\hbar}\int dy \langle q - y/2|\rho(t)|q + y/2\rangle e^{iyp/\hbar}. \tag{B.1}$$

The Wigner function, $\rho_w(q,p,t)$, which is a real "c-number" function, plays the role of the quantum state operator in the Wigner-Weyl representation of quantum mechanics. It generally takes on negative values in non-vanishing regions of its "phase space" domain, $\{q,p\} \in R$, and therefore may not be interpreted as a probability distribution.

Each Hermitian operator, $A(q,p)$, in the standard representation, is also associated with a "c-number" function,

$$A_w(q,p) = \int dy \langle q - y/2|A(q,p)|q + y/2\rangle e^{iyp/\hbar}. \tag{B.2}$$

Observable quantities are obtained from the prescription,

$$\langle A(q,p)\rangle = \int dq \int dp\ \rho_w(q,p)\ A_w(q,p). \tag{B.3}$$

The Wigner-Weyl representation is an exact representation of quantum mechanics in the sense that,

$$\int dq \int dp\ \rho_w(q,p)\ A_w(q,p) = \mathrm{Tr}[A(q,p)\rho], \tag{B.4}$$

for any Weyl-ordered operator $A(q,p)$.

The time-dependence of the Wigner function can be expressed in the following form [71],

$$\frac{d\rho_W(q,p)}{dt} = \{H, \rho_W(q,p)\} + \sum_{n=1}^{\infty} \left(\frac{\hbar}{2}\right)^{2n} \frac{(-1)^n}{(2n+1)!} \frac{\partial^{2n+1}\rho_W(q,p)}{\partial p^{2n+1}} \frac{\partial^{2n+1}H}{\partial q^{2n+1}}, \tag{B.5}$$

with an obvious connection to the time-dependence of the Liouville ensemble. Here $\{\cdot,\cdot\}$ denotes the classical Poisson bracket. As noted by Takahashi [91] and others, the quantum corrections to the Liouville flow (sometimes called the "Moyal terms") do not trivially vanish as "$\hbar \to 0$", in spite of their explicit proportionality to powers of $\hbar$. The Wigner distribution has an implicit dependence on $\hbar$, and factors of $(q/\hbar)^n$ may be expected from the $\partial^n/\partial_{p^n}$ derivatives in Eq. (B.5).

A clearer picture of the origin of quantum corrections to the Liouville picture is obtained by considering the differences that arise in the time-development of "observable" quantities. The time-development of the quantum expectation value $\langle A(q,p)\rangle$, corresponding to a time-independent Weyl-ordered operator, $A(q,p)$, follows from Eqs. (B.5) and (B.3): after integrating by parts, and assuming the surface terms vanish (for physically realistic states),

$$\left[\frac{\partial^k \rho_W(q,p)}{\partial p^k} \frac{\partial^j A}{\partial p^j}\right]_{\infty}^{-\infty} = 0, \tag{B.6}$$

it follows that,

$$\frac{d\langle A_w(q,p)\rangle}{dt} = \{H_w, A_w\} + \sum_{n=1}^{\infty} \left(\frac{\hbar}{2}\right)^{2n} \frac{(-1)^{n+1}}{(2n+1)!} \frac{\partial^{2n+1}A}{\partial p^{2n+1}} \frac{\partial^{2n+1}H}{\partial q^{2n+1}}. \tag{B.7}$$

This expression demonstrates that quantum *dynamical* corrections to the classical Liouville flow do not arise unless the Hamiltonian contains at least cubic powers of q, and, furthermore, *explicit* corrections do not arise unless the observable A contains at least cubic powers of p. These conclusions were determined previously by Ballentine and McRae in the specific case of the Henon-Heiles model [11]. As before, the quantum corrections may not be expected to vanish trivially in the limit "$\hbar \to 0$" since the Moyal terms may contain implicit dependence on $\hbar$.

Bibliography

[1] H. Ammann, R. Gray, I. Shvarchuck, and N. Christensen, Phys. Rev. Lett. **80**, 4111 (1998).

[2] V.I. Arnold, *Mathematical Methods of Classical Mechanics* (Springer-Verlag, New York, 1978).

[3] L.E. Ballentine, Rev. Mod. Phys. **42**, 358 (1970).

[4] L. E. Ballentine, Phys. Rev. A **44**, 4126 (1991).

[5] L. E. Ballentine, Phys. Rev. A **44**, 4133 (1991).

[6] L. E. Ballentine, Phys. Rev. A **47**, 2592 (1993).

[7] L.E. Ballentine, Y. Yang, and J.P. Zibin, Phys. Rev. A **50**, 2854 (1994).

[8] L.E. Ballentine in *Fundamental Problems in Quantum Physics*, Eds. M. Ferrero and A. van der Merwe (Kluwer Academic Publishers, 1995).

[9] L.E. Ballentine, *Quantum Mechanics* (World Scientific, Singapore, 1996).

[10] L.E. Ballentine and J. Zibin, Phys. Rev. A **54**, 3813 (1996).

[11] L.E. Ballentine and S.M. McRae, Phys. Rev. A **58**, 1799 (1998).

[12] L.E. Ballentine, Phys. Rev. A **63**, 024101 (2001).

[13] L.E. Ballentine, private communication.

[14] J.E. Bayfield and P.M. Koch, Phys. Rev. Lett. **33**, 258 (1974).

[15] G.P. Berman and G.M. Zaslavsky, Physica **91A**, 450 (1978).

[16] M.V. Berry, N.L. Balasz, M. Tabor, and A. Voros, Ann. Phys. **122**, 26 (1979).

[17] M.V. Berry and N.L. Balasz, J. Phys. A: Math. Gen. **12**, 625 (1979).

[18] L. Bonci, P. Grigolini, Phys. Rev. A **54**, 112 (1996).

[19] F. Borgonovi, I. Guarneri, F.M. Izrailev, Phys. Rev. E **57**, 5291 (1998).

[20] P. Boyd, G. Midlin, R. Gilmore, and H. Solari, The Astrophysical Journal **431**, 425-431 (1994).

[21] A. Braun, P. Gerwinski, F. Haake, H. Schomerus, Z. Phys. B **100**, 115 (1996).

[22] G. Casati and B.V. Chirikov, in *Quantum Chaos: Between Order and Disorder* (Cambridge University Press, Cambridge, 1995).

[23] G. Casati and B.V. Chirikov, Phys. Rev. Letters **75**, 350 (1995).

[24] B.V. Chirikov, F.M. Izrailev, and D.L. Shepelyansky, Sov. Sci. Rev. C2, 209 (1981).

[25] B.V. Chirikov, F.M. Israilev, and D.L. Shepelyansky, Physica D **33**, 77 (1988).

[26] J.I. Cirac and P. Zoller, Phys Rev Lett **74**, 4091 (1995).

[27] D. Cory and Y. Weinstein, private communication.

[28] S.R. Degroot, *La Transformation de Weyl et la Fonction de Wigner: une Forme Alternative de la Mecanique Quantique* (Les Presses Universitaires de Montreal, Montreal, 1974).

[29] D.P. DiVincenzo, Phys. Rev. A **51**, 1015 (1995).

[30] J.R. Dorfman, *An Introduction to Chaos in NonEquilibrium Statistical Mechanics* (Cambridge University Press, Cambridge, 1999).

[31] B. Eckhardt, S. Fishman, J. Keating, O. Agam, J. Main, and K. Muller, Phys. Rev. E **52**, 5893 (1995).

[32] A.R. Edmonds, *Angular Momentum in Quantum Mechanics* (Princeton University Press, Princeton, 1957).

[33] P. Ehrenfest, Z. Physik **45**, 455 (1927).

[34] A. Einstein, B. Podolsky, and N. Rosen, Phys. Rev. **47**, 777 (1935).

[35] J. Emerson and L.E. Ballentine, Phys. Rev. A **63**, 052103 (2001); quant-ph/0011020.

[36] J. Emerson and L.E. Ballentine, Phys. Rev. E **64**, 026217 (2001); quant-ph/0103050.

[37] A. Farini, S. Boccaletti, and F.T. Arecchi, Phys. Rev. E. **53**, 4447 (1996).

[38] M. Feingold and A. Peres, Physica **9D** 433 (1983).

[39] M. Feingold, N. Moiseyev, and A. Peres, Phys. Rev. A **30**, 509 (1984).

[40] M. Feingold, N. Moiseyev, and A. Peres , Chem. Phys. Lett.

[41] M. Feingold and A. Peres, Phys. Rev. A **34**, 591 (1986). **117**, 344 (1985).

[42] J. Ford, G. Mantica, G. Ristow, Physica D **50**, 493-520, (1991).

[43] J. Ford and M. Ilg, Phys. Rev. A **45**, 6165, 1992.

[44] J. Ford and G. Mantica, Am. J. Phys 60 (12), 1086, (1992).

[45] R.F. Fox and B.L. Lan, Phys. Rev. A **41**, 2952 (1990).

[46] R.F. Fox and T.C. Elston, Phys. Rev. E **50**, 2553 (1994).

[47] R.F. Fox and T.C. Elston, Phys. Rev. E **49**, 3683 (1994).

[48] H. Frahm and H.J. Mikeska, Z. Phys. B **60**, 117 (1985).

[49] P. Gaspard, *Chaos, Scattering and Statistical Mechanics* (Cambridge University Press, Cambridge, 1998).

[50] D. Giulini, E. Joos, C. Kiefer, J. Kupsch, I. Stamatescu, and H. D. Zeh, *Decoherence and the Appearance of a Classical World in Quantum Theory* (Springer, Berlin, 1996).

[51] H. Goldstein, *Classical Mechanics*, 2nd ed. (Addison-Wesley, Reading, 1980).

[52] J. Gong and P. Brumer, Phys. Rev. E **60**, 1643 (1999).

[53] M.C. Gutzwiller, Chaos in Classical and Quantum Mechanics (Springer-Verlag, New York, 1990).

[54] F. Haake, M. Kus and R. Scharf, Z. Phys. B **65**, 361 (1987).

[55] F. Haake, *Quantum Signatures of Chaos* (Springer-Verlag, New York, 1991).

[56] S. Habib, K. Shizume and W.H. Zurek, Phys. Rev. Lett. **80**, 4361 (1998).

[57] B.S. Helmkamp and D.A. Browne, Phys. Rev. E **49**, 1831 (1994).

[58] B.S. Helmkamp and D.A. Browne, Phys. Rev. Lett. **76**, 3691 (1996).

[59] Ph. Jacquod and J.-P. Amiet, J. Phys. A **30**, 2963 (1997).

[60] R.V. Jensen, Nature **355**, 311 (1992).

[61] E. Joos and H.D. Zeh, Condensed Matter **59**, 223-243 (1985).

[62] A.R. Kolovsky, Phys. Rev. Letters **76**, 340 (1996).

[63] B.L. Lan and R.F. Fox, Phys. Rev. A **43**, 646 (1991).

[64] J.G. Leopold and I.C. Percival, Phys. Rev. Lett. **41**, 944 (1978).

[65] R.L. Liboff, *Introductory Quantum Mechanics* (Addison-Wesley, Reading, 1989).

[66] A.J. Lichtenberg and M.A. Lieberman, *Regular and Chaotic Motion* (Springer-Verlag, New York, 1992).

[67] A. Messiah, *Quantum Mechanics* (Wiley, New York, 1966).

[68] E. Merzbacher, *Quantum Mechanics* (Wiley, New York, 1970).

[69] G.J. Milburn, S. Schneider, and D.F.V. James, *Ion Trap Quantum Computing with Warm Ions*, Fortschritte der Physik, 801-810, **48** (2000); quant-ph/9908037.

[70] P. Miller and S. Sarkar, Phys. Rev. E **60**, 1542 (1999).

[71] J.E. Moyal, Proc. Cambridge Phys. Soc. **45**, 99 (1949).

[72] A. Perelomov, *Generalized Coherent States and Their Applications*, (Springer-Verlag, New York , 1986).

[73] A. Peres, Phys. Rev. A **30**, 504 (1984).

[74] A. Peres, Phys. Rev. A **30**, 1610 (1984).

[75] A. Peres, *Quantum Theory: Concepts and Methods* (Kluwer, Dordrecht, 1993).

[76] A. Peres, Phys. Rev. E **53**, 4524 (1996).

[77] M. Price, S. Somaroo, A. Dunlop, T. Havel, and D. Cory, Phys. Rev. A **60**, 2777 (1999).

[78] D. T. Robb and L. E. Reichl, Phys. Rev. E **57**, 2458 (1998).

[79] R. Roncaglia, L. Bonci, B.J. West, and P. Grigolini, Phys. Rev. E **51**, 5524 (1995).

[80] M.E. Rose, *Elementary Theory of Angular Momentum* (Wiley, New York, 1957).

[81] J.J. Sakurai, *Modern Quantum Mechanics* (Benjamin-Cummings, Menlo Park Calif., 1985).

[82] R. Schack and C. Caves, Phys. Rev. Lett. **69**, 3413 (1992).

[83] R. Schack and C. Caves, Phys. Rev. Lett. **71**, 525 (1993).

[84] R. Schack, G. D'Ariano, and C. Caves, Phys. Rev. E **50**, 972(1994).

[85] R. Schack and C. Caves, Phys. Rev. E **53**, 3257 (1996).

[86] R. Schack and C. Caves, quant-ph/9810050.

[87] R. Schack, Phys. Rev. A **57**, (1998); quant-ph/9705016.

[88] L.I. Schiff, *Quantum Mechanics*(McGraw-Hill, New York, 1968).

[89] A.I. Schnirelman, in *KAM Theory and Semiclassical Approximations to Eigenfunctions* (Spinger-Verlag, New York, 1993).

[90] M. Tabor, *Chaos and Integrability in Nonlinear Dynamics* (Wiley, New York, 1989).

[91] K. Takahashi, Prog. Theor. Phys. Supp. 98 (1989).

[92] S. Tomsovic and E.J. Heller, Phys. Rev. E **47**, 282 (1993).

[93] E.P. Wigner, Phys. Rev. 40, 749 (1932).

[94] J. Wisdom, S. Peale, and F. Mignard, Icarus **58**, 137 (1984)

[95] G.M. Zaslavsky, Phy. Rep. **80**, 157 (1981).

[96] W.H. Zurek and J.P. Paz, Phys. Rev. Lett. **72**, 2508 (1994).

[97] W.H. Zurek and J.P. Paz, Phys. Rev. Letters **75**, 351 (1995).

[98] W.H. Zurek and J.P. Paz, Physica D **83**, 300 (1995).

[99] W.H. Zurek, Physica Scripta **T76**, 186 (1998).